IVYSPRING INTERNATIONAL PUBLISHER

Theranostics

2027; 17(1): 366-403. doi: 10.7150/thno.139570

Review

Recent progress in magnetic nanoparticles: classification, morphological features, and applications for cancer treatment

Shuang Bai[1,3,4*]✉, Kai Ma[1,2*], Yupei Zhang[1,2], Juanjuan Wang[1], Long Liu[1], Shuqin Xu[1], Yi Lv[1,2,3,4]✉

1. Shaanxi Province Center for Regenerative Medicine and Surgery Engineering Research, the First Affiliated Hospital of Xi'an Jiaotong University, Xi'an, 710061, China.
2. School of Future Technology, Xi'an Jiaotong University, Xi'an, 710061, China.
3. National Local Joint Engineering Research Center for Precision Surgery & Regenerative Medicine, the First Affiliated Hospital of Xi'an Jiaotong University, Xi'an, 710061, China.
4. Shaanxi Provincial Key Laboratory of Magnetic Medicine, the First Affiliated Hospital of Xi'an Jiaotong University, Xi'an 710061, China.

* S. Bai and K. Ma contributed equally to this work.

✉ Corresponding authors: E-mail: Shuangbai@xjtufh.edu.cn (S. Bai); luyi169@xjtu.edu.cn (Y. Lv).

© 2027 The Author(s). This is an open access article distributed under the Creative Commons Attribution 4.0 International Licence, subject to the Publisher's Terms of Use at https://ivyspring.com/terms.

Received: 2026.06.19; Accepted: 2026.09.29; Published: 2027.01.01

Abstract

With the continuous development of magnetic nanotechnology, new applications for cancer treatment have gradually appeared in recent years. Magnetism, covering fields, forces and thermal effects, has gradually been used in oncology to develop a new type of cancer therapy system. This paper reviews the recent all-around development of magnetic nanoparticles (MNPs) for cancer diagnosis and therapy. First, we introduce the main types of MNPs and discuss their magnetic response mechanisms. In addition to the traditional magnetic control factors of chemical composition and intrinsic structure of magnetic domains, this review also summarizes the regulatory laws for geometric structural parameters such as magnetic anisotropy, particle microscopic morphology and particle size on the magnetic response characteristics of MNPs. Next, we introduce the therapeutic applications of MNPs in oncology, such as magnetic targeting, magnetic hyperthermia, magnetic force-mediated therapy, and precision treatment enabled by magnetically actuated nanorobots. Finally, the main problems and future directions of MNPs in biomedical applications are systematically introduced. This paper takes the properties of materials and relates them to magnetic-field-sensitive functions and biological responses; it aims to build a full-featured database of advantages in magnetic-field-regulated nanocarriers for cancer diagnosis and treatment, uncover the fundamental mechanisms by which magnetic effects boost anti-tumor effects, and provide a practical foundation for developing MNP-based cancer therapy systems.

Keywords: magnetic nanoparticles, magnetic anisotropy, magnetic treatment, tumor theranostics

1. Introduction

Energy technologies are based on acoustics, optics, electricity and magnetism, etc., and have recently gained attention for their applications in the treatment of cancer. Among them, magnetic technology has several advantages; it is non-invasive, can reach deep tissues, is relatively safe and can be easily controlled remotely. Among the various magnetic-based systems, magnetic nanoparticles (MNPs) have gradually emerged as one of the representative and promising materials due to their tunable composition, size, shape, surface chemical properties and magnetic responsiveness [1-3]. The above attributes have given MNPs many design options for therapeutic platforms and have promoted their application in oncology.

Recently, with the progress of physics, materials science and engineering, MNPs have been applied to medicine. Elemental metal MNPs, metal oxide MNPs, metal alloy MNPs, carbides/nitrides MNPs, and rare-earth-based permanent magnets are all types of MNPs. They exhibit distinct magnetic properties and biological functions. In addition, magnetic anisotropy, size effect and shape effect collectively alter the physicochemical properties of these MNPs to modify

their magnetic response, hysteresis loss and mechanical force generation. These features have given MNPs diverse applications in cancer therapy. Magnetic targeting and surface functionalization modification can be used to enhance the accumulation of magnetic nanocarriers at the tumor site and reduce damage to normal tissues [4-6]. Under an alternating magnetic field (AMF), MNPs can dissipate energy as heat through Néel relaxation and Brownian relaxation, and thus cause damage to tumor cells by local heating [7]. The shape of MNPs will also change how they respond mechanically to a magnetic field. Nanorods and nanodiscs can generate rotational or pushing forces, such as torque, tension, shear, and compression; these may damage the cell membrane and organelle structure of cancer cells and thus kill the cancer cells [8].

Meanwhile, the development of intelligent control and robotics has also extended the biomedical application range of magnetic response systems. At present, most studies are concentrated on magnetic navigation, magnetic actuation, and microrobot platforms, which apply controllable forces and torques to magnetized devices for the non-contact remote manipulation of catheters, microrobots, and endoscopes. This technique is commonly defined as robotic remote magnetic navigation (RMN). RMN features non-invasive magnetic field regulation and unimpeded penetration across biological tissues, making it capable of *in vivo* visualization of anatomically narrow or otherwise inaccessible deep-seated tissue regions. Therefore, several studies have applied RMN to targeted therapeutic delivery [9, 10], drug delivery [11-13], cellular and subcellular characterization [14-16], and microsurgery [17, 18].

Magnetic microrobots have been prepared in various shapes for microsurgery, such as fish-like, rod-like, spiral, and spherical shapes [19-24]. Such morphological features govern locomotion and steerability, enabling the robots to navigate within curved, confined environments. For example, in endovascular neurosurgery, a robotic manipulator can remotely steer a guidewire, and a motorized module enables its automated advancement. Real-time imaging is acquired to facilitate remote guidewire navigation toward lesions within anatomically complex regions. Such remote operation also lowers ionizing radiation exposure of surgeons during fluoroscopy-guided procedures [25]. Based on the above studies, it can be concluded that magnetic actuation and robot control technology are suitable support means for biomedical intervention in confined spaces.

Recent developments in magnetic actuation and robotic control have expanded the applications of MNPs beyond local heating and passive cargo transport. Based on the previous review of the biomedical applications of MNPs [26, 27], this paper will investigate how the material characteristics and the application of a magnetic field affect therapeutic effects. Particles of the same chemical composition will have different thermal, mechanical and motion properties in a gradient, AMF and rotating magnetic field (RMF).

The above are the connections among them. First, we will study how composition, magnetic anisotropy, particle size and shape affect the magnetic response and therapeutic effect. The design principles of these materials have been applied in magnetic targeting, magnetic hyperthermia, magnetic force therapy, responsive drug delivery and magnetic micro/nanorobotic systems. The framework can be used to compare the contributions of material properties and applied magnetic-field parameters in different therapeutic modes. We also summarize the existing evidence on how magnetic heating and mechanical actuation trigger cellular stress responses (Figure 1). Finally, the review identifies several reasons for the difficulty of clinical application, such as a lack of correlation between laboratory performance and *in vivo* results. At the same time, the systematic requirements for clinical application are also considered; that is to say, all problems of material preparation, magnetic control, imaging, delivery, and safety assessment must be addressed simultaneously. The purpose of this paper is to summarize the recent research results in material design, application of magnetic fields and biological environment that have enhanced the therapeutic effect of MNPs.

2. Magnetic Nanoparticles

MNPs are composed of iron-, cobalt- and nickel-based oxides, alloys or composites, and have found many applications in various fields, such as magnetic fluids, magnetic data storage, magnetic resonance imaging (MRI), magnetic refrigeration, hyperthermia, biomedicine, catalysis, and environmental remediation [28-36]. The unique properties of MNPs, such as superparamagnetism, depend on their structure. Fortunately, current chemical technology allows the synthesis of MNPs with desired sizes, structures, shapes, as well as oxidation resistance, despite the surface effects and magnetic dipole interactions. In this section, we first describe the types of MNPs, including metal oxides, metal alloys, carbides and nitrides, and rare earth-based permanent magnets. Then, we illustrate the magnetic anisotropy of MNPs and examine how particle size and morphology influence their magnetization and coercivity (H_c), and the transition from ferromagnetic

to superparamagnetic behavior.

2.1 Typical magnetic nanoparticles

2.1.1 Elemental metals

Elemental metals, represented by Fe, Co, and Ni nanoparticles, constitute a fundamental category of MNPs and provide an important basis for understanding other magnetic metal-based nanomaterials. Owing to their strong ferromagnetic responses and relatively high magnetization, these metallic nanoparticles are attractive for magnetic manipulation, MRI-related contrast enhancement, and magnetic-heating applications [37, 38]. However, their magnetic performance is not only dictated by elemental composition, but also strongly affected by magnetocrystalline anisotropy, shape anisotropy, surface anisotropy, particle size, morphology, and interparticle coupling [39, 40]. Ferromagnetic nanoparticles have high surface energy and strong magnetic dipole interactions, are easily aggregated, and therefore need to be surface-stabilized. Therefore, in order to improve colloidal stability, reduce dipolar interactions and enhance biocompatibility, organic surfactants, polymers, silica, carbon, noble metals or lipid coatings are often added [41, 42]. Although elemental Fe, Co and Ni nanoparticles have the magnetic advantage of being magnetic, they still have problems with oxidation instability, potential metal-ion toxicity, aggregation and long-term biosafety; thus, direct biomedical application is inferior to that of iron oxide-based MNPs [43]. To further clarify the biomedical relevance of different magnetic compositions, their representative materials, magnetic features, major advantages, limitations, and cancer-related applications are summarized in Table 1.

2.1.2 Metal oxide magnetic nanoparticles

Metal oxide magnetic nanoparticles are a class of metallic materials with strong magnetic response (saturation magnetization [M_s], remanence [M_r], and H_c), high catalytic activity, and stable crystal structure. Among metal oxide nanoparticles, iron oxide is the most common naturally occurring material. Fe_3O_4 adopts a cubic inverse-spinel structure containing a tetrahedral part occupied by Fe^{3+} and an octahedral part composed of Fe^{2+} and Fe^{3+} (Figure 2A) [44, 45]. This unique structure endows Fe_3O_4 with excellent magnetic and physicochemical properties. Cobalt oxide exists in various polymorphs, including CoO, Co_2O_3, and Co_3O_4. Among them, Co_3O_4, the most stable cobalt oxide, is a spinel-type structure composed of Co^{2+} and Co^{3+} (Figure 2B) [46, 47]. Typically, nickel oxide appears in three forms, including NiO (Figure 2C) [48], NiO_2, and Ni_2O_3. Nickel oxide of different crystalline phases, including cubic, rhombohedral, monoclinic, and hexagonal crystals, can be obtained through special synthesis

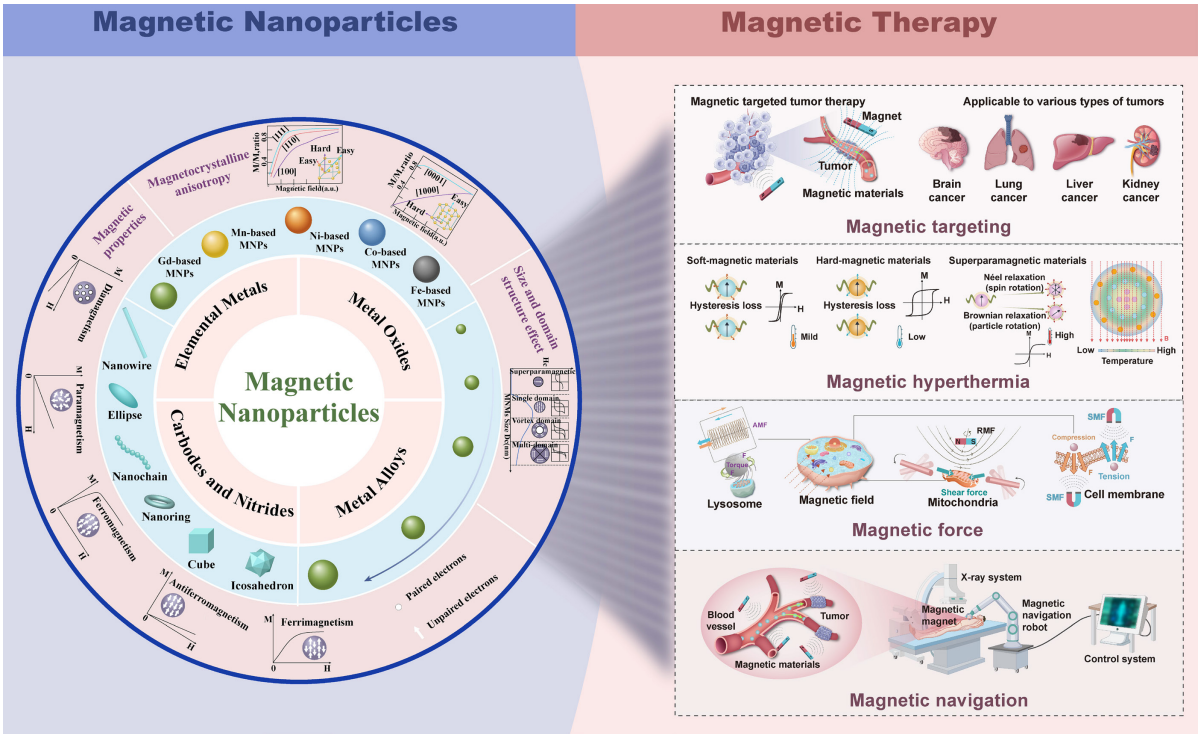

Figure 1. Magnetic materials provide field-programmable platforms for precision cancer therapy. Adjustable compositions, nanostructures and magnetic responses can achieve remote control of tumor targeting, localized hyperthermia, mechanical force generation and magnetic navigation; therefore, they are promising for spatiotemporally regulated and minimally invasive therapeutic applications.

methods or reaction conditions [49]. Song *et al*. synthesized NiO nanoflowers with narrow hysteretic loops using nickel ethylene glycol as a precursor, exhibiting typical ferromagnetic behavior (H_c: 100 Oe, M_r: 0.015 emu/g) [50]. In addition, manganese oxides exist in four forms: MnO, MnO_2, Mn_2O_3, and Mn_3O_4. MnO_2 has four crystalline structures, α, β, γ, and δ, these crystal forms can be modulated by altering reactant concentrations, temperature, as well as reaction duration [51, 52]. It is worth noting that at room temperature to 130 K, MnO obeys the Curie-Weiss law, while Mn_3O_4 has a significantly higher susceptibility than MnO, due to its large effective magnetic moment (theoretical μ_{eff}= 9.15 μ_B) [53].

2.1.3 Metal alloy magnetic nanoparticles

Metal alloy MNPs are usually composed of two magnetic monometallic nanoparticles, which have high magnetocrystalline and chemical stability. The most representative metal alloy MNPs are FePd and FePt. FePt alloys have two structural configurations: the chemically disordered face-centered cubic (fcc, A_1) phase and face-centered tetragonal (fct, $L1_0$) phase (Figure 3) [54, 55]. The Fe-Pt arrangement is layered, and Fe atoms form strong spin-orbit coupling with high magnetic moments and Pt atoms, resulting in high magnetocrystalline anisotropy (the magnetocrystalline anisotropy constant K is 10^7 J/m^3) [56-58]. Notably, the high K value enables FePt alloy, at a size < 2 nm, to maintain excellent magnetic and thermal stability, making it the best candidate material for ultra-high-density thin film magnetic recording media [59]. In addition, CoPt alloys also have a high magnetocrystalline anisotropy (4×10^6 J/m^3) and an M_s up to 800 emu/cm^3 [60, 61]. Various CoPt alloy nanoparticles can be obtained by special synthetic strategies for FePt NPs [62]. The composition, shape, and size of the fct phase are critical parameters in designing hard magnetic CoPt and FePt. Takahashi *et al*. found that FePt NPs cannot form an ordered arrangement at sizes below 4 nm [63]. For CoPt and FePt nanoparticles with a size smaller than 3 nm, even if there are ordered multiple twin morphologies, they cannot exhibit hard magnetic behavior. This phenomenon is consistent with the difficulties faced when stabilizing the $L1_0$ phase in uncoated FePt nanoparticles through heat treatment processes [64, 65].

Table 1. Comparison of representative magnetic nanoparticle compositions for cancer biomedical applications.

Magnetic composition	Representative materials	M_r	H_c	M_s	T_c	Biomedical advantages
Elemental metals	Fe, Co, Ni	Phase- and size-dependent; generally high	Tunable; soft to hard magnetic	Generally high	Generally higher than 37 °C	High magnetic moment; strong field response
Metal oxides	Fe_3O_4, γ-Fe_2O_3, $MnFe_2O_4$	Low/near-zero for SPIONs	Low or near-zero for SPIONs; higher in anisotropic ferrites	Moderate; size-dependent	Composition-dependent; higher than 37 °C	Favorable biocompatibility; easy functionalization; established MRI/ MHT application
Metal alloys	FePt, CoPt	Higher in hard-magnetic phases	Phase- and anisotropy-dependent	Moderate to high	Generally higher than 37 °C	High anisotropy; multifunctional potential
Carbides/nitrides	Fe_5C_2, Fe_3C	Low to moderate, phase-dependent	Low to moderate	Moderate to high	Phase-dependent; higher than 37 °C	Tunable magnetism; chemical stability
Rare earth-based magnets	$Nd_2Fe_{14}B$, $SmCo_5$, Sm_2Co_{17}	High	High	High	High	High H_c; stable M_r

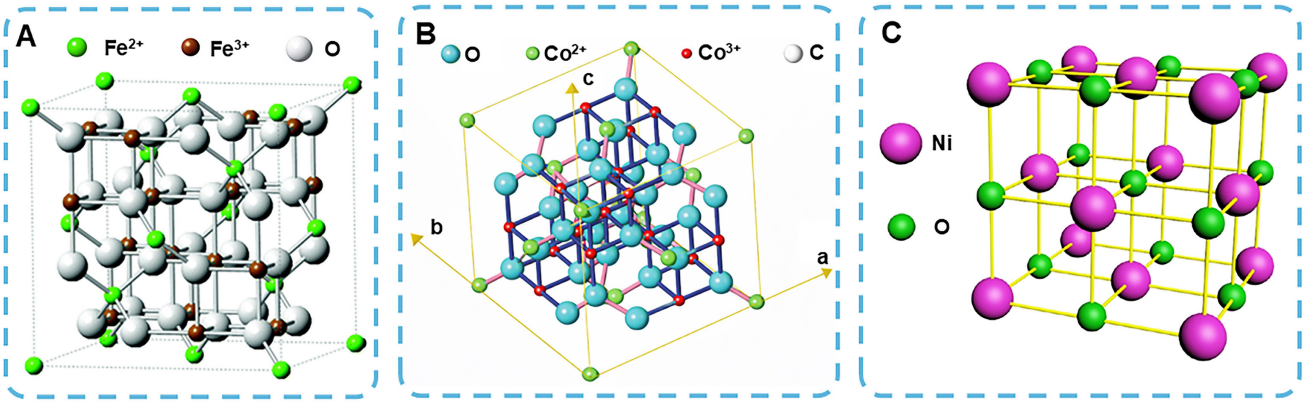

Figure 2. (A) Crystal structure of Fe_3O_4. The green, brown and gray atoms represent Fe^{2+}, Fe^{3+} and oxygen, respectively. Reproduced with permission [45]. Copyright 2011, The Royal Society of Chemistry. **(B)** Spinel structure of Co_3O_4 crystal. Reproduced with permission [47]. Copyright 2009, Springer Nature. **(C)** NiO cubic crystal structure. Reproduced with permission [48]. Copyright 2021, Science Press.

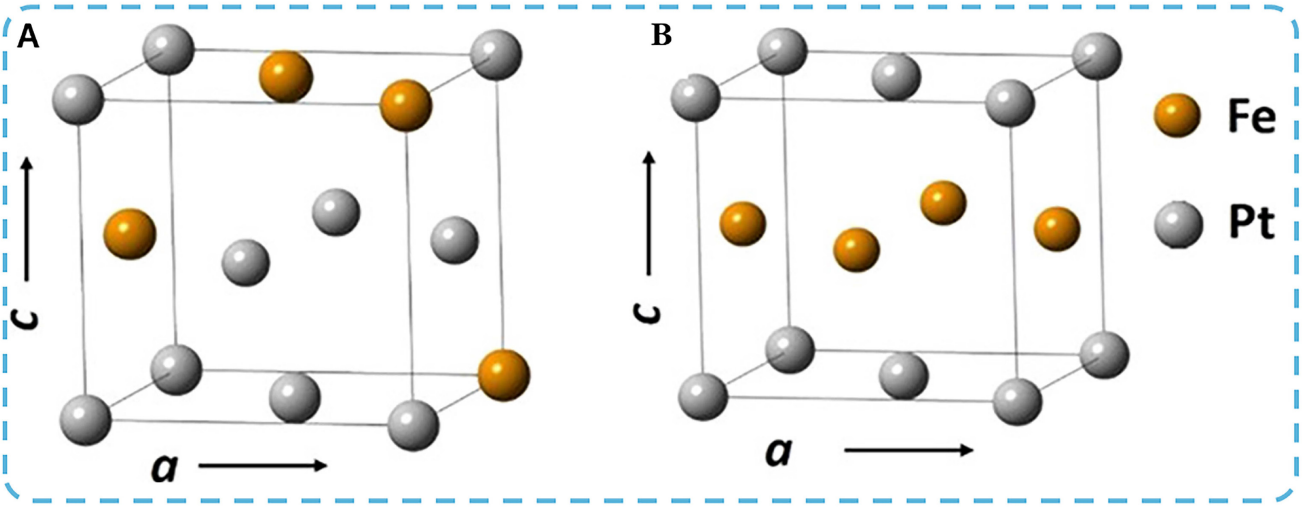

Figure 3. (A) A_1-FePt (or fcc-FePt) and **(B)** $L1_0$-FePt (or fct-FePt) structures of FePt alloys. Reproduced with permission [55]. Copyright 2023, American Chemical Society.

2.1.4 Carbide and nitride magnetic nanoparticles

The electron-rich bonds formed by C/N with magnetic metals confer carbides and nitrides with special electronic, catalytic, and magnetic properties [66-69]. Fe-C compounds contain the electronic structures and geometry of ionic and neutral Fe-C clusters, such as Fe_2C, FeC_n (n = 2-5), Fe_2C_n (n = 1-3), $Fe_nC/Fe_nC^+/Fe_nC^-$ (n = 1-6). In theory, strong Fe-C chemical bonding decreases the local magnetic moments of Fe atoms [70]. Yang *et al.* innovatively proposed the mechanism responsible for the surface stability of halogen ions on ionic nuclei and the penetration process of carbon atoms (Figure 4A), and a "seed conversion" strategy to prepare different phases of iron carbide nanoparticles, such as hexagonal and monoclinic Fe_2C (Figure 4B,C), monoclinic Fe_5C_2 NPs (Figure 4D) and orthorhombic Fe_3C (Figure 4E) [70]. All the iron carbide nanoparticles are in a near-monodisperse state, achieving an M_s up to 101.2 emu/g and a curie temperature (T_c) of 497.8 K (Figure 4F,G). Consistent with theoretical results, all nanoparticles demonstrate a lower M_s under simulation compared to bcc-Fe (Figure 4F). It is worth noting that Cl^- adsorbs on the Fe surface, preventing the adsorption of C atoms (Figure 4A); therefore, different iron carbide nanoparticles can be synthesized by adjusting the Cl^- content.

Furthermore, nitride MNPs have emerged as a research focus due to their remarkable magnetic and catalytic properties. For example, iron nitride phases FeN, Fe_2N, Fe_3N, Fe_4N, and $Fe_{16}N_2$ can undergo transitions from ferromagnetic to non-magnetic and even antiferromagnetic states, rendering them promising nanomagnetic and spintronic materials [71]. As for the carbides and nitrides of nickel, early reports have confused Ni_3C with hcp-Ni. In fact, the two show significant differences in their crystal structures. Ni_3C has a rhombohedral lattice structure, and hcp-Ni has a hexagonal close-packed structure [72]. In addition, Ni_3C is weakly magnetic or non-magnetic [73] and shows some magnetism in a disordered condition or at the nanoscale. In Ni_3C materials, the interaction between Ni 3d electrons and C 2p electrons near the Fermi level promotes forced exchange splitting, which in turn affects the magnetic properties of the nanoparticles [74]. The increase in C concentration may induce changes in the electronic structure, thus decreasing and quenching the magnetic moment at the critical value. For Ni-N bonding, the Ni sublattices in fcc-$NiN_{0.125}$ and fcc-$NiN_{0.25}$ are much more ordered than the fcc lattice, and therefore exhibit significant local magnetic moments [74].

2.1.5 Rare earth-based permanent magnets

Rare earth (RE) permanent magnets can be divided into neodymium iron boron (NdFeB) and samarium cobalt (SmCo) types. Common RE permanent magnets are represented by $Nd_2Fe_{14}B$, $SmCo_5$, and Sm_2Co_{17}. Energy product ($(BH)_{max}$) is an index to measure the strength, energy storage capacity, and reliability of permanent magnet materials. The $(BH)_{max}$ is about 56 MGOe in NdFeB magnets, and 14-28 MGOe in SmCo magnets [75]. However, the SmCo magnets have a higher T_c than the NdFeB magnets. The T_c of $SmCo_5$ is 750 °C, and that of Sm_2Co_{17} is more than 800 °C, both higher than the 400 °C of $Nd_2Fe_{14}B$ and 465 °C of ferrite [76]. Among SmCo-type permanent magnets, $SmCo_5$ has high magnetic strength and temperature stability, and a crystalline structure (Figure 5A) [77]. In the $Nd_2Fe_{14}B$ structure, RE elements (Nd) are arranged alternately

with highly magnetized Fe nets, offering high $(BH)_{max}$ and uniaxial anisotropy (Figure 5B) [77-79]. So far, NdFeB magnets, owing to their high $(BH)_{max}$ and H_c, have been integrated into various magnetic technologies for clinical treatments.

Overall, these material classes differ not only in chemical composition and crystal structure, but also in how their magnetic parameters are regulated at the nanoscale. Oxide-based MNPs usually exhibit relatively favorable biocompatibility and are often designed to display superparamagnetic or ferrimagnetic behavior, whereas alloy- and rare earth-based systems generally possess stronger magnetocrystalline anisotropy, higher H_c, or larger magnetic moments. The magnetic properties of carbide-based and nitride-based MNPs generally vary across different crystal structures. Doping with carbon or nitrogen modifies the electronic structure and local magnetic moments. However, such performance differences may stem from other factors. In fact, M_r, H_c, M_s, and T_c are all affected by crystal symmetry, spin-orbit coupling, particle size, shape, surface spin disorder, and magnetic domain structure. The above factors will determine the magnetic anisotropy and magnetic reversal process of the particles and regulate the response of the particles to an external magnetic field. Therefore, the evaluation of MNPs performance requires consideration of constituent materials, nanostructures, and surrounding particle environments. The following section discusses these key determinants, with an emphasis on magnetocrystalline anisotropy, shape anisotropy, and size effects.

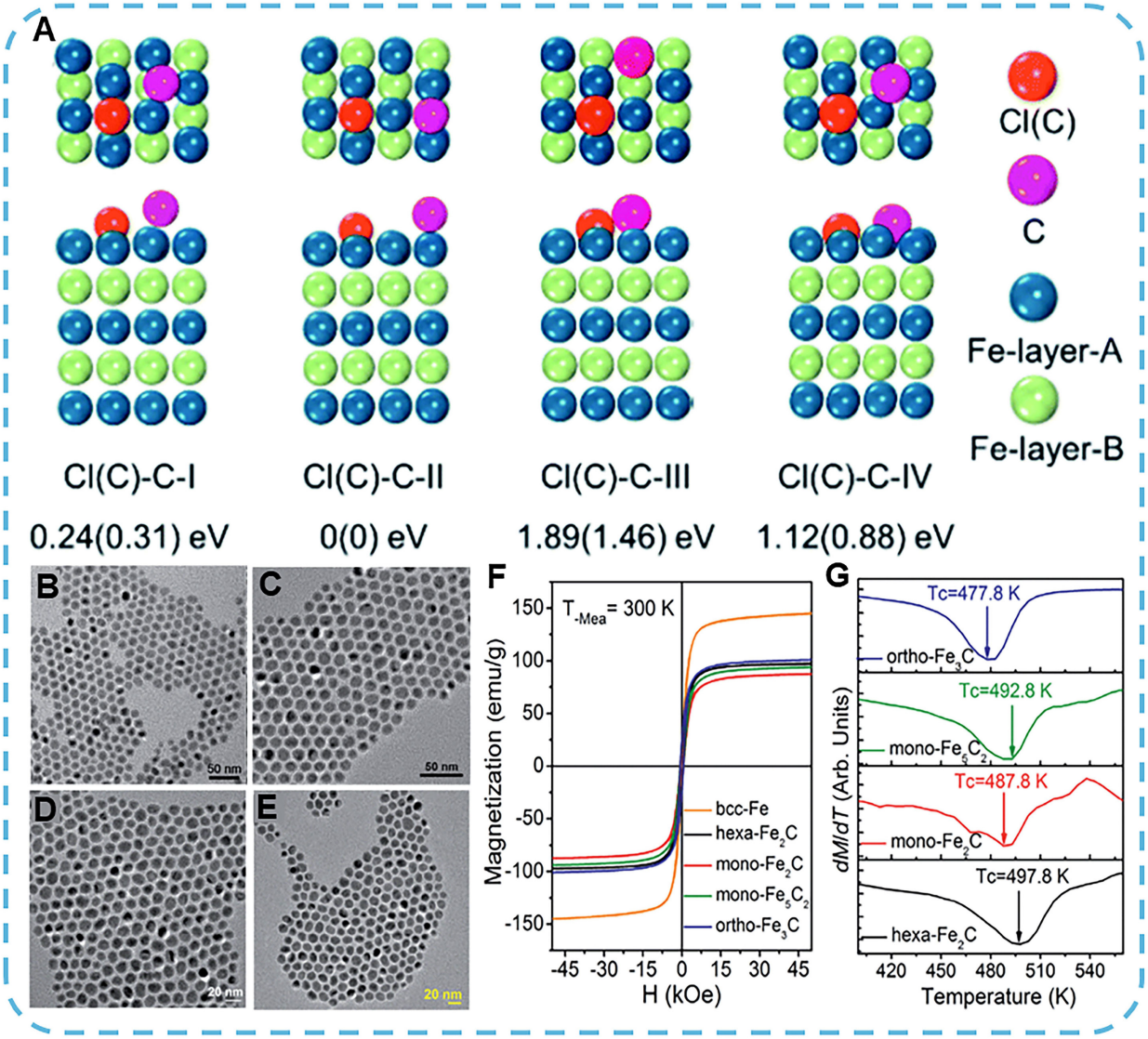

Figure 4. (A) Top and side views illustrating the effect of Cl^- adsorption on carbon atom penetration. TEM images of **(B)** hexagonal Fe_2C, **(C)** monoclinic Fe_2C, **(D)** monoclinic Fe_5C_2, and **(E)** orthorhombic Fe_3C NPs. **(F)** Hysteresis loops of iron and iron carbides at 300 K. **(G)** T_c of iron carbide (dM/dT curve). Reproduced with permission [70]. Copyright 2017, The Royal Society of Chemistry.

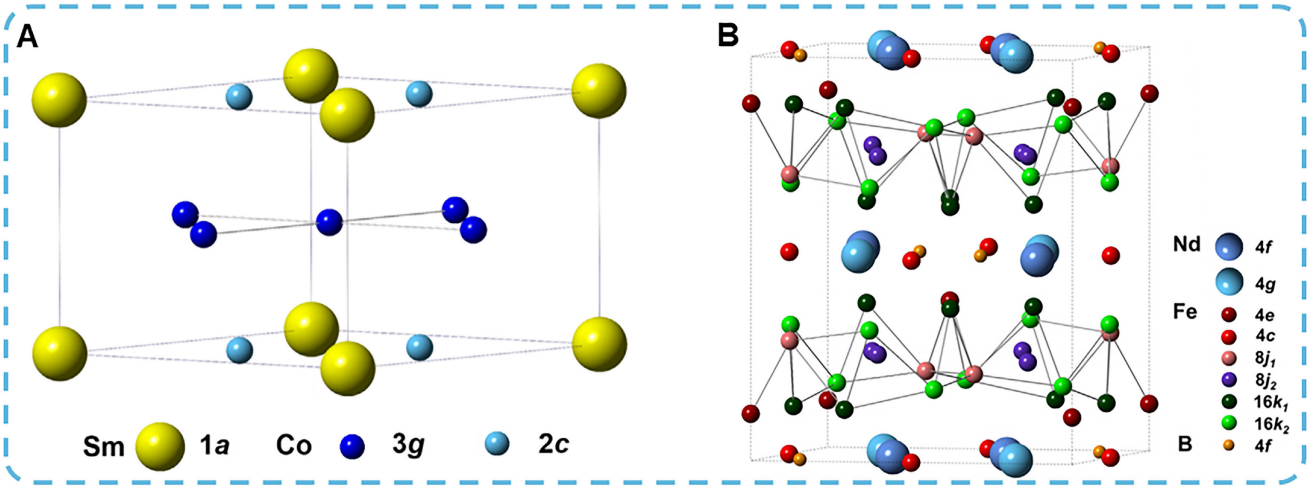

Figure 5. The crystal structure of **(A)** $SmCo_5$ and **(B)** $Nd_2Fe_{14}B$. Reproduced with permission [77]. Copyright 2017, Wiley-VCH Verlag GmbH & Co. KGaA.

2.2 Fundamental properties of magnetic nanoparticles

2.2.1 Magnetocrystalline anisotropy

Anisotropy refers to physical or chemical properties varying with direction. Crystalline ferromagnetic materials, due to the atomic moments of crystal structures, present a high magnetocrystalline anisotropy [80]. Within a crystal structure, crystal axes along which magnetization occurs readily are referred to as magnetic easy axes, whereas axes along which magnetization is difficult to achieve are termed magnetic hard axes. Generally, magnetic materials with a cubic structure possess multiple easy axes and exhibit low magnetocrystalline anisotropy, and are known as "soft magnetic materials". Conversely, magnetic materials with a hexagonal structure exhibit high magnetocrystalline anisotropy and H_c, and are termed "hard magnetic materials".

2.2.2 Shape anisotropy

Shape anisotropy originates from the geometric morphology of MNPs and strongly governs their overall magnetic response. The remanent magnetization in the non-closed direction of MNPs produces a "demagnetizing field" (H_d) within the material, which points in the direction opposite to the applied external field (Figure 6A) [55]. The strength of H_d scales linearly with the magnetization and can be expressed as: $H_d = N_d M$, where N_d is the demagnetizing factor, and M is the magnetization. In a spherical structure, the net shape anisotropy is zero, because the N_d values at the directions of the three main axes are equal. In prolate and oblate spheroids, N_d is determined by the components at the crystal axes. For prolate spheroids, an increase in the aspect ratio leads to a larger N_d at the a-axis or b-axis, and a smaller N_d at the c-axis (Figure 6B). For oblate spheroids, an increase in the aspect ratio increases N_d at the a-axis and decreases N_d along the b-axis and c-axis, resulting in a lower magnetic energy at the a-axis and a more stable magnetization (Figure 6C). Notably, the effect of shape anisotropy on magnetization is determined by the shape anisotropy energy E_{sh} as follows:

$$E_{sh} = \frac{\mu_0 M_s^2}{2}(N_a - N_c)\sin^2\theta = K_{sh}\sin^2\theta \quad (1)$$

where μ_0 represents the permeability of free space, M_s represents the saturation magnetization of the material, N_a and N_c correspond to the demagnetization factors along the a-axis and c-axis, respectively, θ represents the angle between the c-axis and the magnetization direction, K_{sh} represents the shape anisotropy constant [81, 82].

Furthermore, nanoparticle morphology influences not only the H_d distribution but also the resultant magnetic behavior. Shape anisotropy shows morphology-dependent magnetic effects at the nanoscale. The transmission electron microscopy images in Figure 6D show MNPs with multipods, spheres, wire-like, rod-like, cubic, and octahedral morphologies [83-88]. The various M_s, blocking temperatures and magnetization reversal behaviors are generally caused by differences in exposed crystal facets, surface coordination, and spin disorder. For example, multipod-like and spherical Fe_3O_4 nanoparticles exhibit lower M_s values, with considerable differences in their superparamagnetic blocking temperatures (Figure 6E). Complex faceting enhances surface spin disorder and thus reduces the net magnetization. By contrast, nanoparticles with nanowires, nanorods, nanocubes, and nanooctahedra exhibit the opposite trend (Figure 6F) [88]. Generally, they deliver higher M_s values due to more regular

structures, reduced exposed faceting, and better ordered spin arrangements. The cubic and octahedral structures generally have a relatively large M_s because of their regular faceting (Figure 6G) [87]. Therefore, particle shapes affect the direction of demagnetizing factors and change the microscopic arrangement of surface spins and magnetic domains, thereby tuning the magnetic response of MNPs.

2.2.3 Size effect

Size effect plays a certain role in determining the magnetic properties of MNPs. As material size decreases from bulk to nanoscale, quantum effects, enlarged specific surface area, and finite-size effects become prominent. Therefore, the magnetic domain structure and magnetization reversal mechanism, as well as thermal stability, have all changed considerably. Bulk magnetic materials are generally divided into multiple magnetic domains and domain walls to minimize the total magnetic energy of the system. At the nanoscale, however, when particle size falls below a critical threshold, domain walls are no longer energetically favorable. Electron spins within the particles align in parallel under ferromagnetic exchange interaction, forming a uniformly magnetized single-domain structure [30]. The critical size is termed the single-domain diameter (D_{sd}). Most magnetic materials have a size of a few nanometres for D_{sd}. Materials with a large effective anisotropy constant (K) for D_{sd} can be expanded to the micrometer scale. Single-domain MNPs are typically magnetized by the magnetic anisotropy energy (KV) and do not have multiple domains. Thus, they generally have a higher H_c and are more sensitive to external magnetic fields.

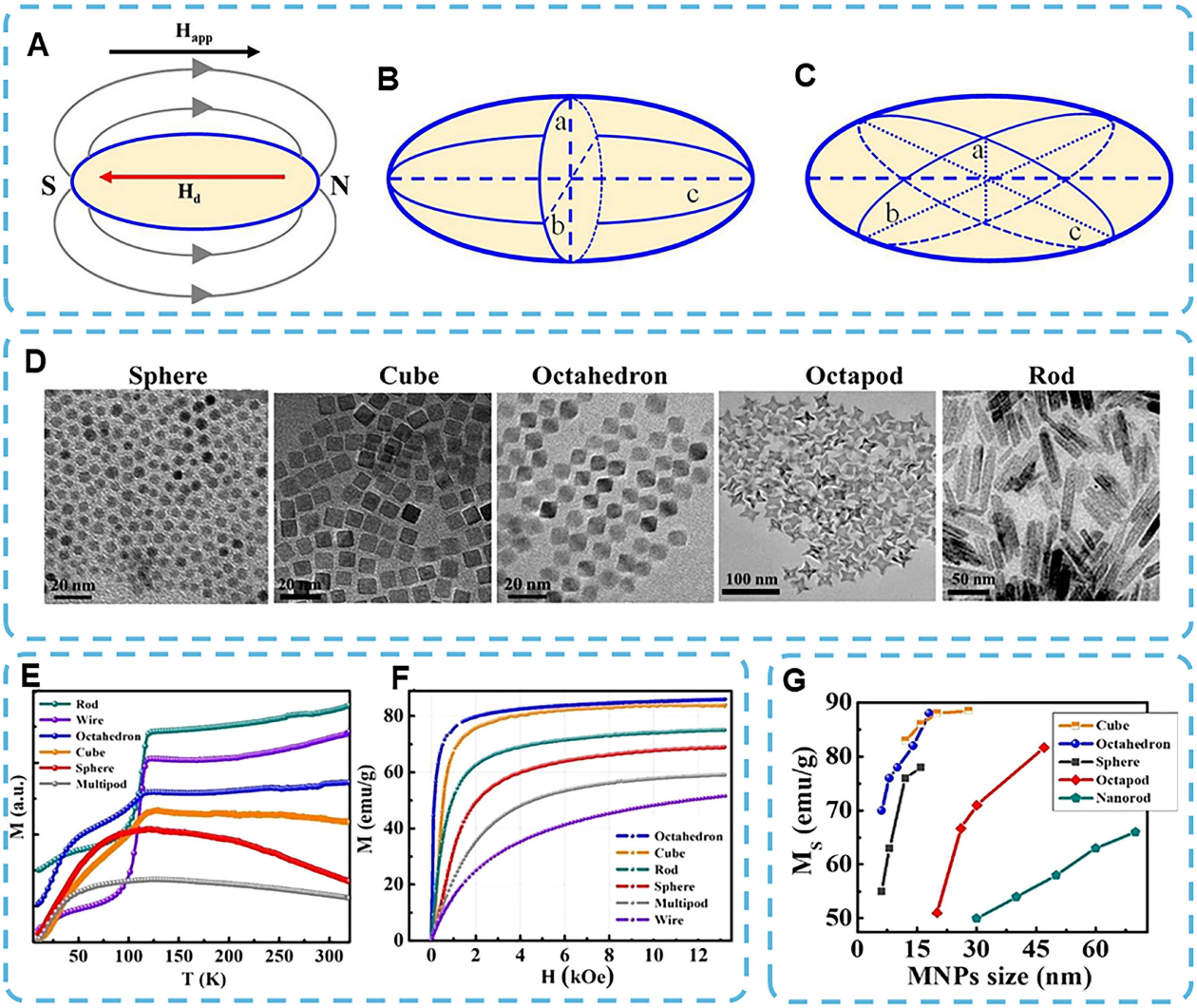

Figure 6. (A) Schematic of demagnetization field lines of a magnetized ellipsoid. **(B)** A prolate spheroid and **(C)** an oblate spheroid. Reproduced with permission [55]. Copyright 2023, American Chemical Society. **(D)** TEM images of Fe_3O_4 spheres, cubes, octahedra, octopods, and nanorods. Reproduced with permission [86]. Copyright 2015, The Royal Society of Chemistry. Reproduced with permission [83-85]. Copyright 2007, American Chemical Society, 2013, Nature Publishing Group, and 2014, American Chemical Society, respectively. **(E)** Zero-field cooling (ZFC) magnetization curves for Fe_3O_4 NPs with different shapes at an applied field of 50 Oe and **(F)** room-temperature field-dependent initial magnetization curves, respectively. Reproduced with permission [88]. Copyright, 2020, IOP Publishing. **(G)** Size-dependent M_s for Fe_3O_4 NPs of different shapes. Reproduced with permission [87]. Copyright, 2019, MDPI.

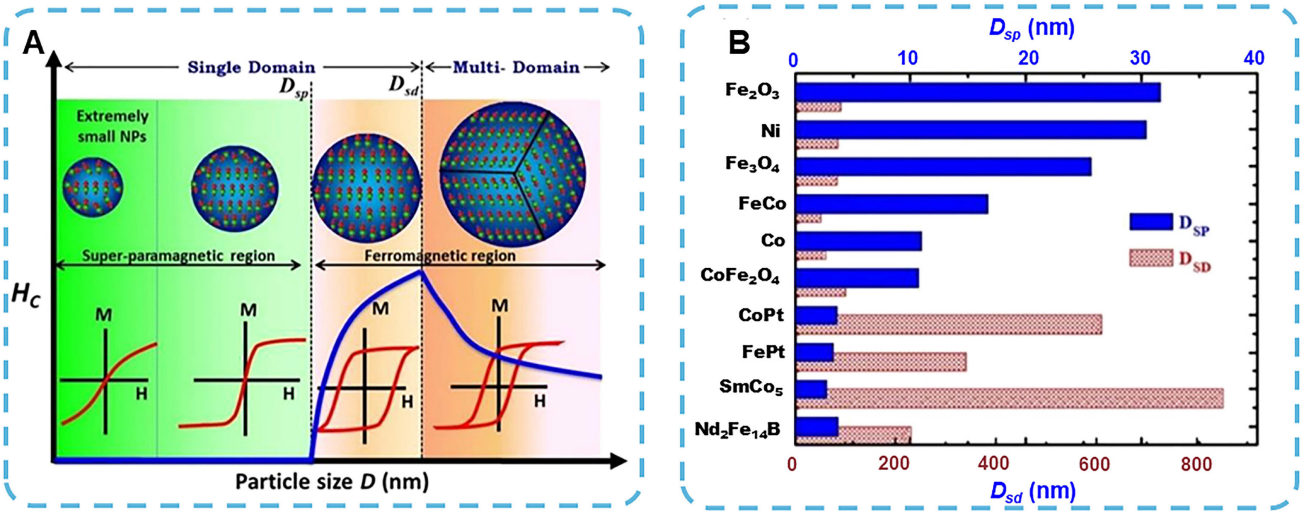

Figure 7. (A) MNP-size-dependent magnetization and H_c. The H_c of ferromagnetic materials first increases with the decrease of particle size. When the particle size is reduced to sustain a single magnetic domain, the H_c reaches the maximum and then gradually decreases. When the particle size is small enough, H_c decreases to zero, and the nanoparticles enter a superparamagnetic state (blue line in the figure). Reproduced with permission [82]. Copyright 2018, Elsevier. **(B)** D_{sd} and D_{sp} of different magnetic nanomaterials. Reproduced with permission [90]. Copyright 2013, IOP Publishing.

However, as the particle size decreases further, the reduction in particle volume (V) results in a continuous decrease in KV, and thus a gradual decline in H_c [89]. When the particle size is small enough that the thermal energy k_BT (k_B: Boltzmann constant, T: absolute temperature) exceeds the anisotropy energy, random fluctuations in the magnetic moments will occur due to thermal fluctuations. The particles thus enter a superparamagnetic state. At this point, stable M_r and H_c are no longer observed, and the corresponding critical size is generally called the superparamagnetic size (D_{sp}) (Figure 7A). Therefore, the magnetic behavior of MNPs generally changes from multi-domain to single-domain and finally to superparamagnetic as the particle size decreases. Based on the intrinsic material parameters, such as magnetocrystalline anisotropy and M_s, the corresponding critical sizes are determined, and these have extensive applications in data storage, magnetic sensing, as well as biomedical imaging and therapy. Most technical and medical applications of MNPs require a particle size of less than 20 nm, and the superparamagnetic critical size for different materials is generally in the range of 5-20 nm. Figure 7B shows the single-domain sizes, and corresponding superparamagnetic thresholds are provided for several typical magnetic materials [90, 91].

3. Magnetic Therapy

Due to its promising therapeutic effects, minimal invasiveness and broad applicability, magnetic nanoparticle-mediated therapy has gradually attracted attention in the field of oncology. Various cancer treatment modalities have been developed, including magnetic-targeting therapy, magnetic hyperthermia, magnetic mechanical therapy and magnetically actuated intelligent systems. These strategies generally leverage the controllable accumulation, heat generation, mechanical actuation and navigation of MNPs to improve the precision and efficacy of tumor therapy. Table 2 shows the latest research achievements in various MNP-mediated therapeutic strategies. Recent developments in MNP-based cancer therapy are introduced in this section, including magnetic targeting, magnetic hyperthermia, magnetic mechanical therapy and magnetic field-guided navigation systems.

3.1 Magnetic targeting and magnetically responsive therapeutic systems

Nanomedicine targets directly affect the effects of anti-cancer drugs. Nanomedicines aim to target the tumor by adding surface ligands for active targeting or by employing the enhanced permeability and retention (EPR) effect for passive targeting [110]. Dense extracellular matrix (ECM) and a high interstitial fluid pressure in the tumor tissue are also hindrances to nanoparticle distribution. Thus, the delivery efficiency is generally less than 10% of the administered dose, and the median is about 0.7% [111]. Therefore, it is not effective. Enhancing retention within the tumor and deep-tissue penetration of nanomedicine are still problems. Simple operation and economic feasibility have been used to apply magnetic targeting in nanomedicine delivery.

MNPs are intravenously administered magnetic functional carriers that enter the systemic circulation through the peripheral veins and can be guided to accumulate at the target lesion site by an external

directional magnetic field. In the 1960s, Freeman and others first proposed the idea of magnetic targeting to group circulating magnetic particles in blood vessels by applying a magnetic field [112]. A favorable result was achieved by Zimmerman and others in 1976; they were able to load red blood cells with magnetic materials and the chemotherapy drug methotrexate to provide a foundation for clinical application [113]. Lubbe and others then used MNPs to deliver epirubicin-loaded ferrofluids in patients with advanced tumors. The formulation was well-tolerated, and among the 14 trial subjects, favorable tumor localization based on the magnetic formulation was achieved in 6 patients (42.86%). Thus, it was determined that magnetically guided drug delivery has potential for clinical translation [114, 115]. Following the above preclinical studies, magnetic catheters have been developed to enhance steering accuracy [116], and magnetically guided nanoparticles that induce thrombosis in intracranial aneurysms have also been prepared [117, 118].

Table 2. A summary of magnetic therapy in different application modes.

System	Magnetic material	Magnetic type	Magnetic field mode	Therapeutic modality	Disease model	Therapeutic mechanism	Ref.
PAMNs	γ-Fe_2O_3	Superpara-magnetic	Static gradient field	Magnetic targeting	Early ischemic stroke	Static-field-guided magnetic targeting with localized NO generation	[9]
MSP-6h/-24h/-72h.	Fe_3O_4	Superpara-magnetic	RMF	Magnetic navigation	Intestinal fluid model	Low-field magnetic navigation with coating-tunable on-site cargo release	[11]
NV-IONP-Lapa	Fe_3O_4	Superpara-magnetic	Static gradient field	Magnetic targeting	Ovarian cancer	Magnetic targeting-enhanced cellular uptake for ROS-amplified chemodynamic therapy	[92]
FeGa@P(VDF-TrFE)	FeGa	Ferromagnetic	RMF and AMF	Magnetic navigation and magnetoelectric drug release	Cervical cancer	Single-field magnetic steering with magnetoelectrically triggered on-demand drug release	[93]
PLGA (Fe/PLGA)	Fe	Ferromagnetic	AMF	Magnetothermal	Breast cancer	*In situ* phase transformation enables localized retention for efficient magnetic hyperthermia	[94]
Ir@$MnFe_2O_4$ NPs	$MnFe_2O_4$	Superparamagnetic	AMF	Magnetothermal	Cervical cancer	AMF-triggered mitochondrial magnetothermal heating that enhances chemodynamic therapy	[95]
MCNPs	Zn-doped iron oxide	Superparamagnetic	AMF	Magnetothermal	Breast and malignant brain tumor	Magnetically facilitated intracellular delivery coupled with localized hyperthermia	[96]
$ZnCoFe_2O_4$@$ZnMnFe_2O_4$-RGD-TPP	$ZnCoFe_2O_4$@$ZnMnFe_2O_4$	Superparamagnetic	AMF	Magnetothermal	Hepatocellular carcinoma	Mitochondria-targeted magnetothermal ICD with macrophage activation	[97]
FVIOs	Fe_3O_4	Ferrimagnetic vortex domain	AMF	Magnetothermal	Breast cancer	High-SAR mild magnetic hyperthermia inducing ICD and potentiating PD-L1 blockade	[98]
TPP-MNPs	Zn-doped iron oxide	Ferrimagnetic	RMF	Magnetic force	Glioblastoma	RMF-induced nanospinning for mitochondria-localized mechanical damage	[99]
SMNPs	Fe_3O_4	Superparamagnetic	Low-frequency alternating current field	Magnetic force	Breast cancer	Low-frequency magnetomechanical cytoskeletal disruption with cancer-cell selectivity	[100]
SPIONs	SPIONs	Superparamagnetic	PMF	Magnetic force	Liver cancer	Pulsed-field-induced LMP and apoptosis	[101]
MNPs	Fe_3O_4	Ferromagnetic	Low-frequency RMF	Magnetic force	Glioblastoma	Frequency- and surface-dependent magnetomechanical control of cell-death pathways	[102]
RGD-MNMs	Zn-doped iron oxide	Ferrimagnetic	RMF	Magnetic force	Glioblastoma	Adaptive RMF-programmed nanomotor swarming for lysosome-mediated apoptosis	[103]
IONs@Cys@PEI@RGD	Zn-doped iron oxide	Ferrimagnetic	RMF and AMF	Magnetic force and magnetothermal	Glioblastoma	Magnetically programmed force–heat co-induction for ROS-mediated cell death	[104]
LAMP1-SPION	SPIONs	Superparamagnetic	Low-frequency DMF	Magnetic force	Insulinoma and Pancreatic beta	Low-frequency rotational magnetomechanical disruption of lysosomes to induce apoptosis	[105]

System	Magnetic material	Magnetic type	Magnetic field mode	Therapeutic modality	Disease model	Therapeutic mechanism	Ref.
HAPF	Ferumoxytol-based iron oxide	Superparamagnetic	Low-frequency AMF	Magnetic force	Hepatocellular carcinoma	Magneto-activated NK-cell cytotoxicity with MRI cell tracking	[106]
BMHR	Fe_3O_4	Superparamagnetic	RMF and AMF	Magnetic navigation	*In vitro* targeted delivery model	Field-programmed multimodal locomotion for obstacle-crossing targeted cargo delivery	[107]
BMMs	Fe_3O_4	Superparamagnetic	Rotating or precessing magnetic fields	Magnetic navigation	Cervical cancer	Magnetically reconfigurable multimer assembly with high-maneuverability locomotion	[108]
(Pd@Au)/Fe_3O_4@Sp-DOX	Fe_3O_4	Ferrimagnetic	RMF	Magnetic navigation	Renal cancer	Rotating-field-guided high-speed propulsion for targeted cargo delivery	[109]

In addition to the materials of MNP-based systems, the therapeutic efficacy can also be modulated by an external magnetic actuation platform. Permanent magnets can produce a strong static magnetic field (SMF) without an external power supply or Joule heating, and are suitable for stationary targeting and local retention at the surface or intraoperative site [119]. However, the magnetic fields cannot be changed dynamically. Mechanical relocation is usually required, the field strength declines rapidly with distance, and thus targeting deep-seated tumors remains a problem [120]. Electromagnetic systems can flexibly adjust the strength, direction, polarity and gradient of the field to change magnetic force and torque dynamically and coordinately [121]. They have the disadvantages of high energy consumption, Joule heating that requires active cooling, and relatively complex and expensive equipment [122]. The platform needs to be able to adjust the tumor depth and field of view, support image compatibility, and meet the requirements of clinical application.

Magnetic actuation platforms share the same basic goal: to create a strong, spatially varying magnetic field and combine it with suitable magnetization characteristics of MNPs for high-efficiency targeting. Although larger MNPs are more magnetic, their larger volume can lead to ferromagnetism and, thus, attract other particles in a magnet [121]. Such particles are quickly eliminated by the mononuclear phagocyte system (MPS), have a very short circulation half-life, and may cause thrombosis. Cobalt doping can enhance the M_s, but the resulting cytotoxicity is not suitable for use in biomedicine. A too-steep magnetic field gradient is also detrimental to the accuracy of targeting and biodistribution specificity. Although there are some defects, magnetic fields can pass through living tissues freely; thus, magnetic targeting remains a feasible method to cross the biological barrier for drug delivery. Recently, some researchers have also studied its anti-cancer and neuroprotective effects. Wang *et al*. constructed NV-IONP-Lapa by encapsulating β-lapachone (Lapa) and iron oxide nanoparticles (IONPs) within extracellular vesicle-mimicking carriers. Under the direction of an external magnetic field, the intracellular uptake efficiency of NV-IONP-Lapa is enhanced, thereby improving cellular invasion and tumor selectivity (Figure 8A). After cellular uptake, Lapa is modified by NADPH quinone oxidoreductase 1 (NQO1) to generate H_2O_2 and reduce intracellular glutathione (GSH); thus, it exacerbates oxidative stress. Meanwhile, iron ions released from IONPs in the acidic tumor microenvironment (TME) trigger tumor cell apoptosis through the Fenton reaction. T_2-weighted MRI shows a dose-dependent signal change in human ovarian cancer cells after treatment with NVIONP-LAPA, and thus can be effectively MR-imaged. *In vivo*, magnetic guidance enhances the accumulation of tumor-specific tissue by about 10-fold and reduces off-target deposition in the liver and spleen. Noteworthy is that magnetically guided NV-IONP-Lapa has achieved near-complete tumor ablation within 21 days and is now being explored for image-guided therapy [92].

Magnetic-target drug delivery has shown some promise in clinical trials for cancer treatment, but wide-scale application has not been achieved and is still uncertain [123]. The other is that, due to poor contrast at the site of a deep-seated tumor, magnetic targeting is less effective. The distance between circulating MNPs and target lesions, as well as the spatial distribution of magnetic fields, are significant problems. Most of the traditional preparation methods for MNPs use only one external magnet for concentration, and the efficiency drops substantially with an increase in the distance from the magnet. As the distance between the magnet and the target tissue increases, both the magnetic field strength and gradient decay exponentially (Figure 8B); thus, there is a limited penetration depth and MNPs are less effectively accumulated at deeper sites. Relevant studies indicate that effective magnetic targeting can only be achieved when the tumor is approximately 5 mm from the magnet surface [123, 124]. This depth-dependent limitation indicates that conventional

single-magnet targeting is more applicable to superficial tumors or locally accessible lesions, whereas well-engineered magnetic field configurations are required for deeper targets. To overcome these drawbacks, the geometry and placement of magnetic field sources must be optimized with respect to target tissues. It is necessary to account for tissue architecture and other local physiological barriers when determining the magnetic force required for effective nanoparticle guidance in drug delivery system (DDS).

Recently, dual-magnet systems have received much attention for high-efficiency magnetic targeting. Tay *et al*. used a north-north (N-N) magnet configuration to generate a central field-free point (FFP), which has been applied in magnetic particle imaging systems since then (Figure 8C) [125]. FFP is a place where MNPs switch from a magnetic saturation state to a demagnetized state and emit MPI signals [126]. Liu and others have also employed a south-south magnet arrangement to create a narrow zero-field region in a strong, uniform magnetic field gradient (Figure 8D) [127]. Another effective design is the north-south type, and it has a relatively uniform magnetic field gradient at its center (Figure 8E) [128]. These configurations enable MNP aggregation *via* intrinsic magnetic interactions; the particles specifically bind to death receptor 4 (DR4) on colon cancer cells and trigger apoptosis through a ligand-like signaling mechanism (Figure 8F).

A key limitation of a single permanent magnet is that its produced magnetic field has a relatively restricted effective penetration range and low field gradient in biological tissues, which inevitably leads to non-uniform magnetophoresis of MNPs at greater tissue depths. At the same time, a dual-magnet structure establishes an extended magnetic-field gradient in the neighborhood of both magnets. Spatial symmetry reduces fluctuations in magnetic force and maintains a near-constant speed for MNPs in the S-S system. The dual-magnet system can increase the concentration of MNPs by about five times over the general EPR effect in solid tumors and improve intratumoral distribution threefold [127]. The dual-magnet arrangement can generate a stronger magnetic driving force for the desired migration and tissue penetration of MNPs. However, the above advantage may not be fully realized *in vivo, as* predicted by the static-field model. Previous studies have shown that the magnet configuration, magnetic field strength, and the distance between the magnet and the tumor all affect the capture efficiency of magnetic carriers, and this problem becomes more prominent in deep-tissue delivery [129]. In terms of control by magnetic field,

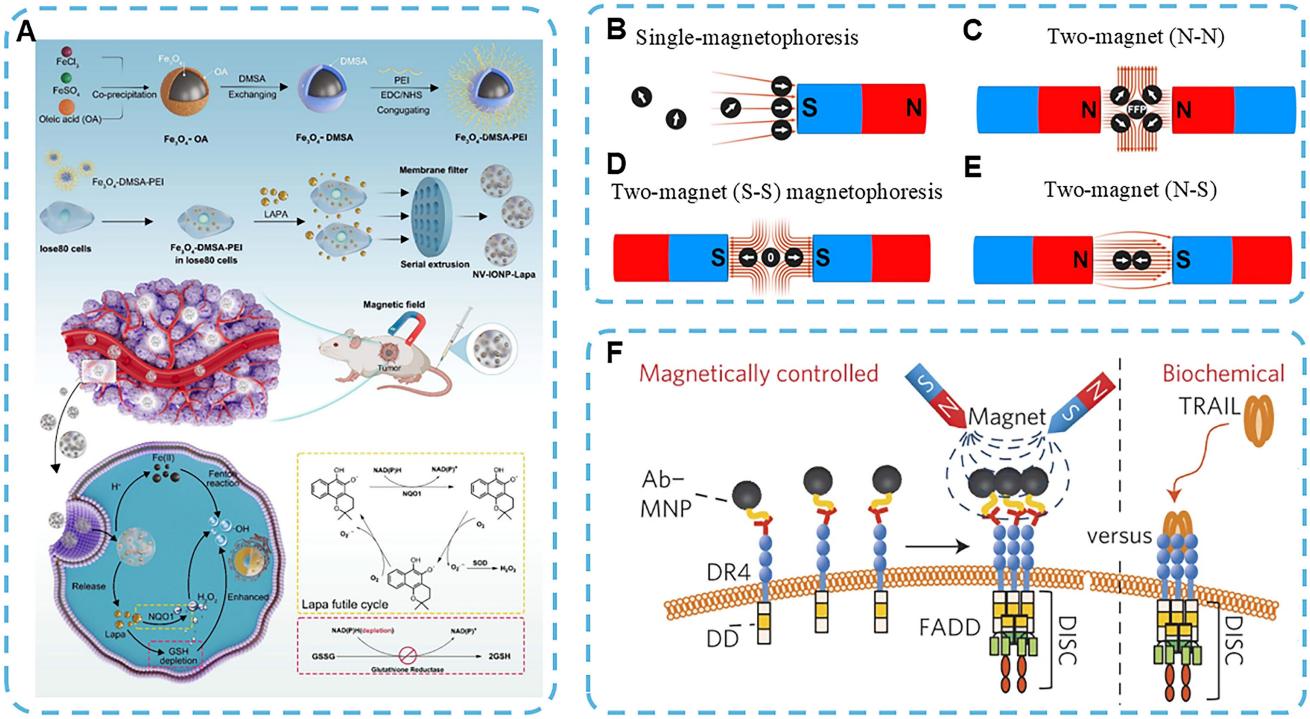

Figure 8. (A) Schematic illustration of the synthesis of engineered NV-IONP-Lapa nanoparticles designed for enhanced targeted CDT and their therapeutic mechanism against ovarian cancer. Reproduced with permission [92]. Copyright 2024, American Chemical Society. **(B)** Diagram of a conventional magnetic targeting system based on a single-magnet configuration. **(C)** Schematic representation of a dual-magnet configuration with oppositely aligned N-N poles. **(D)** Dual-magnet configuration with S-S poles arranged in opposition. **(E)** Dual-magnet configuration with N-S pole orientation. Reproduced with permission [247]. Copyright 2020, American Chemical Society. **(F)** Mechanism of magnetic switch-induced apoptotic signaling, mimicking the biochemical action of TRAIL *via* DR4 receptor activation. Reproduced with permission [128]. Copyright 2012, Springer Nature.

the formation of an FFP or a zero-field region is relatively sensitive to small displacements in space of the external magnetic field outside the target position. Studies on MPI and magnetic actuation have also demonstrated that precise localization of the FFP is required for stable particle manipulation [130]. Nevertheless, under real physiological conditions, target regions are not static. Respiratory motion, cardiac pulsation, blood flow, and gastrointestinal peristalsis all induce local tissue displacement, resulting in misalignment between the pre-defined zero-field zone and the actual lesion site. Furthermore, aberrant tumor vasculature, dense ECM, and elevated interstitial fluid pressure can further impede the intratumoral distribution and deep penetration of MNPs [131]. Accordingly, future magnetic navigation systems may need to integrate real-time imaging, motion correction at target sites, and closed-loop feedback control to enhance spatial matching between the magnetic field region and dynamically moving target tissues.

Beyond the aforementioned motion-control errors, clinical translation is also constrained by the increased source-to-target distance encountered in human tumors. Even optimized external magnetic configurations may fail to overcome the rapid attenuation of magnetic field strength with increasing tissue depth. External magnetic targeting is still a relatively simple and practical method for superficial tumors and lesions that are suitable for local therapy. At the same time, for high-precision MNP delivery of deep-seated tumors, one may need to reduce the effective distance between the magnetic source and the target tissue or generate more concentrated, programmable field gradients. Potential strategies include implantable or locally positioned magnetic components, catheter/guidewire-assisted interventional magnetic navigation, gradient-coil-based electromagnetic systems, and MRI-guided magnetic targeting [132-134]. The above methods may improve field focusing and realize real-time monitoring of MNP biodistribution; however, nanoparticle design, magnetic field geometry, delivery route, imaging guidance and clinical workflow all require concurrent optimization.

Although magnetic targeting increases the local concentration of MNP carriers at the lesion sites, subsequent drug release remains largely passive. To address this, magnetically responsive intelligent delivery systems have been developed, in which magnetic fields serve as both guidance tools and remote triggers for therapeutic action. Such systems can control the therapeutic activation process after the carrier localization, thereby improving treatment accuracy and reducing off-target exposure. For instance, Chen *et al*. prepared FeGa@P(VDF-TrFE) core-shell magnetoelectric nanowires capable of magnetically controlling drug release under both rotating and AMF (Figure 9A) [93]. Under magnetic stimulation, PFM phase imaging shows that some dark areas are brightening (yellow arrow), indicating that some ferroelectric domains have reversed their polarization due to the applied magnetic field (Figure 9B, D). Simultaneously, changes in piezoresponse amplitude are observed. The domains with low initial amplitudes had high amplitudes (dashed square), and the domains with high amplitudes showed the reverse trend (dashed circle) (Figure 9C, E). The above phenomena are due to magnetostriction-induced deformation of the FeGa core, which transmits mechanical strain to the piezoelectric P(VDF-TrFE) shell and alters its surface polarization.

Besides controlled drug release, the nanowires can also be magnetically moved programmatically. Under low-amplitude RMF, they show tumbling and surface-walking behavior (Figure 9F-I), and conical magnetic fields induce three-dimensional swimming (Figure 9J-M); therefore, precise navigation and accurate tumor targeting are expected. Polydopamine (PDA)-surface coating can be used to load drugs. Exposure to an AMF induces a transient modification of surface polarization *via* magnetoelectric coupling, disrupting non-covalent bonds between paclitaxel (PTX) and PDA, and thereby releasing the drug (Figure 9N). Based on the above *in vitro* experiments, the *via*bility of cancer cells after being treated with drug-loaded nanowires in an AMF was approximately 60%. Magnetic hyperthermia and passive drug diffusion yield minimal cytotoxicity; therefore, drug release is caused by the magnetoelectric effect. Exposure to a SMF does not induce cell death, suggesting that surface charge compensation likely stabilizes the polarized state and inhibits PTX release. These properties can be exploited to generate a stable, continuously RMF during *in vivo* nanoparticle administration, which prevents premature drug release and mitigates off-target effects in healthy tissues.

3.2 Magnetic Hyperthermia

Cancer therapies powered by external energy sources offer promising benefits for improving therapeutic outcomes and currently represent one of the most actively investigated research directions in the oncology field. Representative modalities include thermotherapy [135], photothermal therapy [136], photodynamic therapy [137], electrodynamic therapy [138], X-ray therapy [139], and microwave dynamic/thermal therapy [140]. In 1957, Gilchrist *et al*. first proposed magnetic hyperthermia therapy (MHT).

At present, MHT generally involves the administration of magnetic iron oxide nanoparticles (MIONPs), followed by exposure to an AMF to produce localized heating and induce tumor ablation [141, 142]. Although normal tissues exhibit greater heat tolerance than tumor tissues, a major challenge for the clinical translation of MHT is achieving spatially confined and uniform heating restricted to tumors while preserving adjacent healthy tissues. Upon exposure to an AMF, MNPs produce heat *via* hysteresis loss, and the efficiency of this process is highly sensitive to particle size. (Figure 10A,B). To realize intracellular localized heating and reduce off-target damage, MNP-mediated MHT has two main advantages: deep tissue penetration and magnetically guided selective ablation of malignant cells with negligible damage to surrounding normal tissues. Under AMF exposure, the two primary relaxation mechanisms responsible for heat dissipation in MNPs are Brownian relaxation and Néel relaxation, characterized by their respective relaxation time constants τ_B and τ_N [143-145].

$$\tau_B = \frac{3\eta V_H}{k_B T} \quad (2)$$

$$\tau_N = \tau_0 \exp\left[\frac{K_{eff} V}{k_B T}\right] \quad (3)$$

Brownian relaxation is related to the viscosity (η) of the dispersive medium and the hydrodynamic volume (V_H) of MNPs, where k_B is the Boltzmann constant and T is the absolute temperature. Néel relaxation is determined by the product of magnetic anisotropy energy ($K_{eff}V$) and particle volume (V). Under an AMF, internal Néel fluctuations of magnetic moments coupled with external Brownian motion together cause energy dissipation in single-domain MNPs and generate heat (Figure 10B) [143]. The heating performance of MNPs is commonly quantified by the specific loss power or specific absorption rate (SAR), calculated as follows [146]:

$$SAR = \frac{C\,m}{m_{mag}}\left(\frac{dT}{dt}\right) \quad (4)$$

C represents the specific heat capacity of the colloidal dispersion ($J \cdot g^{-1} \cdot K^{-1}$); m represents the total mass of the colloid (g); m_{mag} represents the mass of the magnetic material used for normalization (g); and dT/dt represents the initial slope of the temperature-time curve ($K \cdot s^{-1}$). For iron-based MNPs, SAR may also be normalized to the iron mass, depending on the reporting convention. SAR is related to the inherent magnetic properties of MNPs and the strength and frequency of the applied AMF.

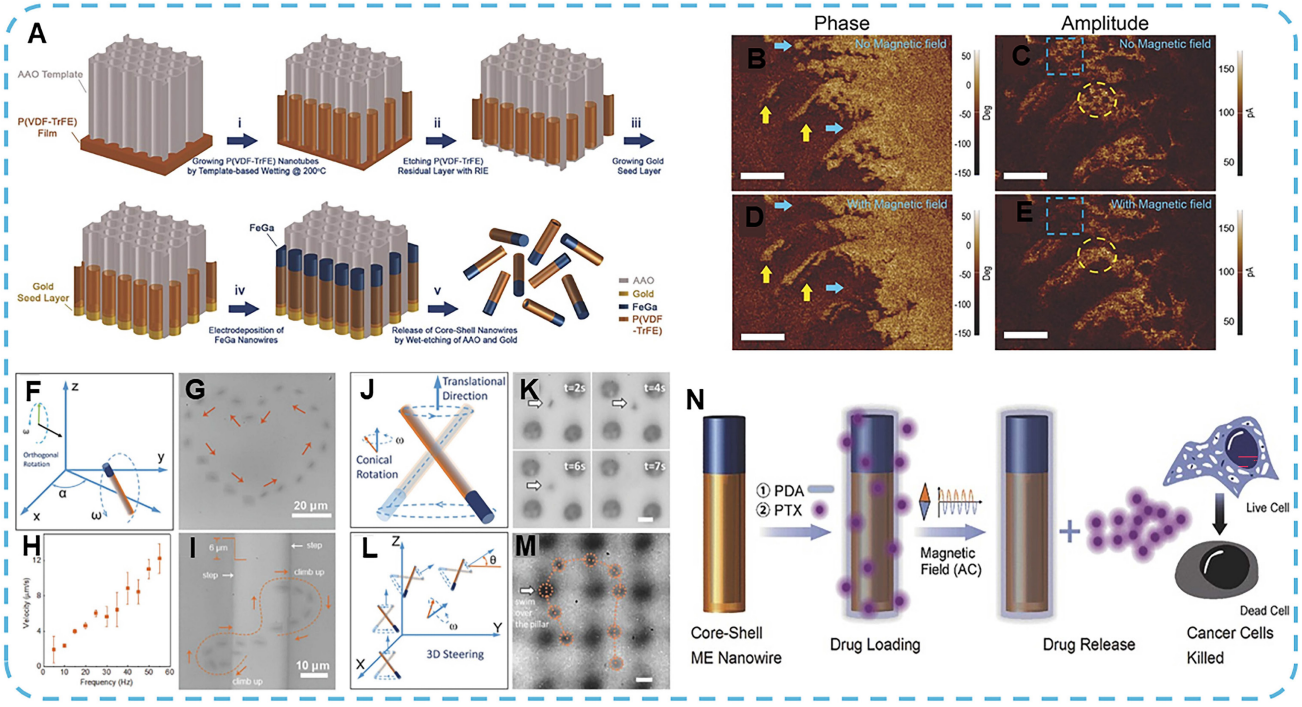

Figure 9. (A) Schematic illustration of the synthesis of FeGa@P(VDF-TrFE) core–shell nanowires exhibiting magnetic responsiveness. **(B,D)** PFM phase images of FeGa@P(VDF-TrFE) nanowires without **(B)** and with **(D)** magnetic field exposure. **(C,E)** Corresponding PFM amplitude images without **(C)** and with **(E)** magnetic field. Scale bars in (**B–E**) represent 200 nm. **(F)** Schematic showing the nanowire rotating perpendicular to the x–y plane. **(G)** Directed movement of the nanowire along a predetermined path. **(H)** Graph showing the average translational velocity of the nanowire as a function of magnetic field frequency. **(I)** Trajectories of nanowires migrating along vertical surfaces. **(J)** Schematic of nanowire actuation in a conically rotating magnetic field. **(K)** Nanowire displacement away from the substrate under conical field manipulation. **(L)** Controlled modulation of motion direction by adjusting the pitch angle (ϑ). **(M)** Three-dimensional U-shaped swimming trajectory of nanowires under magnetic actuation. Scale bars in **(K)** and **(M)** represent 5 μm. **(N)** Schematic illustration of magnetically triggered drug release from nanowires under an alternating magnetic field. Reproduced with permission [93]. Copyright 2017, Wiley-VCH.

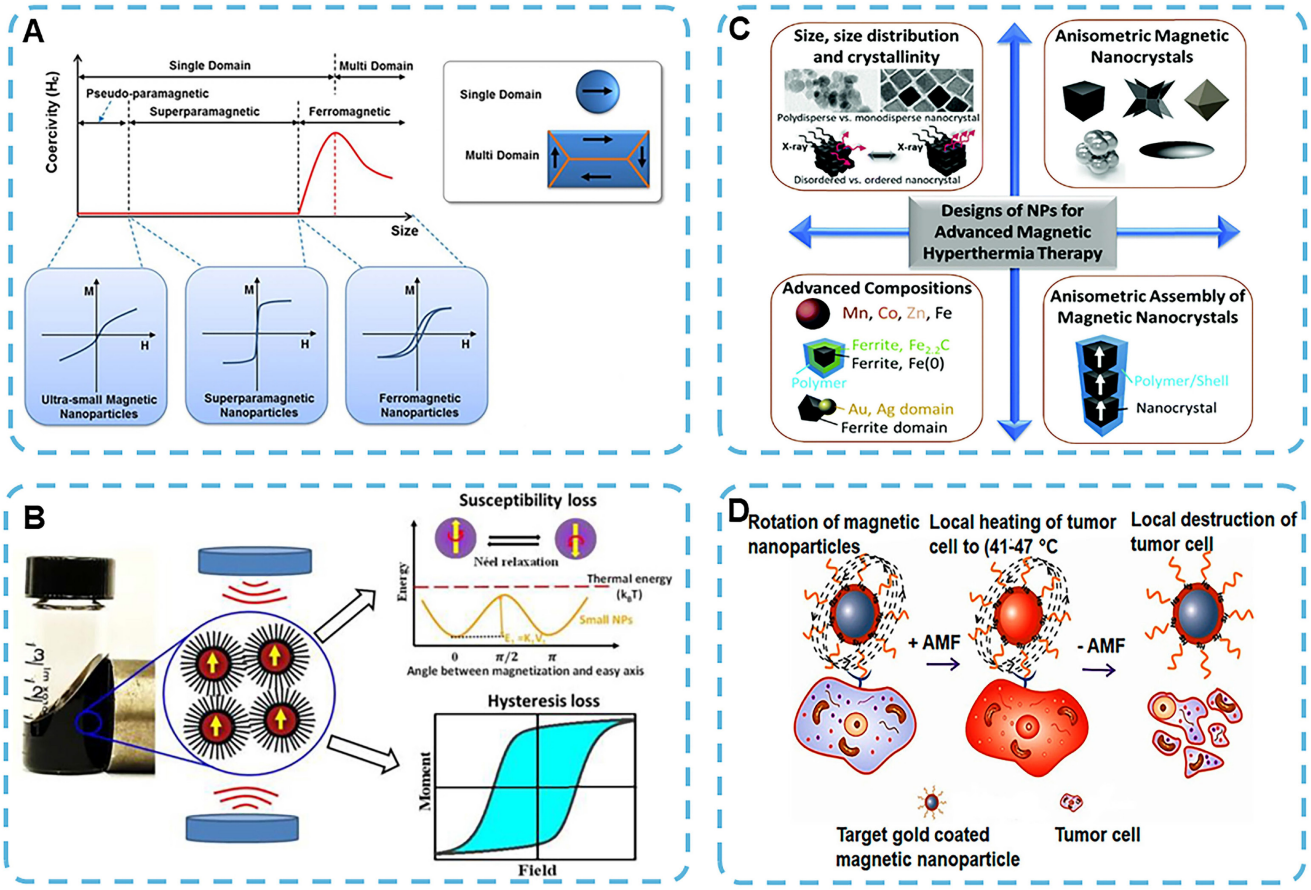

Figure 10. (A) Hysteresis loops of ultrasmall magnetic nanoparticles, superparamagnetic nanoparticles, and ferromagnetic nanoparticles, illustrating the effect of particle size on H_c. Reproduced with permission [162]. Copyright 2020, Ivyspring International. **(B)** Schematic illustration of magnetic heating mechanisms in magnetic nanoparticles under an alternating magnetic field, including susceptibility loss and hysteresis loss. Reproduced with permission [55]. Copyright 2023, American Chemical Society. **(C)** Design strategies for magnetic nanoparticles (MNPs) tailored for MHT. Reproduced with permission [2]. Copyright 2021, The Royal Society of Chemistry. **(D)** Localized heating effect of MNPs under an AMF, maintaining cancer cell temperature within the therapeutic range of 41–47 °C. Reproduced with permission [248]. Copyright 2017, MDPI.

For biosafety considerations, AMF parameters are limited by the safety threshold $H \times f < 5 \times 10^9$ $A \cdot m^{-1} \cdot s^{-1}$ [147]. Accordingly, research efforts have focused on optimizing magnetic material selection and engineering structural parameters, including core size, crystal structure, morphology, and surface coating, to boost SAR values (Figure 10C). These modifications influence key magnetic characteristics, including magnetocrystalline anisotropy (k), M_s, magnetic susceptibility, and relaxation dynamics. SAR is strongly correlated with M_s and is also modulated by particle size, which displays a non-linear relationship with SAR due to surface spin disorder and k-dependent magnetic anisotropy effects [148-150]. For example, Majeed *et al*. developed silica-coated IONPs, demonstrating that the silica shell enhances Brownian motion and consequently increases SAR compared to uncoated nanoparticles [151]. However, an excessively thick silica layer will instead reduce the SAR. This is clinically *via*ble: a relatively high SAR can be leveraged to lower the therapeutic dosage, thereby improving biosafety and treatment efficacy [152]. Carbide- and nitride-based MNPs have also been studied as new heating platforms in addition to the traditional iron oxide system because their phase-dependent magnetization, magnetic anisotropy, and T_c may affect energy dissipation under AMF exposure. Nevertheless, their application in cancer MHT is less mature compared with IONPs, and further data regarding colloidal stability, biosafety, and reproducible *in vivo* heating performance are required.

Benefiting from its excellent deep tissue penetration performance and spatiotemporally controllable remote heating capability, MHT has been established as a promising treatment option applicable to multiple solid tumor types in the prostate, lungs, breast, and liver. MHT generally raises the temperature in the tumor through MNPs to 41-47 °C (Figure 10D) and thus causes apoptosis or necrosis of cancer cells by thermal stress [153, 154]. Achieving precise thermal effects allows for selective and uniform destruction of tumor tissue while protecting the surrounding normal tissues. Given the clinical safety limit for the amplitude-frequency product ($H \times f$) of AMF, thermal conversion efficiency of MNPs needs to be high enough to achieve a therapeutic effect.

Among the available nanomaterials, superparamagnetic iron oxide nanoparticles (SPIONs) are used more frequently in MHT due to their strong magnetic properties and excellent biocompatibility. Nanoparticles can be magnetized to the tumor site and generate local hyperthermia when exposed to AMF with minimal off-target heating.

In addition to MNPs administered *via* systemic circulation, multiple types of magnetically responsive implants designed for local retention have been developed to achieve superior spatial control and long-term stability. Chen *et al*. designed a multi-functional phase-transition nanocomposite for minimally invasive implantation (Figure 11A). In this system, polylactic-co-glycolic acid (PLGA) is blended with iron powder to form a highly injectable Fe/PLGA gel (L-Fe-PLGA). The gel solidifies upon contact with physiological fluids to form an *in situ* implant (S-Fe-PLGA). An anchor is used at the tumor site to convert electromagnetic energy into heat *via* an AMF, and the local temperature is raised to over 70 ℃. Thermal elevation results in full-thickness tumor destruction within three days, with no recurrence observed after one month. Clinically approved materials are used to enhance the biocompatibility and reduce the long-term toxicity of the system [94]. Beyond their intrinsic direct cytotoxicity, magnetothermal effects can act as a trigger for controlled drug release. Rao *et al*. demonstrated that hysteresis heat produced by MNPs upon AMF exposure can trigger the release of small molecules from thermosensitive liposomes after a short 20-second lag (Figure 11B) [155]. This approach enables targeted delivery of neuromodulators to the targeted neural region at a specific time and place, and the magnetothermal strategy is versatile for cancer treatment and neuromodulation.

In addition to generating localized thermal stress within the surrounding microenvironment, MHT concurrently induces nanoscale modulations in the molecular structure and physiological properties of endogenous biomolecules in the lesion region [156-158]. Some studies have demonstrated that individual MNPs can elevate the temperature in their immediate vicinity, thereby affecting adjacent or bound molecules. The localized thermal effect is expected to improve the anti-tumor effect of MNP-mediated MHT. For example, under an AMF, accumulated MNPs within lysosomes elevate the local temperature and reactive oxygen species (ROS) level, thereby triggering lysosomal cell death [159, 160]. Gordon *et al*. demonstrated that internalized MNPs exert stronger pro-apoptotic or necrotic effects owing to the insulating nature of the cell membrane, which consequently amplifies intracellular thermal stress [161]. Therefore, the hypothesis is supported. The advantages of magnetocalorically induced local hyperthermia are as follows: (i) reduced heat dissipation in surrounding tissues; (ii) achievement of targeted and spatially specific thermal ablation; and (iii) the capacity to modulate the functions or interactions of specific biomolecules under AMF-mediated heating, enabling selective destruction of tumor cells [162].

Lysosomes represent one of the most extensively investigated subcellular targets for MNP-mediated MHT. As acidic degradative organelles, lysosomes are rich in hydrolases and are responsible for macromolecule degradation, autophagy, and cell death regulation. Once MNPs are sequestered within lysosomes, AMF exposure triggers the generation of heat and ROS. This leads to lysosomal membrane permeabilization (LMP) and subsequent leakage of lysosomal enzymes into the cytosol, disrupting intracellular homeostasis and ultimately inducing apoptosis, necrosis, or inflammatory cell death [27]. Domenech *et al*. have shown that surface-functionalized MNPs can actively target tumor cells with elevated epidermal growth factor receptor (EGFR) expression, and upon exposure to an AMF, selectively induce LMP and ROS generation, thus reducing cell *via*bility [160]. Sanchez *et al*. also found that iron oxide nanocrystals entrapped within lysosomes can induce LMP in *in vitro* endocrine tumor cell models under low-intensity AMF, even at very low concentrations [163].

Mitochondria are also well-recognized targets for MHT, as they govern adenosine triphosphate (ATP) production, redox homeostasis, calcium signaling, and apoptosis. Shen *et al*. have developed a mitochondria-targeted magnetothermogenic nanozyme ($Ir@MnFe_2O_4$ NPs) for AMF-induced synergistic tumor therapy (Figure 11C) [95]. These nanozymes, directed by iridium (III) complexes (Ir), precisely accumulate in the mitochondria (Figure 11D) and produce localized thermal stress under an AMF, thereby damaging mitochondria. Within the GSH-rich microenvironment of cancer cells, Fe^{3+} in the nanozyme is reduced to Fe^{2+}, which promotes the Fenton reaction and generates hydroxyl radicals ($^{\cdot}OH$). This leads to oxidative cytotoxicity and disruption of cellular redox homeostasis. Shah *et al*. also reported a tumor-targeted magnetic core-shell nanoparticle (MCNP) system capable of delivering a mitochondria-targeting pro-apoptotic amphipathic tail-anchored peptide (ATAP) to metastatic breast and malignant brain tumor cells. Upon delivery, MCNP-ATAP induces mitochondrial dysfunction, which is further exacerbated by local magnetic hyperthermia. Compared with free ATAP, MCNP-mediated delivery leads to more severe loss of

mitochondrial membrane potential and enhanced mitochondrial disruption, thereby elevating the apoptotic rate. In addition, this system allows noninvasive cellular tracking *via* magnetic resonance and dark-field imaging, offering complementary diagnostic information alongside therapeutic functions [96].

External thermal stimulation can also induce mitochondrial heat stress, which propagates to mitochondria-associated endoplasmic reticulum (ER) membranes and initiates ER stress-mediated apoptotic signaling. Jiang *et al*. developed a dual-targeted nanoparticle, $ZnCoFe_2O_4$@$ZnMnFe_2O_4$-RGD-TPP (MRT), to selectively induce mitochondrial thermal stress under AMF exposure [97]. The arginyl-glycyl-aspartic acid (RGD) motif facilitates MRT binding to tumor cells, while triphenylphosphonium bromide (TPP) enables mitochondrial targeting (Figure 12A). AMF stimulates MRT to generate localized heat; mitochondrial dysfunction and excessive ROS production occur. Mitochondrial heat stress suppresses Mfn2; therefore, there is increased ER stress and activation of the PERK-eIF2α signaling pathway. This cascade induces immunogenic cell death (ICD), promotes the polarization of tumor-associated macrophages towards the pro-inflammatory M1 phenotype, and stimulates systemic anti-tumor immunity (Figure 12B). In a hepatocellular carcinoma model, MRT-mediated AMF exposure raises the subcutaneous tumor temperature to around 50 °C and causes substantial ablation of tumor cells. In addition, the induction of mitochondrial stress can inhibit the proliferation of the tumor locally and trigger immune responses that suppress distant tumors; thus, magnetothermal immunotherapy has shown some promise.

According to the above evidence, MHT can induce long-lasting anti-tumor immune responses through multiple mechanisms [164-166]. As early as 1998, Kobayashi and others reported that MHT activates the systemic immune function and enhances antitumor effects [167]. Notably, after MHT, $CD4^+$ and $CD8^+$ T cells were found infiltrating the tumor tissue; otherwise, no immune cells were present in the untreated control. The resulting immune response is also long-lasting. Subsequent studies have found that MHT-induced upregulation of heat shock protein 70 (HSP70) promotes the chaperoning of tumor-associated antigens and enhances their presentation by antigen-presenting cell (APC) *via* the MHC-I

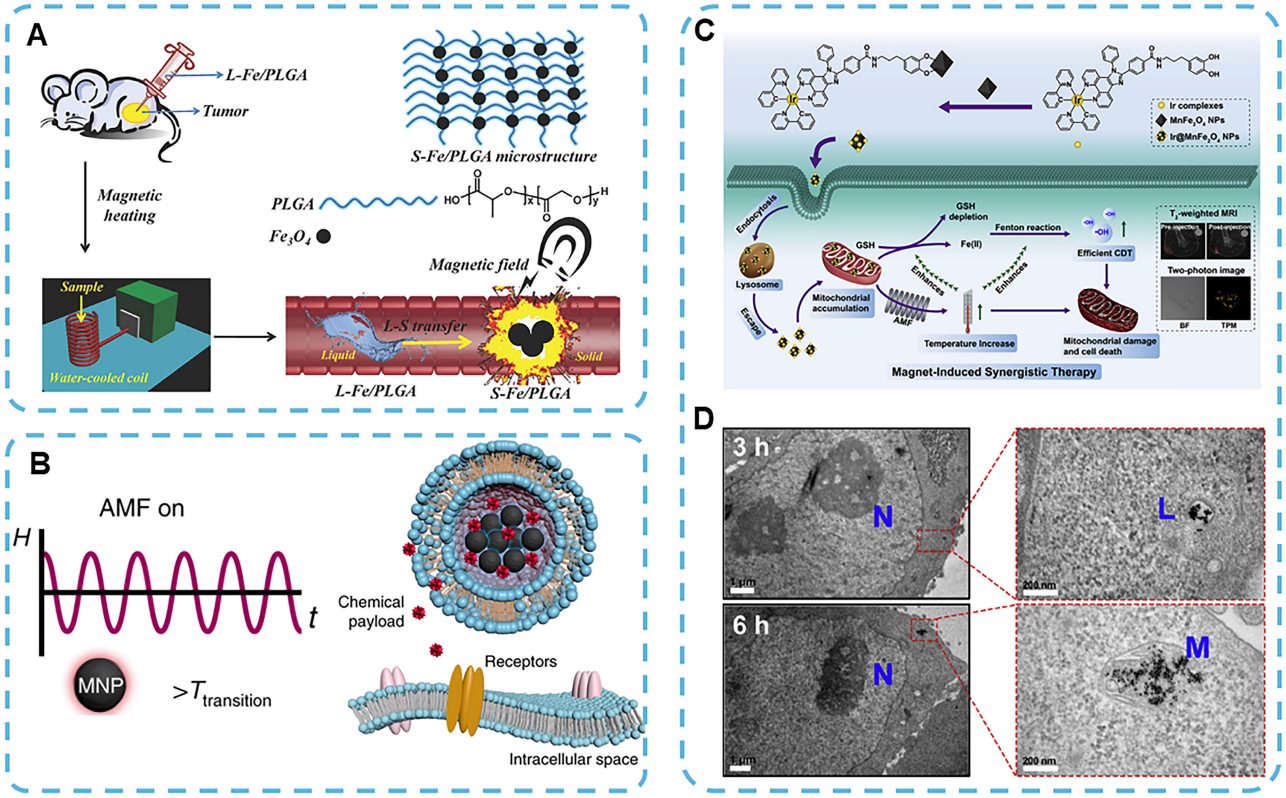

Figure 11. (A) Schematic illustration of tumor ablation mediated by MHT using phase-transition materials L-Fe/PLGA and S-Fe/PLGA. Reproduced with permission [94]. Copyright 2014, Wiley-VCH. **(B)** Experimental setup demonstrating the use of magnetoliposomes for triggered chemical payload release under an AMF. Reproduced with permission [155]. Copyright 2019, Springer Nature. **(C)** Synthetic route for mitochondria-targeted magnetothermogenic nanomaterials (Ir@$MnFe_2O_4$ NPs) and schematic representation of AMF-induced synergistic therapeutic mechanisms. **(D)** Bio-transmission electron microscopy (Bio-TEM) images showing the intracellular distribution of Ir@$MnFe_2O_4$ NPs in HeLa cells at 3 and 6 hours post-incubation. N: nucleus; L: lysosome; M: mitochondrion. Reproduced with permission [95]. Copyright 2020, Elsevier.

pathway, thereby activating cytotoxic CD8⁺ T lymphocytes [168, 169]. Liu and others have shown that MHT can also trigger an immune response by releasing tumor antigens [98]. PEGylated ferrimagnetic vortex-domain iron oxide nanorings (FVIOs) for MHT were engineered with a uniform vortex structure and a 70 nm diameter; they also have excellent heat conversion properties (SAR = 3337 W/g Fe at 365 kHz, 46 kA/m) (Figure 12C-F). In the presence of AMF, FVIOs induce calreticulin (CRT) translocation to the cell surface, a feature of ICD, and thus promote APC recruitment. CRT exposure promotes macrophage polarization and activates downstream immune cells. *In vivo* investigations have confirmed that MHT mediated by FVIOs significantly enhances systemic cytokine production—including interferon-gamma (IFN-γ), tumor necrosis factor-alpha (TNF-α), interleukin-6 (IL-6), and interleukin-18 (IL-18)—compared to AMF or FVIOs alone. Magnetothermal treatment nearly eradicates 4T1 breast tumors, and when combined with anti-PD-1 immune checkpoint blockade, results in complete tumor ablation. Furthermore, mild hyperthermia induced by FVIOs promotes immune cell infiltration within the TME and effectively inhibits both distant metastasis and the growth of secondary tumors.

MHT can also promote immune cell migration and drug delivery by triggering thermally induced biophysical changes. Hyperthermia within the range of 40-43 °C improves oxygenation by dilating arterioles and increasing vascular permeability, thereby recruiting T cells and dendritic cells from the draining lymph nodes to the tumor site [170-172]. MHT also upregulates intercellular adhesion molecule-1 (ICAM-1) and other vascular adhesion molecules *via* the IL-6 signaling pathway and promotes immune cell infiltration [173]. MHT-induced thermal stress also damages the tumor ECM and increases vascular and interstitial permeability, thereby facilitating the penetration of cytotoxic drugs and nanoparticle-based therapeutics while enhancing intratumoral drug delivery.

3.3 Magnetic Force-Induced Tumor Therapy

Magnetomechanical control of cells has garnered increasing attention in recent years. It is now established that mechanical force acts as an essential regulator of cell behavior and tissue homeostasis in cancer. Mechanical cues regulate how cells perceive and respond to their physical microenvironment; therefore, based on the above evidence, magnetism can be employed in cancer therapy to modify the structure of malignant cells and induce apoptosis [174]. Most studies have determined that mechanical force is a key reason for changes in cell-cell and cell-matrix contacts, and thus various other cell functions, such as division, differentiation, and immunity, are regulated [175, 176]. When exogenous mechanical

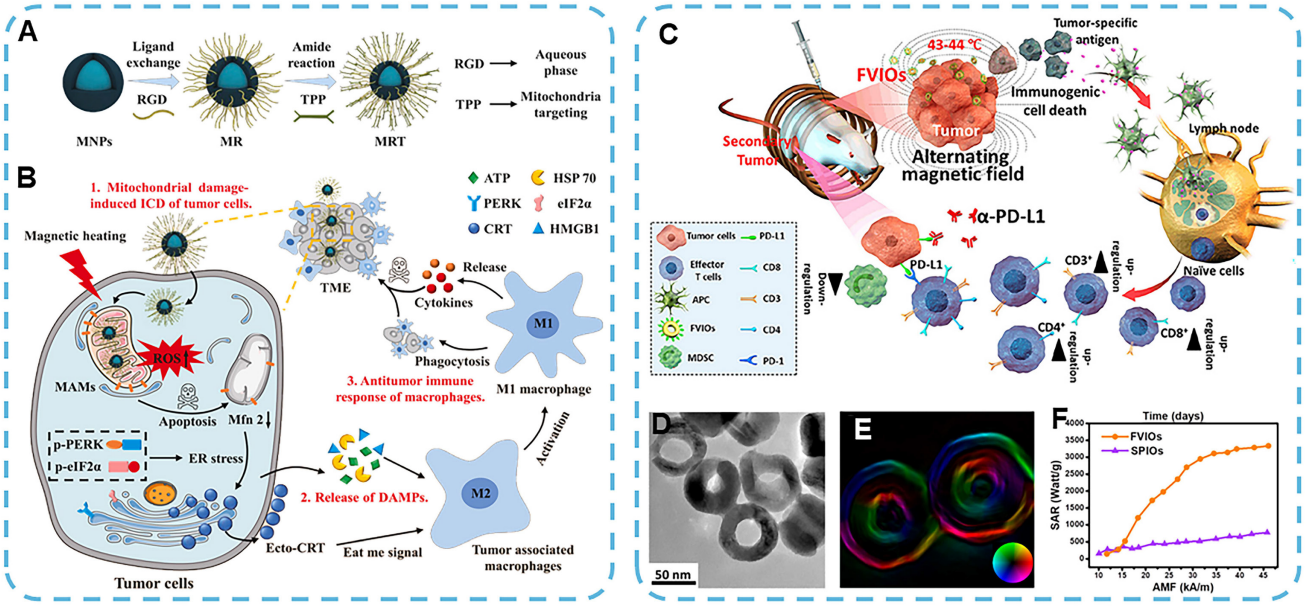

Figure 12. (A) Schematic illustration of the synthesis of MNPs-RGD-TPP (MRT) nanoparticles. **(B)** Mechanism by which MRT nanoparticles induce mitochondrial heat stress to promote ICD: (1) MRT nanoparticles disrupt mitochondrial function in tumor cells, triggering ICD. (2) Mitochondrial heat stress induces ER stress, promoting the release of damage-associated molecular patterns (DAMPs), including ecto-CRT, ATP, HMGB1, and HSP70. (3) These DAMPs facilitate the polarization of tumor-associated macrophages (TAMs) from an immunosuppressive M2 phenotype to a pro-inflammatory M1 phenotype, thereby enhancing tumor cell phagocytosis and the release of cytotoxic cytokines. Reproduced with permission [97]. Copyright 2022, Elsevier. **(C)** Schematic representation of anti-tumor immune activation mediated by FVIO nanorings through mild magnetic hyperthermia in combination with immune checkpoint blockade therapy. **(D)** Transmission electron microscopy (TEM) image and **(E)** Lorentz TEM image of PEGylated FVIO nanorings. **(F)** Comparison of specific absorption rate (SAR) between PEGylated FVIO and SPIONs under an AMF at 365 kHz. Reproduced with permission [98]. Copyright 2019, American Chemical Society.

forces exceed a threshold, they can disrupt cellular integrity and initiate cytotoxic cascades, thereby enhancing the efficacy of cancer therapies [176-179]. In 2021, Ardem Patapoutian received the Nobel Prize in Physiology or Medicine for discovering the molecular foundation of mechanosensation and extending the range of biological effects caused by mechanical stimulation [180].

Magnetic fields induce various types of mechanical stress on magnetoresponsive nanomaterials, including torque, tension, shear stress and compression, leading to changes in their structure and apoptosis of cancer cells. By changing the applied magnetic field and the shape of MNP, both the size and distribution of mechanical stress can be adjusted (Figure 13A). The biological effects of magnetically induced mechanical stimulation are significantly affected by the size, location and manner of application of mechanical load. Localized forces in the piconewton (pN) range can generally change mechanosensitive structures and start mechanotransduction without causing damage to the structure [181, 182]. With an increase in mechanical stress, forces in the range of hundreds of pN to nN can cause significant deformation of cellular membranes and cytoskeletal structures, and under suitable loading conditions, may result in structural damage or membrane rupture [183, 184]. The above values should be considered approximate mechanical environments rather than general upper bounds, as the biological response is also influenced by factors such as force concentration, loading frequency, contact shape, membrane stress, etc., in other cells. Therefore, magnetomechanical cancer therapy holds promise as a novel, physics-based non-invasive cancer treatment modality.

AMF generates oscillating magnetic fields (OMF) or RMF, exerting lateral mechanical stimuli such as shear and compressive stress on cell membranes and intracellular organelles [185]. AMF drives anisotropic MNPs (e.g., magnetic nanorods) to align and rotate along their longitudinal axes *via* magnetic torque, producing propeller-like motion that induces local mechanical stress. Consequently, the generated shear and compressive forces physically disrupt cancer cell membranes through a "slicing" effect [99, 186]. At the same time, there are also MNPs in a circle around a fixed point in RMF. For example, in the case of RMF, magnetic nanohelices can rotate and move along their helical axes to generate spiral shear forces that mechanically "mill" cancer cells by continuous rotational deformation [187, 188]. The modes of magnetic actuation produce different mechanical stresses in the cell structure (Figure 13B) [100]. MNPs of different shapes can be subjected to vertical compression or tension, and needle-like or sharp-edged MNPs generate a high local compressive force and are thus more effective against highly permeable or structurally damaged cancer cells [176-178]. Modification of the outer surface can also enhance the mechanical advantage of shape-specific MNPs and enable specific binding to target cell membranes or subcellular organelles. Anchoring will directly induce mechanical stress in the target membrane, receptor, cytoskeleton or subcellular organelle *via* magnetic-field-induced displacement. The resulting biological response varies according to the location, size and type of force application. Local magnetic forces at the plasma membrane can open the mechanosensitive ion channel Piezo1 and cause an influx of Ca^{2+} [182, 189]. Mechanical stimulation can also be transmitted by adhesion complexes and the actin cytoskeleton to regulate YAP/TAZ activity [190]. However, direct involvement in cell apoptosis in magnetomechanical tumor models has not been confirmed. Oscillation of lysosome-targeted SPIONs at the organelle level can lead to LMP and subsequent apoptosis [105]. Another study found that MNPs accumulated in lysosomes can disrupt the actin cytoskeleton without detectable lysosomal leakage, and thus different modes of intracellular action may occur simultaneously [100]. Besides these lysosomal effects, magnetic aggregation of DR4-targeted nanoparticles can promote DR4 clustering and activate the extrinsic apoptotic pathway [128]. Overall, the biological response to magnetomechanical stimulation depends on nanoparticle localization as well as the type and magnitude of applied force, including shear, torque, compression, and tension.

Shear force refers to a mechanical stress that arises from a directional "cutting" motion, causing one segment of an organelle to slide relative to another [185-187, 191]. RMF is applied to the MNPs for spinning and rotation, and shear forces are generated by rubbing, scraping, milling, slicing, etc. The size of the shear stress is also affected by the specific shape of the MNPs and other factors in the magnetic field. The above reasons will damage the structure of the cell by causing membrane rupture and releasing intracellular contents; therefore, either apoptosis or necrosis will occur (Figure 14A). The mechanism and range of shear-induced cytotoxicity for MNPs are affected by MNP shape, surface modification, and magnetic field strength. Zhao *et al*. have shown that rod-shaped MNPs can generate a larger shear force than spherical ones and are thus more effective at ablating cancer cells [192]. Rod-shaped MNPs cause significant shape deformation of cancer cells in the presence of AMF and reduce cell *via*bility considerably compared to spherical counterparts. Rotationally sheared MNPs

reduced the size of tumors in a mouse breast cancer model compared with the control group. More recently, Cheng *et al*. developed a magnetic nanocube platform that self-assembles into rod-like structures under RMF (15 Hz, 40 mT). These rod-shaped assemblies exert slicing shear forces on cells *via* dynamic rotational motion (Figure 14B,C) [99, 103, 104]. Additionally, mitochondrial-targeted surface modification of MNPs enables direct transmission of shear forces to mitochondrial membranes, triggering the efflux of pro-apoptotic proteins such as cytochrome c into the cytoplasm (Figure 14D) [99].

Torque describes the rotational mechanical moment generated when a force acts at a distance from a rotational axis. Under AMF, rotating MNPs generate torque that distorts cellular structures upon direct interaction with plasma membranes or subcellular organelles (Figure 15A). Tunable torque-mediated deformation can be achieved by engineering MNP geometry, adding organelle-targeted surface functionalization, or changing the frequency of the applied magnetic field to extend the therapeutic effect of magnetomechanical oncology [193]. Zhang *et al*. showed that magnetic nanospheres bonded to lysosomes could be subjected to an AMF (20 Hz, 30 mT), thereby exerting a direct torque on the lysosomal membrane and causing twisting and damage to its structure (Figure 15B) [105, 194]. When the applied torque exceeds the mechanical limit of the membrane, it will break, thus resulting in cancer apoptosis and impaired cancer growth. Master and others used a polymer network to fix the nanospheres more securely to lysosomal membranes and enhanced torque transmission and therapeutic effect [100]. Park *et al*. developed ligand-functionalized magnetic nanospindles for selective mitochondrial targeting in 2021. Low-frequency AMF stimulation (0.5-20 Hz, 1 mT) generates torque directly at the mitochondrial surface of these nanospindles and thus causes mechanical deformation and functional impairment (Figure 15C) [195]. External torque triggers excessive mitophagy and mitochondrial dysregulation in tumor cells, leading to apoptotic cell death.

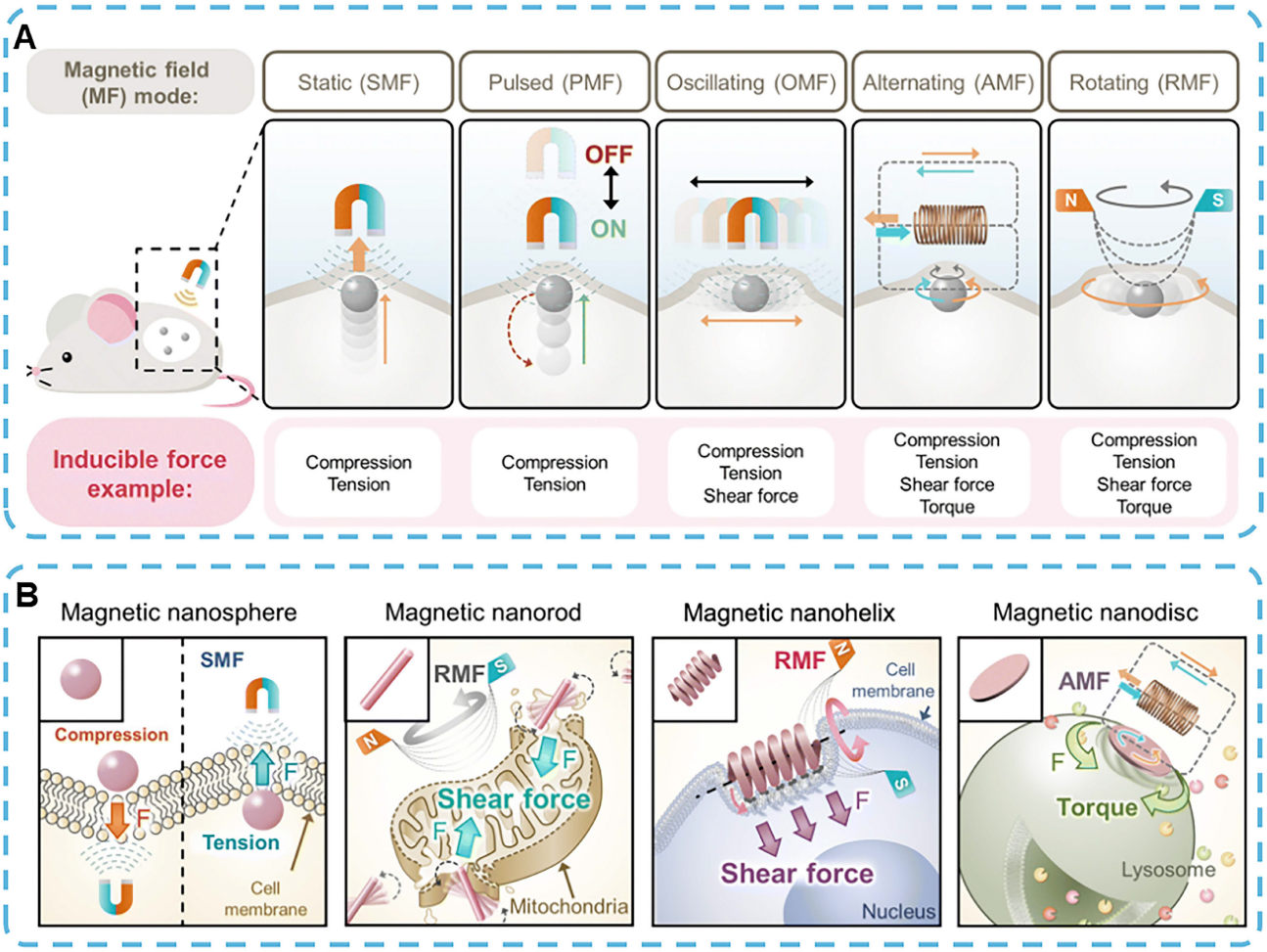

Figure 13. Versatile mechanical cancer therapy enabled by magnetic fields and MNPs. **(A)** Schematic illustration showing how MNPs exhibit diverse mechanical motions under various magnetic field modes. **(B)** Schematic representation of shape-dependent MNPs exerting specific mechanical forces on subcellular organelles of cancer cells when exposed to different magnetic field configurations. Reproduced with permission [8]. Copyright 2023, Royal Society of Chemistry.

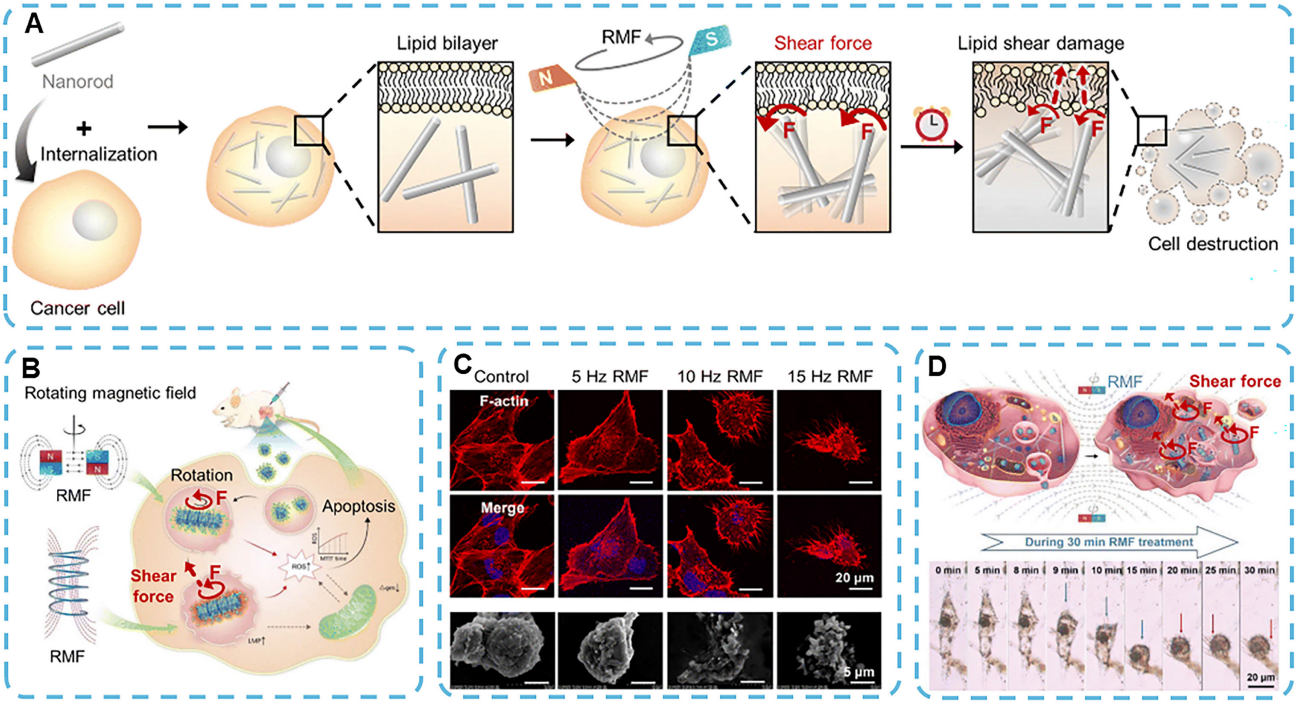

Figure 14. Magnetic shear force-mediated tumor therapy. **(A)** Schematic illustration of cancer cell disruption mediated by magnetic nanorods, which generate shear forces on the cell membrane under a RMF. Reproduced with permission [8]. Copyright 2023, Royal Society of Chemistry. **(B)** Under RMF exposure, rod-shaped magnetic nanocubes produce shear forces that promote tumor cell apoptosis through ROS generation. Reproduced with permission [104]. Copyright 2020, Wiley-VCH. **(C)** Immunofluorescence and SEM images illustrating morphological changes in cancer cells subjected to RMF-induced shear forces at varying frequencies. The cytoskeleton and nuclei are stained with phalloidin and DAPI, respectively. Scale bars: 20 μm (immunofluorescence), 5 μm (SEM). Reproduced with permission [103]. Copyright 2021, American Chemical Society. **(D)** Schematic illustration of mitochondria-targeted MNPs generating localized shear forces under RMFs to induce cancer cell apoptosis. Reproduced with permission [99]. Copyright 2020, Wiley-VCH.

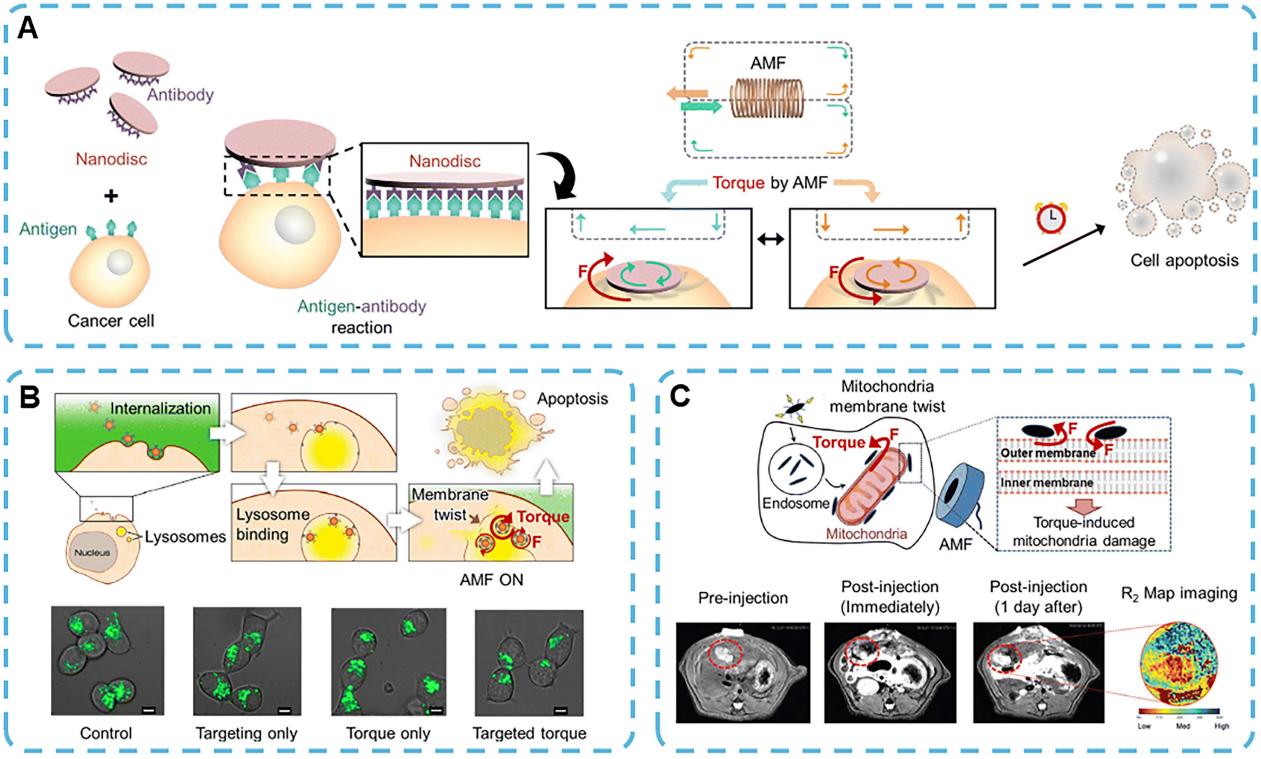

Figure 15. AMF-induced torque-mediated cancer therapy. **(A)** Schematic illustration of a magnetic nanodisc disrupting tumor cells by exerting rotational torque on the cell membrane under AMF exposure. Reproduced with permission [8]. Copyright 2023, Royal Society of Chemistry. **(B)** Torque generated by the rotation of magnetic nanospheres under AMF induces lysosomal membrane permeabilization, triggering apoptotic pathways in cancer cells. Fluorescence microscopy images depict lysosomal disruption, visualized using Lyso-Tracker Green. Scale bars: 5 μm. Reproduced with permission [105]. Copyright 2014, American Chemical Society. **(C)** Schematic illustration of mitochondrial destruction induced by torque from magnetic nanospindles' rotation under AMF. *In vivo* T_2-weighted MRI images show signal variations before and after injection of MNPs. Reproduced with permission [195]. Copyright 2021, Royal Society of Chemistry.

Compression and tension are fundamental mechanical forces that cause inward compressive stress and outward tensile stress on cell membranes and intracellular organelles. Compression can directly damage membranes and impair cells; tension or cyclic mechanical vibration, which alternates between compression and tension, can open mechanosensitive ion channels and activate other intracellular signaling pathways to alter diverse cell functions (Figure 16A) [128, 196]. Recent studies have demonstrated that targeted mechanical vibration can potentiate anti-cancer immune response. In 2021, Sim *et al*. developed a magnetic-responsive nanocomplex incorporating SPIONs for natural killer (NK) cell labeling [106]. Upon exposure to a low-frequency AMF (1 Hz, 1.5 mT), the nanocomplex undergoes dynamic mechanical oscillation, subjecting NK cells to repeated compression and extension. Mechanical stimulation on the NK cell surface alters mechanosensitive structures and enhances their cytotoxic activity against tumor cells (Figure 16B). Lunov *et al*. confirmed that mechanical stress applied to lysosomes can induce apoptosis in cancer cells (Figure 16C) [101]. Magnetic nanospheres are internalized *via* endocytosis and trafficked to lysosomes. Upon exposure to a high-intensity pulsed magnetic field (PMF; 8 T, 15 μs pulse width), they abruptly generate tensile stress, inducing lysosomal membrane damage and subsequent cytoplasmic release of Granzyme B to trigger apoptosis. Building on this concept, Cho *et al*. applied magnetic tension to selectively activate DR4 on the surface of cancer cells (Figure 16D) [128]. In their study, antibody-functionalized magnetic nanospheres specifically bind to DR4 and are subjected to a SMF to create a local tensile force at receptor sites. Such mechanical stimulation promotes assembly of the death-inducing signaling complex and subsequent caspase-3 activation, thereby triggering apoptosis. This magnetomechanical strategy has achieved promising results against multidrug-resistant cancer cells and is currently under investigation for cancer therapeutic applications.

The above magnetomechanical effects provide a direct path for magnetic-force-mediated cancer therapy. In magnetically actuated micro/nanorobots, magnetic forces and torques are applied in a distinct manner. They no longer serve as primary cytotoxic triggers, but act as control parameters for deformation, locomotion, navigation, tissue penetration, and cargo delivery.

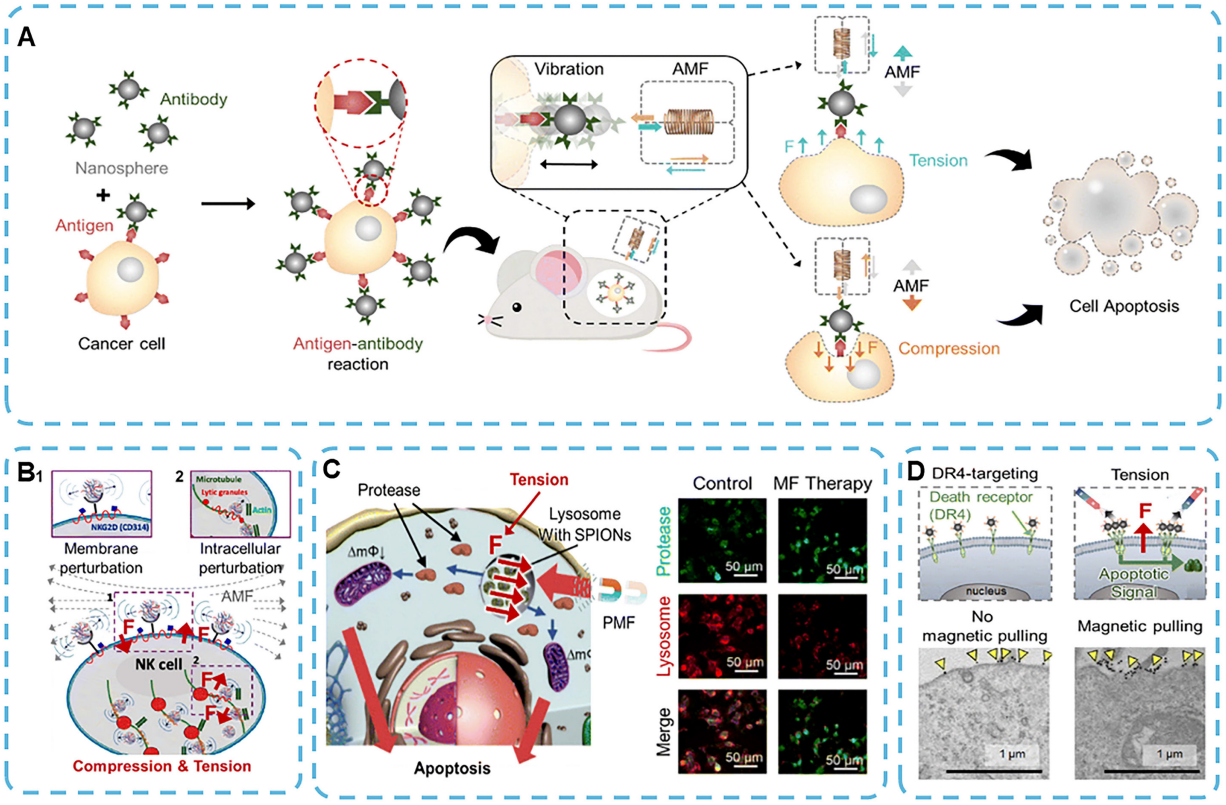

Figure 16. AMF- and PMF-mediated compression- and tension-based cancer therapies. **(A)** Schematic depiction of magnetic nanospheres inducing tumor cell death by exerting compressive and tensile forces on the cell membrane under AMF stimulation. Reproduced with permission [8]. Copyright 2023, Royal Society of Chemistry. **(B)** Schematic illustration showing the activation of NK cells through AMF-induced membrane deformation *via* compressive and tensile stress. Reproduced with permission [106]. Copyright 2021, American Chemical Society. **(C)** Schematic representation and immunofluorescence images demonstrating PMF-induced tension generated by magnetic nanospheres, which promotes cancer cell apoptosis through lysosomal membrane permeabilization. Scale bar: 50 μm. Reproduced with permission [101]. Copyright 2019, MDPI. **(D)** Under a SMF, magnetic nanospheres are drawn toward and bind to specific cell surface receptors, generating tensile forces that activate apoptotic signaling cascades in tumor cells. Scale bar: 1 μm. Reproduced with permission [249]. Copyright 2016, American Chemical Society.

3.4 Magnetic Navigation Micro/Nanorobots Mediated Tumor Therapy

Numerous organisms in nature, such as birds, butterflies, magnetotactic bacteria, and salmon, can perform long-distance navigation by sensing geomagnetic fields [26]. Some species rely on the Earth's magnetic field for spatial orientation and nest selection. Inspired by these biological navigation strategies, researchers have developed magnetic micro/nanorobots for targeted delivery in biomedical applications. These artificial structures are generally micro- or nano-sized, and after functionalization with diagnostic agents, therapeutic payloads or targeting ligands, they can be targeted to different parts of the body for delivery. Micro/nano-robots are classified based on the type of actuation device: magnetic, electrical, chemical (fuel-powered), acoustic (ultrasound-driven), and optical (light-driven). However, all these systems have certain deficiencies. Chemically and ultrasound-driven systems are generally not directionally controllable, and cytotoxic fuels such as urea, hydrogen peroxide or sodium borohydride need to be employed [197, 198]. Light-driven robots need a powerful light source; therefore, they may be less biocompatible, and electrically actuated devices have not undergone clinical trials. At the same time, magnetically actuated micro-/nanorobots can be remotely controlled and are compatible with tissue in a complex physiological environment. These systems have shown extensive applications in various fields of biomedicine, such as targeted drug delivery, biofilm inhibition, cell modulation and real-time *in vivo* biosensing. Therefore, they are now new platforms for minimally invasive and highly controllable therapy. Magnetic medical microrobots can be magnetized for real-time imaging and manipulation in MRI to achieve combined diagnosis and motion control. Magnetic fields have some advantages over other drive modes:

(i) Remote control capability: Magnetic fields are used for wireless, non-contact manipulation of microrobots in complex chemical and biological environments.

(ii) Fuel-free operation: Magnetic propulsion is a type of clean actuation that does not use toxic chemical fuels. It is also highly environmentally friendly; the low-frequency magnetic actuation does not harm the cells and tissues.

(iii) Deep-tissue penetration: Magnetic fields have good soft-tissue permeability and biosafety; thus, they can reach deep-seated, anatomically localized lesion areas *in vivo*.

(iv) Programmability and reconfigurability: Precise motion control of magnetic microrobots can be achieved by modifying the inherent material properties (e.g., magnetic anisotropy and particle morphology) to alter magnetic response behavior [199-201]. The magnetorheological structure can be flexibly changed for various biomedical applications by dynamically adjusting the amplitude, direction, and frequency of the magnetic field [202-205].

(v) Versatility: Magnetic actuation can be used in conjunction with other types of stimulation, such as optical, chemical and acoustic energy, to achieve high-precision control and delivery of various functional cargoes, including single cells and nanotherapeutic agents [206].

(vi) Recyclability: Magnetically assembled micro/nanorobots can be efficiently extracted from biological fluids and tissues by an external magnetic field after use. This way can improve biosafety and reduce systemic and environmental accumulation.

Given their magnetic properties, the three categories of materials often employed in the construction of microrobots are soft magnets, hard magnets and superparamagnetic materials. Generally speaking, the division is based on the necessary characteristics of M_r and H_c, as shown in their respective magnetization curves (Figure 17A-C). M_r is the remanent magnetism that remains in a material after the removal of an external magnetic field, and H_c is the magnetic field strength required to reduce M_r to zero. Both are highly dependent on particle size (Figure 17D). Soft magnetic materials, such as iron- and nickel-based alloys, have a high magnetic susceptibility and M_s but low M_r and H_c values (Figure 17A). A special kind, soft-magnetic soft materials, have soft magnetic properties and mechanical compliance, and a low Young's modulus. When embedded magnetic particles are isotropic and spherical, no magnetic torque is generated owing to the lack of a preferred magnetization axis (Figure 17E). Accordingly, magnetoresponsive gels and elastomers fabricated from isotropic soft-magnetic soft materials undergo deformation driven by magnetic forces originating from spatial magnetic field gradients (Figure 18A,B) [207-209]. Magnetic anisotropy can be imparted to soft-magnetic soft materials by incorporating non-spherical particles or assembling magnetic particles into anisotropic chain-like architectures (Figure 18C,D) [201, 210, 211]. This engineered structural asymmetry disrupts magnetic isotropy, thereby enhancing the material's directional responsiveness to external magnetic fields and significantly improving its actuation performance.

In contrast, hard magnetic materials exhibit high values of both M_r and H_c, which enables them to sustain stable magnetization and function as permanent magnetic sources after polarization (Figure

17B). Therefore, rare-earth-based permanent magnetic materials (e.g., NdFeB and SmCo) are more suitable for fabrication of locally positioned magnetic components and embedded magnetic domains, as well as for device-assisted actuation, rather than serving as conventional systemically injected nanoparticles. Their high M_r and H_c values enable persistent magnetization and programmable deformation in magnetic robotic systems. Nevertheless, their limited biodegradability, potential long-term *in vivo* retention, and composition-associated biosafety risks necessitate rigorous encapsulation strategies and safety assessments before biomedical applications. When hard magnetic particles are embedded within mechanically compliant polymer matrices, the resulting hard-magnetic soft materials can undergo controlled deformation (e.g., bending or shape morphing) under uniform or gradient magnetic fields *via* torque- and force-driven actuation mechanisms (Figure 19A–D). When particle sizes are reduced below a critical threshold, H_c decreases sharply, making the particles highly susceptible to thermal fluctuations and magnetic relaxation (Figure 17D). Ferromagnetic nanoparticles below this threshold display superparamagnetic characteristics: they produce large magnetization under an applied magnetic field but negligible remanent magnetization and H_c once the field is removed (Figure 17C). When such superparamagnetic nanoparticles are embedded within soft magnetic matrices, the resultant composites are referred to as superparamagnetic soft materials. Although superparamagnetic soft materials generate lower magnetic torque and force density compared to their soft or hard magnetic counterparts, they possess a unique ability to produce heat through Néel and Brownian relaxation mechanisms under AMF exposure. This localized thermal effect can be exploited to trigger programmable internal shape transformations (Figure 19E), as well as to regulate expansion–contraction behavior in thermoresponsive composite systems (Figure 19F). Accordingly, superparamagnetic soft materials provide an alternative mode of actuation that extends beyond direct magnetic force or torque-mediated deformation.

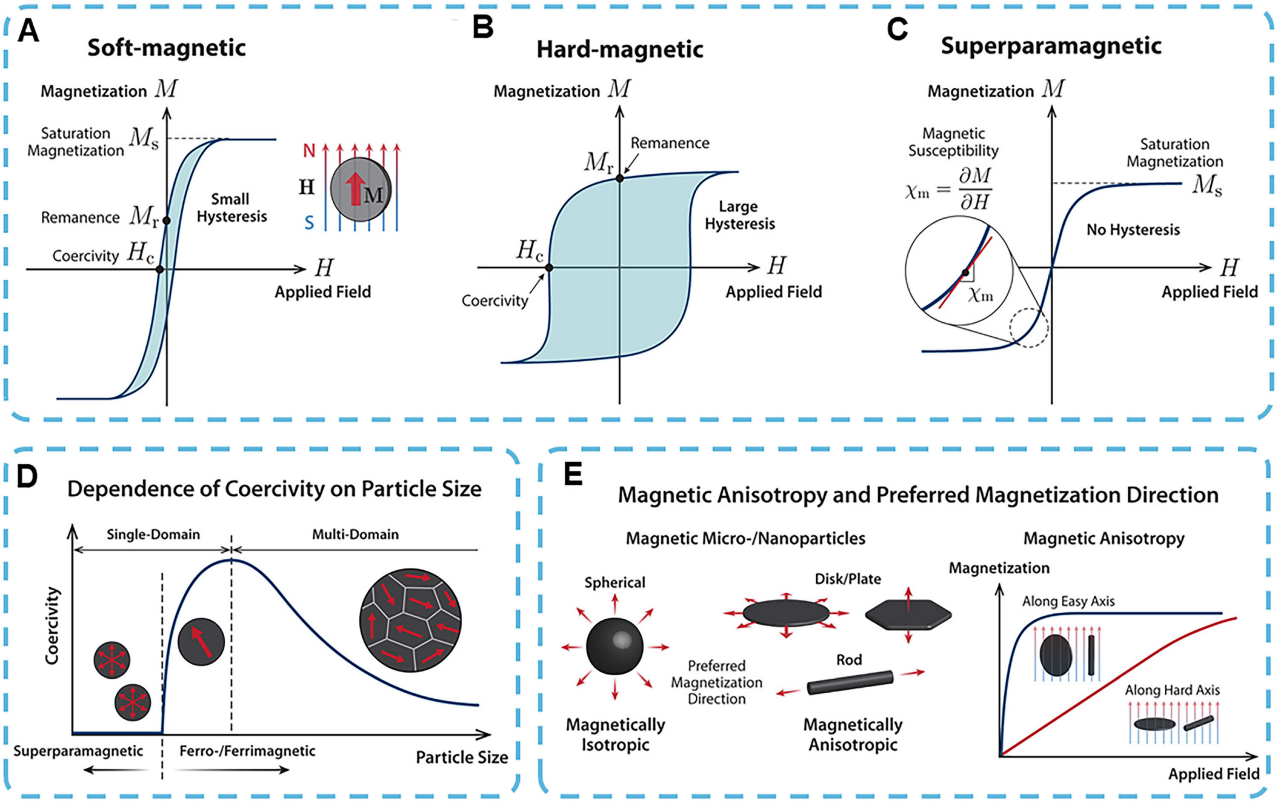

Figure 17. Hysteresis curves of **(A)** magnetic soft materials, **(B)** magnetic hard materials and **(C)** superparamagnetic materials. **(D)** Dependence of magnetic particle H_c on size. **(E)** According to the shape of the magnetic particles and the preferred magnetization direction, they can be divided into magnetically isotropic particles or magnetically anisotropic particles. Reproduced with permission [212]. Copyright 2022, American Chemical Society.

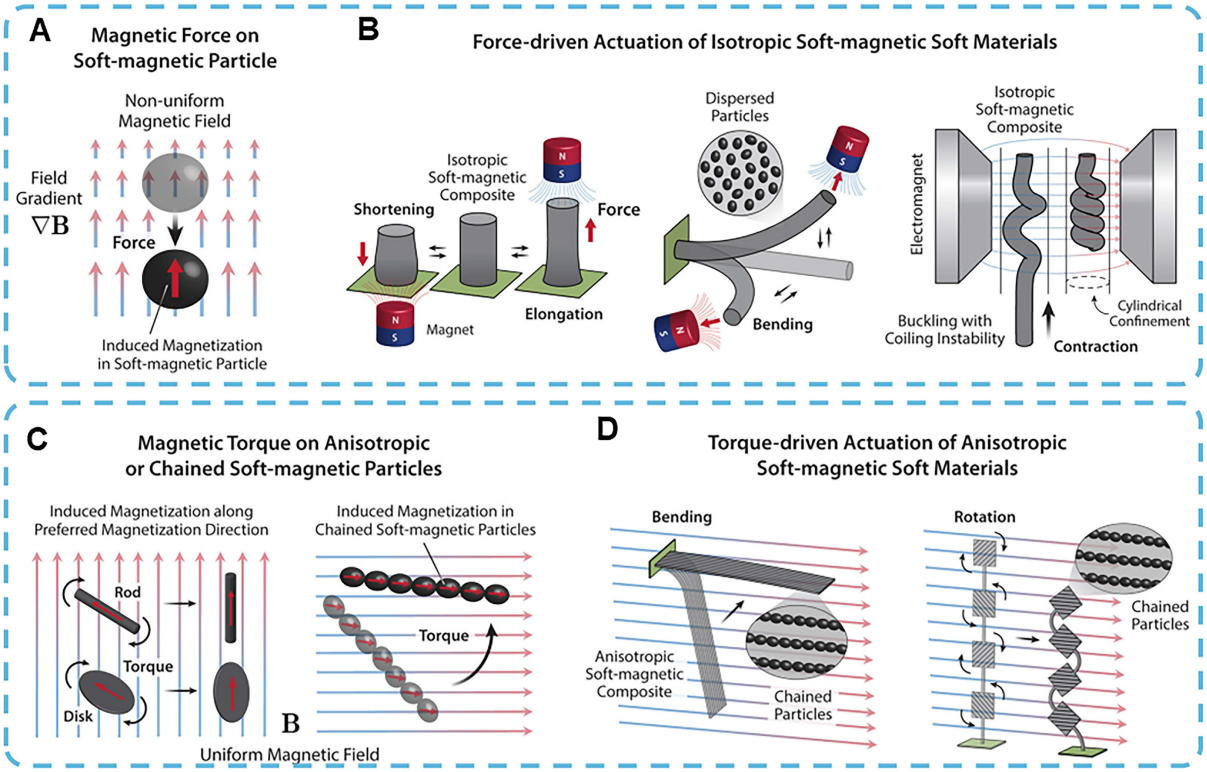

Figure 18. Actuation mechanisms of soft-magnetic soft materials under magnetic fields. **(A)** Magnetic force exerted on a single soft-magnetic particle in a spatially nonuniform magnetic field. **(B)** Force-induced actuation of isotropic soft-magnetic composites *via* gradient fields, resulting in global shape deformation. **(C)** Magnetic torque acting on anisotropic or chain-aligned soft-magnetic particles in spatially uniform magnetic fields. **(D)** Torque-driven actuation of soft-magnetic composites containing chained anisotropic particles. Reproduced with permission [212]. Copyright 2022, American Chemical Society.

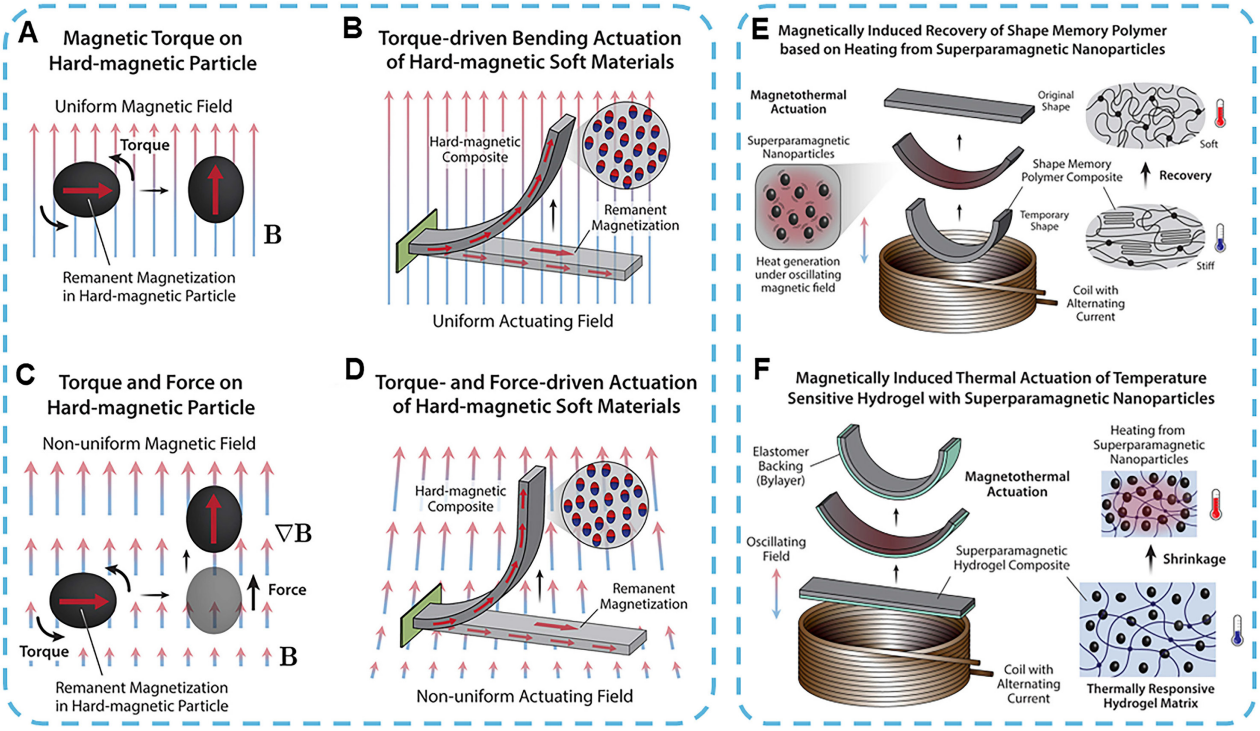

Figure 19. Actuation strategies of hard-magnetic and superparamagnetic soft materials. **(A-D)** Torque- and force-induced bending of hard-magnetic soft composites. **(A)** A magnetized hard-magnetic particle experiences magnetic torque under a spatially uniform magnetic field. **(B)** A rectangular beam composed of a uniformly magnetized hard-magnetic soft composite bends under a uniform magnetic field applied perpendicular to its remanent magnetization. **(C)** Under a spatially nonuniform magnetic field, a magnetized hard-magnetic particle is subjected to both magnetic torque and force. **(D)** In nonuniform fields, initial bending of the hard-magnetic soft composite is induced by torque, followed by continued deformation driven by increasing magnetic force. **(E,F)** Magnetothermal actuation of superparamagnetic soft composites. **(E)** Shape recovery of a shape memory polymer triggered by thermal relaxation generated from superparamagnetic nanoparticles under an AMF. **(F)** Bilayer hydrogel structure undergoes magnetothermal-induced deswelling due to temperature-responsive shrinkage. Reproduced with permission [212]. Copyright 2022, American Chemical Society.

In addition to the inherent magnetic properties of materials, the spatial distribution of external magnetic fields also significantly influences the type of actuation and movement characteristics for magnetic soft robots. A hard magnetic structure with a programmed M_r in a near-uniform magnetic field is driven by magnetic torque. The distal end rotates or bends to be perpendicular to the field, but in the absence of a strong field gradient, there is little net displacement. Therefore, the forward drive is achieved by near-field insertion, fluid flow or auxiliary drive. A spatial magnetic field gradient creates a net magnetic force in the direction of an increase in the magnetic field and thus induces translation. In general, a force and a torque in a non-uniform magnetic field work together rather than independently [212].

Different magnetic field characteristics can be used to implement various navigation strategies for vascular intervention. Torque-dominated systems control the position and bend of the distal end by means of magnetic fields, and forward motion is realized by external means, such as mechanical pushing or fluid flow. Jeon and others are examples. Connect a variable-direction magnetic field to an independent robotic inserter for guidance of a guidewire inside a coronary phantom [213]. Similar strategies have also been used for the neurovascular system: magnetic-field systems are used for steering control, and motorized devices deliver forward propulsion. Pancaldi *et al*. adopted an alternative approach, utilizing magnetic torque to regulate orientation at vascular bifurcations while relying entirely on blood flow for vessel traversal [214]. Gradient-dominated systems differ because magnetic field inhomogeneity itself provides a directionally biased pulling force at the distal tip. The fringe field generated by a clinical MRI scanner has been utilized to guide tethered instruments robotically [215], and built-in MRI gradients have realized stepwise leader-follower navigation of a tethered guidewire [216]. Therefore, torque-dominated navigation generally separates orientation from propulsion, and gradient-dominated navigation links magnetic actuation to translation more directly. The three-dimensional path of the actual vascular environment is jointly determined by vessel geometry, fluid flow, mechanical insertion, magnetic field distribution and tether deformation.

Novel materials and magnetic actuation devices have been developed to enhance the biomedical applications of magnetic micro/nanorobots. These miniaturized agents exhibit promising potential for disease diagnosis and therapy, biosensing, and detoxification, and generally serve as rigid carriers of genes, cells, or chemotherapeutic agents [217-219]. Magnetic actuation under low millitesla-scale field strengths is generally sufficient to drive micro/nanorobots' locomotion while avoiding damage to surrounding healthy tissues [26]. For example, iron-coated biotubes can be driven as drill—like carriers within high-frequency RMF to precisely deliver the anticancer agent camptothecin to tumor sites. *In vitro* experiments have shown that this targeted delivery strategy can effectively eliminate HeLa cells, and magnetically-driven microcarriers have exhibited therapeutic potential [220].

Chen *et al*. also developed a biodegradable magnetic hydrogel robot (BMHR) based on gelatin and Fe_3O_4 nanoparticles capable of autonomous navigation under a closed-loop control system [107]. The BMHR supports four motion modes to follow predefined paths. The navigation module adopts the AI algorithm to compute optimal paths for the robot to reach target locations, while a dilation algorithm maintains safe distances from environmental boundaries for obstacle avoidance, enabling intelligent motion planning. Prolonged exposure to AMF gradually increases the internal temperature of BMHR, and after reaching the upper limit for thermosensitive change, a reversible gel-to-solid phase transition takes place. In addition, BMHR is highly biodegradable and can be gradually degraded in PBS at room temperature. Gelatin has an inherent thermal response, and Fe_3O_4 NPs produce heat in the presence of AMF through Néel relaxation, Brownian relaxation and hysteresis loss. Together, they can target the release of drugs in tumors and suppress the growth of cancer cells. Collectively, the above results show that BMHR can function as an intelligent magnetic-guidance drug-delivery system for cancer treatment and has good prospects for future clinical application.

Given the complexity of the human physiological environment, cargo delivery and release strategies for micro/nanoscale agents in various biological fluids, such as blood, gastric juice and saliva, need to be investigated [26]. Biomedical nanorobots are self-propelled and controllable navigation devices that have attracted extensive attention in recent years for targeted drug delivery and biosensing [221]. Alapan *et al*. have engineered cell-level multifunctional surface microrollers by functionalizing magnetic-responsive Janus microparticles with anti-HER2 antibodies. Microrollers can be functionalized with cancer-targeting ligands or anticancer drugs to achieve targeted delivery to the tumor site in a simulated circulatory system [12]. Although their propulsion performance decreases in the presence of dynamic flow, active upstream motion can still be achieved for the micro-rollers in both two-dimensional (2D) and three-dimensional (3D) flow channels, and they are

also suitable for navigation in a physiological environment.

The foundation of *in vivo* feasibility for magnetic micro/nanorobots is favorable biocompatibility. However, most of the existing designs have high immunogenicity and can cause serious host immune reactions; thus, they may lead to structural damage or platelet activation of the robots and increase the risk of adverse pathological lesions [222]. Biohybrid magnetic microrobots (BMMRs) have been developed to solve the problems of biological incompatibility and cytotoxicity. Gong *et al*. fabricated biohybrid microrobots by magnetizing *Chlorella (Ch.)* cells with Fe_3O_4 nanoparticles and then loaded the chemotherapeutic drug doxorubicin (DOX) into the engineered cells (Figure 20A) [108]. These microrobots can be further organized into chain-structured multimers called biohybrid microrobot multimers (BMMs) *via* dynamic magnetic self-assembly (Figure 20B). BMMs have multiple ways to move, and under different magnetic field conditions, they can roll or tumble to move in any direction accurately (Figure 20C, D). Under the processing magnetic field (B = 70 G, f = 60 Hz, θ = 30°), both the rolling speed and the propulsion performance of dimeric BMMs reached a maximum of 107.6 μm/s, due to the excellent biocompatibility of *Ch.* BMMs are not cytotoxic. Targeted chemotherapy experiments have further validated that BMMs can be magnetically guided to cancer cells, and the acidic TME triggers localized drug release to induce apoptosis in malignant cells.

Wang *et al*. also constructed multifunctional hybrid bio-microrobots, denoted as (Pd@Au) /Fe_3O_4@*Sp*.-DOX, by using non-cytotoxic *Spirulina* (*Sp*.) as a biological scaffold (Figure 20E) [109]. These BMMRs are designed to perform targeted drug delivery and synergistic chemo-photothermal therapy simultaneously (Figure 20F). BMMRs have a high M_s, can be driven by a RMF to achieve a maximum propulsion speed of 526.2 μm/s, and show stable directional motion. DOX-loaded BMMRs can be precisely delivered to the tumor site by magnetic fields and bind to 769-P cancer cells. Subsequent near-infrared (NIR) irradiation induces on-demand in situ drug release and thus causes extensive apoptosis and necrosis of tumor cells. Fe_3O_4 nanoparticles are used as contrast agents for MRI and gold (Au) components are used for CT. Such dual-modal imaging capability endows these microrobots with great potential for real-time image-guided cancer therapy, representing a promising direction for future research.

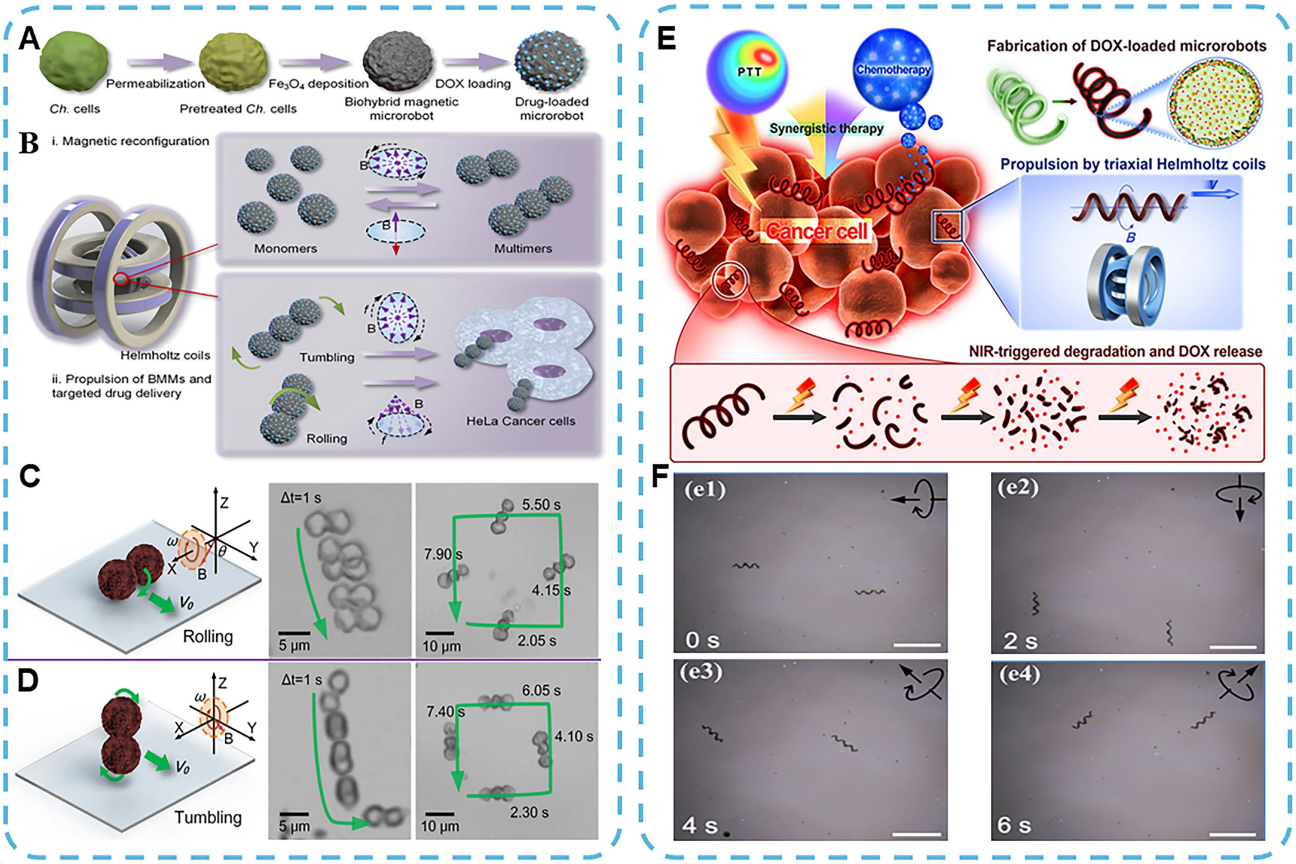

Figure 20. Magnetic biohybrid microrobots and their magnetically actuated locomotion strategies. **(A)** Schematic illustration of the synthesis of BMMs incorporating magnetic Chlorella cells. **(B)** Magnetic self-assembly and propulsion of the fabricated BMMs. **(C)** Rolling locomotion of dimer and trimer BMMs under a processing magnetic field. **(D)**

Tumbling locomotion of dimer and trimer BMMs under a vertically rotating magnetic field. Reproduced with permission [108]. Copyright 2022, American Chemical Society. **(E)** Schematic representation of synergistic chemo–photothermal therapy mediated by BMMRs, with triaxial Helmholtz coils generating magnetic actuation. V indicates translational velocity; B denotes magnetic field strength. **(F)** Time-lapse images showing precise directional propulsion of a BMMR under a rotating magnetic field (RMF, 100 Gs, 20 Hz). Scale bar: 200 μm. Reproduced with permission [109]. Copyright 2019, American Chemical Society.

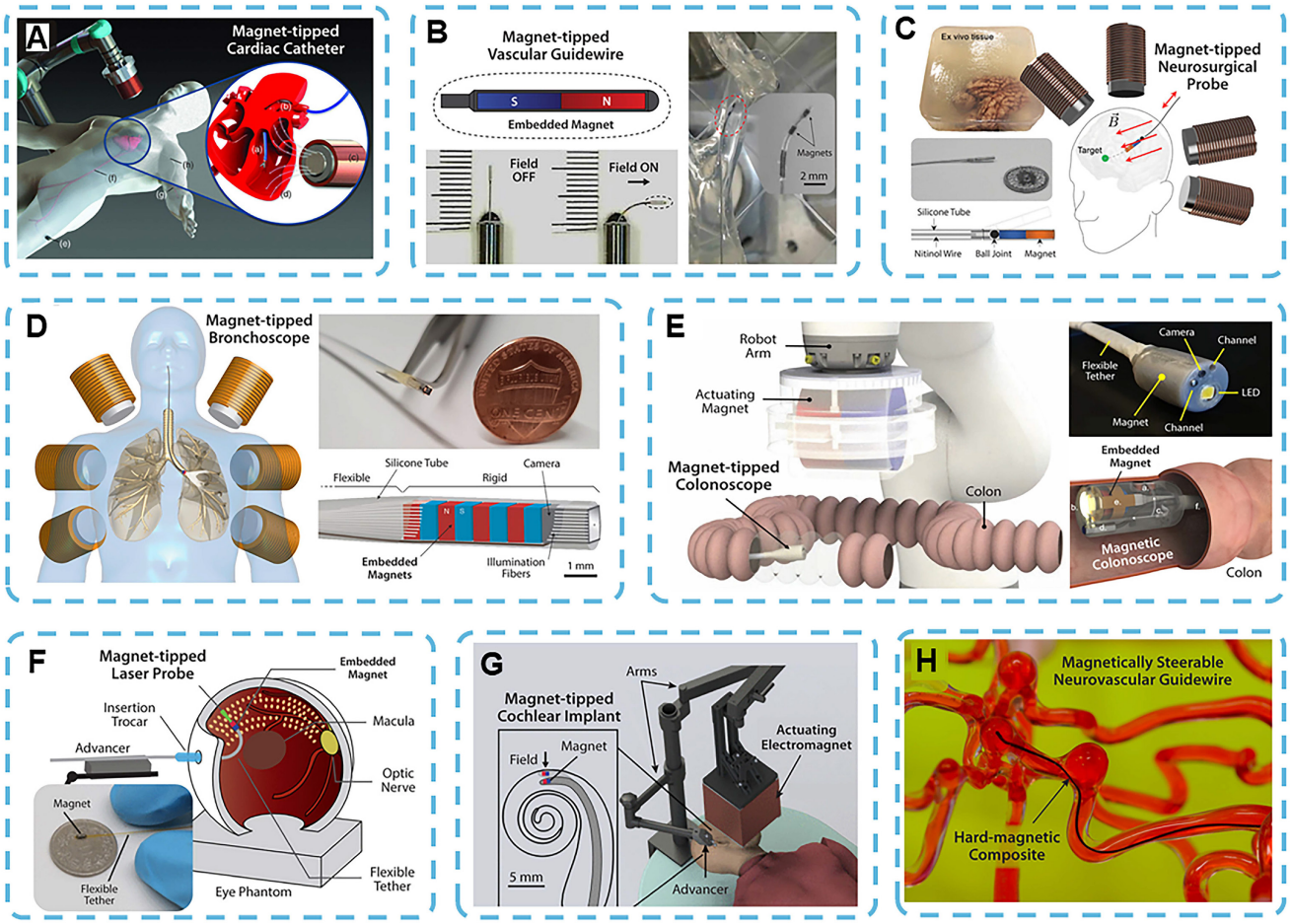

Figure 21. Applications of magnetic micro- and nanorobots in minimally invasive surgical interventions. **(A)** Magnet-tipped catheter designed for minimally invasive cardiac procedures. Reproduced with permission [250]. Copyright 2018, IEEE. **(B)** Magnet-tipped guidewire for endovascular navigation. Reproduced with permission [226, 251]. Copyright 2006, Springer Nature and Copyright 2018, MDPI. **(C)** Magnetically steerable flexible needle for neurosurgical applications. Reproduced with permission [230]. Copyright 2021, IEEE. **(D,E)** Magnetically guided flexible endoscopes incorporating embedded magnets for minimally invasive exploration of **(D)** the bronchial tree (bronchoscope) and **(E)** the colonic lumen (colonoscope). Panel **(D)** reproduced with permission [231]. Copyright 2018, World Scientific Publishing. Panel **(E)** reproduced with permission [232, 233, 252]. Copyright 2019, IEEE, Copyright 2019, American Association for the Advancement of Science and Copyright 2020, Springer Nature. **(F)** Magnetically steerable laser probe for ophthalmic microsurgery targeting retinal disorders. Reproduced with permission [235]. Copyright 2019, IEEE. **(G)** Magnet-tipped cochlear implants integrated with magnetically actuated robotic components. Reproduced with permission [238]. Copyright 2020, IEEE. **(H)** Flexible magnetically steerable guidewire for navigation through complex cerebral vasculature. Reproduced with permission [240]. Copyright 2019, American Association for the Advancement of Science.

In addition to the above applications of targeted drug delivery, magnetic micro/nanorobots can also serve as untethered microgrippers or micro-tweezers to reach deep-tissue sites and navigate narrow capillaries for minimally invasive surgery under remote magnetic control [223, 224]. Barbot *et al.* developed a magnetically actuated microgripper composed of two microrobots with perpendicular magnetization orientations, which collectively yields an average gripping force of 0.5 N. The system has high accuracy, with positioning errors less than 5 μm and orientation errors of only 0.4°. Therefore, magnetic micro/nanorobotics is highly promising for high-precision guidance in minimally invasive surgery [225]. Notably, magnetically steerable tethered devices, such as magnet-tipped catheters and guidewires, have been translated into clinical application in minimally invasive cardiac surgery and intravascular navigation (Figure 21A, B) [226-229]. With the development of control systems and high-performance hard magnetic materials, a wide range of minimally invasive treatments for neurosurgery (Figure 21C) [230], bronchoscopic navigation of the pulmonary airways [231], colonoscopic interventions (Figure 21D, E) [232, 233], retinal surgery for posterior segment diseases (Figure 21F) [234-236], and cochlear implantation (Figure 21G) [237, 238] have been introduced. Recently, submillimeter-scale microrobots made from hard magnetic and soft materials have achieved omnidirectional steering for navigation in

complex neurovascular environments (Figure 21H) [25, 239, 240]. In contrast to conventional designs that integrate a single magnet at the distal end, these soft continuum robots are fabricated by uniformly dispersing magnetic particles throughout the entire polymer matrix. This innovative structural design features miniaturized dimensions and superior flexibility, which greatly reduces the risk of venous thrombosis arising from vascular displacement and vessel wall injury commonly induced by rigid permanent magnets [215, 240].

In short, among the above-mentioned therapeutic modes, the selection of magnetic therapy strategies for particular types of tumors should be based on all-encompassing consideration of factors such as histological characteristics, location in the body, blood supply, tissue barriers and feasibility for clinical application [241, 242]. For superficial tumors such as breast cancer, the short distance between the magnetic source and the lesion renders external magnetic field targeting, local magnetic hyperthermia, and magnetomechanical therapy relatively favorable options [243]. Liver tumors are relatively highly vascularized and can be accessed through the arterial system; therefore, catheter-assisted magnetic targeting and magnetic chemoembolization have been applied [244]. Magnetic carriers of lung tumors are expected to reach the tumor directly *via* inhalation or local injection. Displacement caused by breathing motion and uneven distribution of pulmonary deposits are still practical problems [245, 246]. Nevertheless, most available evidence remains preclinical, and no fixed correspondence has yet been established between the composition of specific MNPs and specific tumor type.

4. Challenges and Perspectives

4.1 Challenges

MNP-based therapeutic strategies have shown excellent results in cancer treatment. However, many serious problems have prevented their widespread application in biomedicine and subsequent clinical translation. Specifically, some outstanding problems of treatment accuracy, *in vivo* environmental adaptability, material biocompatibility, biodegradability and long-term biosafety still need to be solved. Therefore, future research will focus on addressing the current deficiencies to improve the overall therapeutic effect of MNP-based cancer therapy.

(i) Magnetic hyperthermia is now one of the cancer treatments that can alter the behavior of cells and organelles in a localized way by generating heat. However, several restrictive factors prevent its clinical application. In addition to the intrinsic SAR of magnetic materials, the therapeutic effect is also highly dependent on fine-tuning parameters of AMF, tissue thermal diffusion characteristics, and the uniformity of intratumoral nanoparticle dispersion. At present, the following serious defects still exist in this area: low heating efficiency per unit dose; uneven temperature rise in the tumor; an increased risk of non-specific thermal damage to normal tissues; and difficulty in balancing potent therapeutic thermal effect with minimal systemic side effects within a clinically safe magnetic field window. The basic reasons for magnetic-force therapy at the level of cells and organelles are still unknown. Magnetic mechanical therapy has shown various and innovative therapeutic effects, and although it has moved from the stage of basic research to preliminary clinical trials, it is still in the initial phase of clinical application. For example, the first clinical trials in China and the Netherlands have investigated the application of RMFs to drive MNPs for mechanical therapy of osteosarcoma. However, the system has not yet shown broad safety and efficacy in treating patients, and it is not very controllable.

(ii) Another prominent obstacle to the clinical application of MNPs is the loss of their original magnetic characteristics in a complex and dynamic *in vivo* microenvironment. Many physiological phenomena, such as adsorption of serum proteins, *in vivo* biodegradation, blood dilution and nanoparticle aggregation, can change the hydrodynamic size, crystal structure, surface physicochemical properties and interparticle interactions of MNPs. Structural and morphological modifications will also alter the M_s, H_c, magnetic anisotropy, and relaxation characteristics of MNPs; thus, their performance in a physiological environment will be inconsistent or degraded. Therefore, the effectiveness of magnetic hyperthermia, imaging contrast, tumor targeting efficiency and micro/nanorobot actuation performance may be significantly reduced, and the reliability of *in vivo* treatment will also be affected.

(iii) In addition to stable retention of magnetic properties, precise and localized modification of the magnetic therapeutic effect under external magnetic actuation is also needed. The therapeutic effect of MNPs is achieved through the synergistic action of nanoparticle-intrinsic characteristics, external magnetic-field parameters and a heterogeneous local-tissue microenvironment. For magnetic hyperthermia, if the relaxation time is too short, insufficient heat will be generated to effectively destroy the tumor; otherwise, if it is too long, damage to nearby healthy tissues will occur. Unreliable magnetic actuation for magnetic soft materials and micro/nanorobots will cause a loss of function. The size and direction of the

magnetic-actuation force are determined by the distribution of magnetization, magnetic anisotropy, particle arrangement and matrix mechanical properties. A small change in any of the above reasons will lead to abnormal deformation or displacement and therapeutic failure. Therefore, the clinical application of reliable magnetic therapy requires the combined optimization of magnetic characterization, magnetic field design and *in vivo* biological tests. Stand-alone assessment of individual components cannot reveal the root causes of therapeutic failure or off-target adverse effects.

(iv) *In vivo* circulation stability and degradation biosafety of MNPs are also problems for clinical application. Ferrite-based MNPs have an unavoidable release of iron ions at the material level. After entering the cell, MNPs are degraded in acidic lysosomes and release ferrous (Fe^{2+}) and ferric (Fe^{3+}) ions. Excess iron ions produce hydroxyl radicals, cause lipid peroxidation and induce oxidative stress in cells. Although such reactions promote tumor-targeted chemodynamic therapy and ferroptosis, excessive release of iron and a lack of tumor specificity can disrupt the body's systemic iron homeostasis and cause severe damage to essential metabolic and clearance organs. Therefore, we need to develop a strategy that can induce sufficient tumor-site oxidative stress for tumor ablation without causing prolonged iron accumulation and oxidative damage to the adjacent normal tissues.

At the system level, the basic technical problem is how to balance the circulation stability and post-treatment degradability/clearance of magnetic micro/nanorobots. Surface modification strategies to reduce the early clearance of blood cells and extend their *in vivo* circulation time have included PEGylation, zwitterionic coating and cell membrane camouflage. Although PEGylated liposomes have been successfully translated into clinical practice, zwitterionic coatings and cell-membrane-encapsulated magnetic systems (erythrocyte or platelet membrane modification) are still limited to preclinical research. Clinically mature drug carriers, such as liposomes and albumin-bound nanoparticles, have reduced formulation uncertainty; however, their biosafety and applications in integrated magnetic biohybrid micro/nanorobots have not been systematically investigated. Therefore, all-encompassing systematic evaluation of magnetic cores, surface coatings, magnetic field-responsive behavior, degradation products, *in vivo* biodistribution and long-term organ retention is required. The balance between circulation stability and metabolic clearance should be optimized by regulating coating stability, adding biodegradable matrix materials, and screening functional magnetic materials that retain therapeutic effects during treatment and can be degraded and excreted *in vivo* later. Standardized protocols for cell source collection, sterility guarantees, maintenance of membrane integrity, batch-to-batch consistency control and large-scale production are also necessary for future clinical applications of cell membrane-coated delivery systems.

(v) Although MNP-based magnetic therapy has shown good preclinical results, large-scale industrial production and standardized clinical application have not been achieved. At present, the production conditions fail to satisfy the standardized requirements for appropriate manufacturing practice. Scale-up of production may result in a different particle size distribution and colloidal stability for some batches. Ambiguous regulatory classification is also detrimental to clinical application. The criteria for categorizing MNP-based therapeutic products are not clear, and combined systems of MNPs and external magnetic guidance or imaging devices are classified as such. It has not been determined whether to test the nanoparticle-device composite system separately or as a whole, and standardized regulatory rules for such combined platforms have not been issued. Biosafety evaluation also has some deficiencies. Traditional *in vivo* cytotoxicity tests are suitable for the initial screening of materials but fail to detect prolonged harm caused by repeated *in vivo* administration. The biodistribution, degradation and metabolic behavior of MNPs are all highly dependent on surface modification and the route of administration; therefore, the safety data of a single formulation cannot be generalized to other similar systems. Specifically, there has been no systematic study of the long-term tissue retention and oxidative stress-related toxic effects of SPION-based platforms. These shortcomings indicate that standardized preclinical evaluation procedures are needed urgently to enhance the accuracy of extended biosafety confirmation and *in vivo* efficacy tests prior to clinical trials.

4.2 Perspectives

In the future, research on MNP-based precision tumor therapy systems will be organized in three key directions.

(i) Clinically tailored magnetic navigation technology for smart healthcare has excellent application prospects. The next high-level goal is to achieve stable, closed-loop magnetic navigation of deep-seated lesions in complex biological environments. The new focus of the research will be stable real-time perception and control, not algorithmic complexity. At a low Reynolds number, the movement of microrobots is driven by viscous

forces; therefore, they are highly susceptible to local flow variations, changes in medium viscosity, and anatomical structures. Therefore, the model trained in an ideal microchannel may not have the same behavior under physiologically complex conditions.

Imaging feedback is necessary for the current state and trajectory correction, and different imaging modalities have various strengths and applications. Fluorescence microscopy has excellent sensitivity and spatial resolution, but only a small depth of the tissue can be observed. Ultrasound is convenient in daily life and suitable for real-time observation, but its spatial resolution is relatively low, the signal-to-noise ratio is small, and it can be easily obstructed by acoustic shadows caused by bone or gas. Magnetic particle imaging has a low background signal in biological tissues and is used to track particle clusters and guide magnetic hyperthermia. Millimeter-scale resolution is only suitable for observing large-scale changes in population at present, and it cannot monitor individual micro/nanorobots. Therefore, in the future, navigation models will need to be trained and validated in a physiological environment that can simulate imaging noise, feedback delay, fluctuating fluidic resistance and anatomical boundary constraints. Prediction error, along with the following, also occurs: localization error, control delay, trajectory de*via*tion and environmental adaptation. Physiologically relevant training and validation must be conducted before deploying AI-assisted navigation for *in vivo* real-time control.

(ii) To advance MNP-mediated multimodal therapy, a new paradigm is required: move from macro-level phenomenological observations to micro-level dissection of magnetic-triggered biological effects. In the future, for all links, a causal chain will be formed: Magnetic stimulation→MNP-cell interaction → intracellular signaling pathways→key molecular targets → therapeutic effect. Tumor cells and the surrounding stromal cells continuously exchange materials, energy and information in the TME. Future research will systematically explore how the physicochemical properties of MNPs, such as size, shape and surface modification, affect membrane interaction, intracellular transport, metabolic network and cellular stress response. External magnetic fields may alter the interaction mode of MNPs with cells, and their effect on cellular uptake efficiency, subcellular distribution, mechanical force transmission, thermal response and cell fate regulation is not yet fully known. Further exploration of these interaction mechanisms will facilitate the mechanism-driven rational design of MNPs and expand their therapeutic applications in oncology.

Based on the interaction studies above, high-resolution imaging, real-time mechanical measurement, single-cell analysis and multiscale modelling should be combined to explore how MNPs act at the sub-cellular level in nuclei, plasma membranes, cytoskeletons, mitochondria and lysosomes. Only by constructing a continuous mechanistic chain spanning magnetic stimulation-physical response-molecular alteration-biological outcome can we achieve reproducibility, predictability, and rational optimization of MNP-based therapeutic strategies.

(iii) In terms of clinical translation, it is necessary to break away from the traditional material-oriented research model and establish full-chain research standards based on specific clinical indications. The framework should simultaneously cover material safety assessment, therapeutic protocol standardization and unified construction of clinical endpoint systems to accelerate the translation of MNP-based therapeutics. Material design, magnetic-field delivery, imaging and clinical workflows need to be optimized as a whole in this system. Early interdisciplinary cooperation among materials scientists, engineers, oncologists, radiologists, surgeons, and interventional specialists is needed to identify unmet clinical demands, determine administration routes, and develop methods for tracking the location of particles and therapeutic effects. The first clinical trials should focus on indications suitable for nanoparticle delivery, magnetic-field application and controlled therapeutic monitoring. Suitable starting candidates are superficial, locally recurrent or localized unresectable tumors that are accessible by image-guided injection or catheter delivery for local administration, magnetic intervention and imaging-assisted evaluation. Even an ideal lesion needs to meet the following conditions: sufficient depth, good blood supply, high stromal density, the expectation of high concentration of intratumoral nanoparticles, favorable imaging characteristics, and compatibility with the magnetic field source.

Set quality control and performance standards according to the specific purpose of therapy. The general requirements for MNP formulations are particle size and shape, chemical composition, surface chemistry, colloidal stability, sterility, endotoxin levels, batch consistency, etc., and their functions must meet the purposes of use. Magnetic targeting needs reproducible magnetization and response to clinically relevant magnetic field gradients. Continuously generate heat by changing the amplitude, frequency and exposure time of an AMF for magnetic hyperthermia. In addition, the size and direction of the generated force in magnetomechanical therapy, its

transmission to cells and tissues, and the resulting biological response need to be evaluated. Analysis of the propulsion behavior, steering accuracy, force/torque output, imaging feedback and compatibility with delivery devices for a navigation system is required. Therefore, in the future, MNP formulations, magnetic field generators, imaging modalities, delivery devices and clinical workflows will be integrated rather than optimized individually.

5. Conclusion

With the rapid development of nanobiotechnology and oncology, functional MNPs have become one of the leading platforms for developing next-generation cancer nanomedicines. They are able to respond to external magnetic fields and, at the same time, can be used for intelligent construction of structures and shapes. Such customized design enables the control of biological behavior and therapeutic effect; it cannot be achieved with conventional nanomaterials. As shown above, magnetic anisotropy, size effects and shape effects are not only inherent properties of the material but also the basic reasons for the biological behavior and therapeutic effects of these systems in a complex physiological microenvironment. Therefore, the direction of research has shifted from the preparation of basic magneto-responsive materials to the construction of programmable therapeutic platforms. MNPs can now be designed for targeted accumulation in tumors, localized energy conversion, force-mediated biological effects and magnetic-guided locomotion within the tumor. Ultimately, the translational success of MNPs will depend on deep mechanistic understanding and a strong translational system, rather than the endless expansion of material libraries. Only with these foundations can these promising experimental systems evolve into clinically *via*ble platforms for high-precision cancer therapy.

Abbreviations

2D: two-dimensional; 3D: three-dimensional; AMF: alternating magnetic field; APC: antigen-presenting cell; ATAP: amphipathic tail-anchored peptide; ATP: adenosine triphosphate; Au: gold; $(BH)_{max}$: energy product; BMM: biohybrid microrobot multimer; BMMR: biohybrid magnetic microrobot; BMHR: biodegradable magnetic hydrogel robot; DDS: drug delivery system; DOX: doxorubicin; ECM: extracellular matrix; EGFR: epidermal growth factor receptor; EPR: enhanced permeability and retention; ER: endoplasmic reticulum; fcc: face-centered cubic; fct: face-centered tetragonal; FFP: field-free point; FVIO: ferrimagnetic vortex-domain iron oxide nanoring; GSH: glutathione; H_c: coercivity; H_d: demagnetizing field; HSP: heat shock protein; ICAM-1: intercellular adhesion molecule-1; ICD: immunogenic cell death; IFN-γ: interferon-gamma; IL: interleukin; IONP: iron oxide nanoparticle; LMP: lysosomal membrane permeabilization; MCNP: magnetic core-shell nanoparticle; MHT: magnetic hyperthermia therapy; MIONP: magnetic iron oxide nanoparticle; MNPs: magnetic nanoparticles; MPS: mononuclear phagocyte system; M_r: remanence; MRI: magnetic resonance imaging; M_s: saturation magnetization; NIR: near-infrared; NK: natural killer; NQO1: NADPH quinone oxidoreductase 1; OMF: oscillating magnetic field; PDA: polydopamine; PEG: polyethylene glycol; PLGA: polylactic-co-glycolic acid; PMF: pulsed magnetic field; PTX: paclitaxel; RGD: arginyl-glycyl-aspartic acid; RMN: robotic remote magnetic navigation; RMF: rotating magnetic field; ROS: reactive oxygen species; SAR: specific absorption rate; SMF: static magnetic field; SPION: superparamagnetic iron oxide nanoparticle; T_c: Curie temperature; TME: tumor microenvironment; TNF: tumor necrosis factor; TPP: triphenylphosphonium bromide.

Acknowledgments

This work was supported by the National Natural Science Foundation of China (No. 82402501), the Major State Basic Research Development Program of China (No. 2023YFF071370), and the Sanqin Talent Introduction Plan-Youth Project of Shaanxi Province (No. KSQYC202402) and Fundamental Research Funds for Xi'an Jiaotong University (No. xzy012024129).

Author contributions

Shuang Bai and Kai Ma: contributed equally to this work; conceived the study, performed the literature search, and drafted the manuscript. **Yupei Zhang, Juanjuan Wang, and Long Liu:** collected and organized the literature and prepared the figures and tables. **Shuqin Xu:** critically revised the manuscript for important intellectual content. **Yi Lv:** provided overall supervision and finalized the manuscript. **All authors:** read and approved the final manuscript.

Competing Interests

The authors have declared that no competing interest exists.

References

1. Gallo J, Long NJ, Aboagye EO. Magnetic nanoparticles as contrast agents in the diagnosis and treatment of cancer. Chem Soc Rev. 2013; 42: 7816-33.
2. Gavilan H, Avugadda SK, Fernandez-Cabada T, Soni N, Cassani M, Mai BT, et al. Magnetic nanoparticles and clusters for magnetic hyperthermia:

optimizing their heat performance and developing combinatorial therapies to tackle cancer. Chem Soc Rev. 2021; 50: 11614-67.
3. Shi J, Kantoff PW, Wooster R, Farokhzad OC. Cancer nanomedicine: progress, challenges and opportunities. Nat Rev Cancer. 2017; 17: 20-37.
4. Guo Y, Ran Y, Wang Z, Cheng J, Cao Y, Yang C, et al. Magnetic-responsive and targeted cancer nanotheranostics by PA/MR bimodal imaging-guided photothermally triggered immunotherapy. Biomaterials. 2019; 219: 119370.
5. Rahman M. Magnetic Resonance Imaging and Iron-oxide Nanoparticles in the era of Personalized Medicine. Nanotheranostics. 2023; 7: 424-49.
6. Ma K, Xu S, Tao T, Qian J, Cui Q, Rehman SU, et al. Magnetosome-inspired synthesis of soft ferrimagnetic nanoparticles for magnetic tumor targeting. P Natl Acad Sci U S A. 2022; 119: e2211228119.
7. Pershina AG, Efimova LV, Brikunova OY, Nevskaya KV, Sukhinina EV, Hmelevskaya ES, et al. Nano-bio interaction of magnetic nanoparticles with cells in a tumor at the single-cell level. Nano Today. 2024; 56: 102300.
8. An J, Hong H, Won M, Rha H, Ding Q, Kang N, et al. Mechanical stimuli-driven cancer therapeutics. Chem Soc Rev. 2023; 52: 30-46.
9. Li M, Li J, Chen J, Liu Y, Cheng X, Yang F, et al. Platelet Membrane Biomimetic Magnetic Nanocarriers for Targeted Delivery and in Situ Generation of Nitric Oxide in Early Ischemic Stroke. ACS Nano. 2020; 14: 2024-35.
10. Go G, Jeong SG, Yoo A, Han J, Kang B, Kim S, et al. Human adipose-derived mesenchymal stem cell-based medical microrobot system for knee cartilage regeneration in vivo. Sci Robot. 2020; 5: eaay6626.
11. Yan X, Xu J, Zhou Q, Jin D, Vong CI, Feng Q, et al. Molecular cargo delivery using multicellular magnetic microswimmers. Appl Mater Today. 2019; 15: 242-51.
12. Alapan Y, Bozuyuk U, Erkoc P, Karacakol AC, Sitti M. Multifunctional surface microrollers for targeted cargo delivery in physiological blood flow. Sci Robot. 2020; 5: eaba5726.
13. Xu H, Medina-Sánchez M, Maitz MF, Werner C, Schmidt OG. Sperm Micromotors for Cargo Delivery through Flowing Blood. ACS Nano. 2020; 14: 2982-93.
14. Kilinc D, Lee GU. Advances in magnetic tweezers for single molecule and cell biophysics. Integr Biol. 2013; 6: 27-34.
15. Coughlin MF, Bielenberg DR, Lenormand G, Marinkovic M, Waghorne CG, Zetter BR, et al. Cytoskeletal stiffness, friction, and fluidity of cancer cell lines with different metastatic potential. Clin Expl Metastasis. 2013; 30: 237-50.
16. Bonakdar N, Gerum R, Kuhn M, Spörrer M, Lippert A, Schneider W, et al. Mechanical plasticity of cells. Nat Mater. 2016; 15: 1090-4.
17. Vyskočil J, Mayorga-Martinez CC, Jablonská E, Novotný F, Ruml T, Pumera M. Cancer Cells Microsurgery via Asymmetric Bent Surface Au/Ag/Ni Microrobotic Scalpels Through a Transversal Rotating Magnetic Field. ACS Nano. 2020; 14: 8247-56.
18. Chatzipirpiridis G, Ergeneman O, Pokki J, Ullrich F, Fusco S, Ortega JA, et al. Electroforming of Implantable Tubular Magnetic Microrobots for Wireless Ophthalmologic Applications. Adv Healthc Mater. 2015; 4: 209-14.
19. Walker D, Kasdorf BT, Jeong HH, Lieleg O, Fischer P. Enzymatically active biomimetic micropropellers for the penetration of mucin gels. Sci Adv. 2015; 1: e1500501.
20. Huang T-Y, Sakar MS, Mao A, Petruska AJ, Qiu F, Chen X-B, et al. 3D Printed Microtransporters: Compound Micromachines for Spatiotemporally Controlled Delivery of Therapeutic Agents. Adv Mater. 2015; 27: 6644-50.
21. Mair LO, Evans BA, Nacev A, Stepanov PY, Hilaman R, Chowdhury S, et al. Magnetic microkayaks: propulsion of microrods precessing near a surface by kilohertz frequency, rotating magnetic fields. Nanoscale. 2017; 9: 3375-81.
22. Li J, Li X, Luo T, Wang R, Liu C, Chen S, et al. Development of a magnetic microrobot for carrying and delivering targeted cells. Sci Robot. 2018; 3: eaat8829.
23. Li T, Li J, Zhang H, Chang X, Song W, Hu Y, et al. Magnetically Propelled Fish-Like Nanoswimmers. Small. 2016; 12: 6098-105.
24. Ye C, Liu J, Wu X, Wang B, Zhang L, Zheng Y, et al. Hydrophobicity Influence on Swimming Performance of Magnetically Driven Miniature Helical Swimmers. Micromachines (Basel). 2019; 10: 175.
25. Kim Y, Genevriere E, Harker P, Choe J, Balicki M, Regenhardt RW, et al. Telerobotic neurovascular interventions with magnetic manipulation. Sci Robot. 2022; 7: eabg9907.
26. Zhou H, Mayorga-Martinez CC, Pane S, Zhang L, Pumera M. Magnetically Driven Micro and Nanorobots. Chem Rev. 2021; 121: 4999-5041.
27. Pucci C, Degl'Innocenti A, Belenli Gumus M, Ciofani G. Superparamagnetic iron oxide nanoparticles for magnetic hyperthermia: recent advancements, molecular effects, and future directions in the omics era. Biomater Sci. 2022; 10: 2103-21.
28. Na HB, Song IC, Hyeon T. Inorganic Nanoparticles for MRI Contrast Agents. Adv Mater. 2009; 21: 2133-48.
29. Liu F, Hou Y, Gao S. Exchange-coupled nanocomposites: chemical synthesis, characterization and applications. Chem Soc Rev. 2014; 43: 8098-113.
30. Wu L, Mendoza-Garcia A, Li Q, Sun S. Organic Phase Syntheses of Magnetic Nanoparticles and Their Applications. Chem Rev. 2016; 116: 10473-512.
31. Nasir Baig RB, Nadagouda MN, Varma RS. Magnetically retrievable catalysts for asymmetric synthesis. Coor Chem Rev. 2015; 287: 137-56.
32. Smith BR, Gambhir SS. Nanomaterials for In vivo Imaging. Chem Rev. 2017; 117: 901-86.
33. Ulbrich K, Hola K, Subr V, Bakandritsos A, Tucek J, Zboril R. Targeted Drug Delivery with Polymers and Magnetic Nanoparticles: Covalent and Noncovalent Approaches, Release Control, and Clinical Studies. Chem Rev. 2016; 116: 5338-431.
34. Shen C, Oda Y, Matsubara M, Yabuki J, Yamanaka S, Abe H, et al. Magnetorheological Fluids with Surface-Modified Iron Oxide Magnetic Particles with Controlled Size and Shape. ACS Appl Mater Interfaces. 2021; 13: 20581-8.
35. Tejedor I, Kravchenko DE, Gandara-Loe J, Ameloot R, Gascón I, Roubeau O. Gd Metal–Organic Framework Thin Film for On-Chip Local Magnetic Refrigeration. Chem Mater. 2024; 36: 8239-46.
36. Usman M, Byrne JM, Chaudhary A, Orsetti S, Hanna K, Ruby C, et al. Magnetite and Green Rust: Synthesis, Properties, and Environmental Applications of Mixed-Valent Iron Minerals. Chem Rev. 2018; 118: 3251-304.
37. Dash A, Blasiak B, Tomanek B, Banerjee A, Trudel S, Latta P, et al. Colloidally Stable Monodisperse Fe Nanoparticles as T2 Contrast Agents for High-Field Clinical and Preclinical Magnetic Resonance Imaging. ACS Appl Nano Mater. 2021; 4: 1235-42.
38. Wu J, Zhou W, Cheng Q, Yang J. Polyvinylpyrrolidone-stabilized magnetic nickel nanochains for cancer hyperthermia and catalysis applications. RSC Adv. 2015; 5: 22965-71.
39. Carvell J, Ayieta E, Gavrin A, Cheng R, Shah VR, Sokol P. Magnetic properties of iron nanoparticle. J Appl Phys. 2010; 107: 103913.
40. Fu R, Yan Y, Roberts C, Liu Z, Chen Y. The role of dipole interactions in hyperthermia heating colloidal clusters of densely-packed superparamagnetic nanoparticles. Sci Rep. 2018; 8: 4704.
41. Azmoudeh A, Moral S, Sari S, Türk M, Kahveci MU, Doganay GD, et al. Magnetic iron-based nanoparticles encapsulated in graphene/reduced graphene oxide: Synthesis, functionalization and cytotoxicity tests. J Sci: Adv Mater Devices. 2024; 9: 100776.
42. Krishnan RR, Prasad E, Fernandez FB, K.V N, Chandran SR, Johnson E, et al. Hyperthermia heating efficiency of glycine functionalized graphene oxide modified nickel nanoparticles. J Alloys Compd. 2024; 982: 173804.
43. Akhtar MJ, Ahamed M, Alhadlaq H. Cobalt-based nanoparticles strongly diminish CalceinAM fluorescence independently of their cytotoxic potential in human lung cell line. J King Saud Univ Sci. 2023; 36: 102987.
44. Cornell RM, Schwertmann U. Crystal Structure. In: Cornell RM, Schwertmann U, editors. The Iron Oxides: Structure, Properties, Reactions, Occurrences and Uses. Weinheim: Wiley-VCH; 2003. p. 9-38.
45. Yang C, Wu J, Hou Y. Fe3O4 nanostructures: synthesis, growth mechanism, properties and applications. Chem Commun. 2011; 47: 5130-41.
46. Ukhurebor KE, Aigbe UO, Onyancha RB, Balogun VA, Anani OA, Adama KK, et al. An Overview of Magnetic Nanomaterials. In: Aigbe UO, Ukhurebor KE, Onyancha RB, editors. Magnetic Nanomaterials: Synthesis, Characterization and Applications. Cham: Springer International Publishing; 2023. p. 1-20.
47. Xie X, Li Y, Liu Z-Q, Haruta M, Shen W. Low-temperature oxidation of CO catalysed by Co3O4 nanorods. Nature. 2009; 458: 746-9.
48. Wang P-P, Zhang C-X, Hu L-N, Li S-Q, Ren W-H, Hao Y-Y. Research progress of inverted planar perovskite solar cells based on nickel oxide as hole transport layer. Acta Phys Si. 2021; 70: 118801.
49. Devan RS, Patil RA, Lin J-H, Ma Y-R. One-Dimensional Metal-Oxide Nanostructures: Recent Developments in Synthesis, Characterization, and Applications. Adv Funct Mater. 2012; 22: 3326-70.
50. Song LX, Yang ZK, Teng Y, Xia J, Du P. Nickel oxide nanoflowers: formation, structure, magnetic property and adsorptive performance towards organic dyes and heavy metal ions. J Mater Chem A. 2013; 1: 8731-6.
51. Yin B, Zhang S, Jiang H, Qu F, Wu X. Phase-controlled synthesis of polymorphic MnO2 structures for electrochemical energy storage. J Mater Chem A. 2015; 3: 5722-9.
52. Wang K, Cheng Q, Bai J-q, Chen F, Chen J, Wu M, et al. The directional structure transition of MnO2 during the drying process. J Mater Chem A. 2024; 12: 2373-82.

53. Djerdj I, Arčon D, Jagličić Z, Niederberger M. Nonaqueous Synthesis of Manganese Oxide Nanoparticles, Structural Characterization, and Magnetic Properties. J Phys Chem C. 2007; 111: 3614-23.
54. Gutfleisch O, Lyubina J, Müller KH, Schultz L. FePt Hard Magnets. Adv Eng Mater. 2005; 7: 208-12.
55. Ma Z, Mohapatra J, Wei K, Liu JP, Sun S. Magnetic Nanoparticles: Synthesis, Anisotropy, and Applications. Chem Rev. 2023; 123: 3904-43.
56. Burkert T, Eriksson O, Simak SI, Ruban AV, Sanyal B, Nordström L, et al. Magnetic anisotropy of FePt and Fe1−xMnxPt. Phys Rev B. 2005; 71: 134411.
57. Brown G, Kraczek B, Janotti A, Schulthess TC, Stocks GM, Johnson DD. Competition between ferromagnetism and antiferromagnetism in FePt. Phys Rev B. 2003; 68: 052405.
58. Staunton JB, Ostanin S, Razee SSA, Gyorffy BL, Szunyogh L, Ginatempo B, et al. Temperature Dependent Magnetic Anisotropy in Metallic Magnets from an Ab Initio Electronic Structure Theory: L10-Ordered FePt. Phys Rev Lett. 2004; 93: 257204.
59. Weller D, Moser A, Folks L, Best ME, Wen L, Toney MF, et al. High K/sub u/ materials approach to 100 Gbits/in/sup 2. IEEE Trans Magn. 2000; 36: 10-5.
60. Weller D, Brändle H, Gorman G, Lin CJ, Notarys H. Magnetic and magneto-optical properties of cobalt-platinum alloys with perpendicular magnetic anisotropy. Appl Phys Lett. 1992; 61: 2726-8.
61. Sanchez JM, Moran-Lopez JL, Leroux C, Cadeville MC. Magnetic properties and chemical ordering in Co-Pt. J Phys Condens Matter. 1989; 1: 491-6.
62. Yu Y, Yang W, Sun X, Zhu W, Li XZ, Sellmyer DJ, et al. Monodisperse MPt (M = Fe, Co, Ni, Cu, Zn) Nanoparticles Prepared from a Facile Oleylamine Reduction of Metal Salts. Nano Letters. 2014; 14: 2778-82.
63. Takahashi YK, Koyama T, Ohnuma M, Ohkubo T, Hono K. Size dependence of ordering in FePt nanoparticles. J Appl Phys. 2004; 95: 2690-6.
64. Gruner ME, Rollmann G, Entel P, Farle M. Multiply Twinned Morphologies of FePt and CoPt Nanoparticles. Phys Rev Lett. 2008; 100: 087203.
65. Wiedwald U, Klimmer A, Kern B, Han L, Boyen HG, Ziemann P, et al. Lowering of the L1 ordering temperature of FePt nanoparticles by He+ ion irradiation. Appl Phys Lett. 2007; 90: 062508.
66. Yang W, Rehman S, Chu X, Hou Y, Gao S. Transition Metal (Fe, Co and Ni) Carbide and Nitride Nanomaterials: Structure, Chemical Synthesis and Applications. ChemNanoMat. 2015; 1: 376-98.
67. Haglund J, Fernandez Guillermet A, Grimvall G, Korling M. Theory of bonding in transition-metal carbides and nitrides. Phys Rev B Condens Matter. 1993; 48: 11685-91.
68. Tian D, Denny SR, Li K, Wang H, Kattel S, Chen JG. Density functional theory studies of transition metal carbides and nitrides as electrocatalysts. Chem Soc Rev. 2021; 50: 12338-76.
69. Khazaei M, Arai M, Sasaki T, Chung C-Y, Venkataramanan NS, Estili M, et al. Novel Electronic and Magnetic Properties of Two-Dimensional Transition Metal Carbides and Nitrides. Adv Funct Mater. 2013; 23: 2185-92.
70. Yang Z, Zhao T, Huang X, Chu X, Tang T, Ju Y, et al. Modulating the phases of iron carbide nanoparticles: from a perspective of interfering with the carbon penetration of Fe@Fe3O4 by selectively adsorbed halide ions. Chem Sci. 2017; 8: 473-81.
71. Suzuki K, Morita H, Kaneko T, Yoshida H, Fujimori H. Crystal structure and magnetic properties of the compound FeN. J Alloy Compd. 1993; 201: 11-6.
72. He L. Hexagonal close-packed nickel or Ni3C? J Magn Magn Mater. 2010; 322: 1991-3.
73. Zhu Y, Zhang Y, Wang K, Li D, Ding F, Meng D, et al. One-pot synthesis of Ni/Ni3C/Ni3N nanocomposite: Structure, growth mechanism and magnetic properties. Mater Res Bull. 2017; 95: 79-85.
74. Fang CM, Sluiter MHF, van Huis MA, Zandbergen HW. Structural and magnetic properties of NiC and NiN (to) solid solutions from first-principles calculations. Phys Rev B. 2012; 86: 134114.
75. Gutfleisch O, Willard MA, Brück E, Chen CH, Sankar SG, Liu JP. Magnetic Materials and Devices for the 21st Century: Stronger, Lighter, and More Energy Efficient. Adv Mater. 2011; 23: 821-42.
76. Kirchmayr HR. Permanent magnets and hard magnetic materials. J Phys D: Appl Phys. 1996; 29: 2763-78.
77. Yang Z, Qiao S, Sun S. Overview of magnetic nanomaterials. In: Hou Y, Sellmyer DJ, editors. Magnetic Nanomaterials. Weinheim: Wiley-VCH; 2017. p. 1-28.
78. McCallum RW, Lewis LH, Skomski R, Kramer MJ, Anderson IE. Practical Aspects of Modern and Future Permanent Magnets. Annu Rev Mater Res. 2014; 44: 451-77.
79. Kuz'ma YB, Bilonizhko NS, Mykhalenko SI, Stepanchikova GF, Chaban NF. The interaction of transition and rare earth metals with boron. J Less Common Met. 1979; 67: 51-7.
80. Buschow KHJ, de Boer FR. Permanent Magnets. In: Buschow KHJ, de Boer FR, editors. Physics of Magnetism and Magnetic Materials. Boston, MA: Springer US; 2003. p. 105-29.
81. Sellmyer DJ, Zheng M, Skomski R. Magnetism of Fe, Co and Ni nanowires in self-assembled arrays. J Phys Condens Matter. 2001; 13: R433-60.
82. Mohapatra J, Liu JP. Rare-Earth-Free Permanent Magnets: The Past and Future. In: Brück E, editor. Handbook of Magnetic Materials: Amsterdam, Elsevier; 2018. p. 1-57.
83. Kovalenko MV, Bodnarchuk MI, Lechner RT, Hesser G, Schaffler F, Heiss W. Fatty acid salts as stabilizers in size- and shape-controlled nanocrystal synthesis: the case of inverse spinel iron oxide. J Am Chem Soc. 2007; 129: 6352-3.
84. Zhao Z, Zhou Z, Bao J, Wang Z, Hu J, Chi X, et al. Octapod iron oxide nanoparticles as high-performance T2 contrast agents for magnetic resonance imaging. Nat Commun. 2013; 4: 2266.
85. Mitra A, Mohapatra J, Meena SS, Tomy CV, Aslam M. Verwey Transition in Ultrasmall-Sized Octahedral Fe3O4 Nanoparticles. J Phys Chem C. 2014; 118: 19356-62.
86. Mohapatra J, Mitra A, Tyagi H, Bahadur D, Aslam M. Iron oxide nanorods as high-performance magnetic resonance imaging contrast agents. Nanoscale. 2015; 7: 9174-84.
87. Mohapatra J, Xing M, Liu JP. Inductive Thermal Effect of Ferrite Magnetic Nanoparticles. Materials (Basel). 2019; 12: 3208.
88. Mohapatra J, Xing M, Beatty J, Elkins J, Seda T, Mishra SR, et al. Enhancing the magnetic and inductive heating properties of Fe3O4 nanoparticles via morphology control. Nanotechnology. 2020; 31: 275706.
89. Néel L. Influence des fluctuations thermiques sur l'aimantation de grains ferromagnétiques très fins. C R Hebd Seances Acad Sci. 1949; 228: 664-6.
90. Poudyal N, Ping Liu J. Advances in nanostructured permanent magnets research. J Phys D Appl Phys. 2013; 46: 043001.
91. Krishnan K. Biomedical Nanomagnetics: A Spin Through Possibilities in Imaging, Diagnostics, and Therapy. IEEE Trans Magn. 2010; 46: 2523-58.
92. Wang S, Mao Y, Rong S, Liu G, Cao Y, Yang Z, et al. Engineering Magnetic Extracellular Vesicles Mimetics for Enhanced Targeting Chemodynamic Therapy to Overcome Ovary Cancer. ACS Appl Mater Interfaces. 2024; 16: 39021-34.
93. Chen XZ, Hoop M, Shamsudhin N, Huang T, Ozkale B, Li Q, et al. Hybrid Magnetoelectric Nanowires for Nanorobotic Applications: Fabrication, Magnetoelectric Coupling, and Magnetically Assisted In Vitro Targeted Drug Delivery. Adv Mater. 2017; 29: 1605458.
94. Chen Y, Jiang L, Wang R, Lu M, Zhang Q, Zhou Y, et al. Injectable smart phase-transformation implants for highly efficient in vivo magnetic-hyperthermia regression of tumors. Adv Mater. 2014; 26: 7468-73.
95. Shen J, Rees TW, Zhou Z, Yang S, Ji L, Chao H. A mitochondria-targeting magnetothermogenic nanozyme for magnet-induced synergistic cancer therapy. Biomaterials. 2020; 251: 120079.
96. Shah BP, Pasquale N, De G, Tan T, Ma J, Lee KB. Core-shell nanoparticle-based peptide therapeutics and combined hyperthermia for enhanced cancer cell apoptosis. ACS Nano. 2014; 8: 9379-87.
97. Jiang H, Fu H, Guo Y, Hu P, Shi J. Evoking tumor associated macrophages by mitochondria-targeted magnetothermal immunogenic cell death for cancer immunotherapy. Biomaterials. 2022; 289: 121799.
98. Liu X, Zheng J, Sun W, Zhao X, Li Y, Gong N, et al. Ferrimagnetic Vortex Nanoring-Mediated Mild Magnetic Hyperthermia Imparts Potent Immunological Effect for Treating Cancer Metastasis. ACS Nano. 2019; 13: 8811-25.
99. Chen M, Wu J, Ning P, Wang J, Ma Z, Huang L, et al. Remote Control of Mechanical Forces via Mitochondrial-Targeted Magnetic Nanospinners for Efficient Cancer Treatment. Small. 2020; 16: e1905424.
100. Master AM, Williams PN, Pothayee N (Nikorn), Pothayee N (Nipon), Zhang R, Vishwasrao HM, et al. Remote Actuation of Magnetic Nanoparticles For Cancer Cell Selective Treatment Through Cytoskeletal Disruption. Sci Rep. 2016; 6: 33560.
101. Lunov O, Uzhytchak M, Smolkova B, Lunova M, Jirsa M, Dempsey NM, et al. Remote Actuation of Apoptosis in Liver Cancer Cells via Magneto-Mechanical Modulation of Iron Oxide Nanoparticles. Cancers (Basel). 2019; 11: 1873.
102. Thebault C, Marmiesse M, Naud C, Pernet-Gallay K, Billiet E, Joisten H, et al. Magneto-mechanical treatment of human glioblastoma cells with engineered iron oxide powder microparticles for triggering apoptosis. Nanoscale Adv. 2021; 3: 6213-22.
103. Shen Y, Zhang W, Li G, Ning P, Li Z, Chen H, et al. Adaptive Control of Nanomotor Swarms for Magnetic-Field-Programmed Cancer Cell Destruction. ACS Nano. 2021; 15: 20020-31.

104. Wu J, Ning P, Gao R, Feng Q, Shen Y, Zhang Y, et al. Programmable ROS-Mediated Cancer Therapy via Magneto-Inductions. Adv Sci (Weinh). 2020; 7: 1902933.
105. Zhang E, Kircher MF, Koch M, Eliasson L, Goldberg SN, Renstrom E. Dynamic magnetic fields remote-control apoptosis via nanoparticle rotation. ACS Nano. 2014; 8: 3192-201.
106. Sim T, Choi B, Kwon SW, Kim KS, Choi H, Ross A, et al. Magneto-Activation and Magnetic Resonance Imaging of Natural Killer Cells Labeled with Magnetic Nanocomplexes for the Treatment of Solid Tumors. ACS Nano. 2021; 15: 12780-93.
107. Chen X, Tian C, Zhang H, Xie H. Biodegradable Magnetic Hydrogel Robot with Multimodal Locomotion for Targeted Cargo Delivery. ACS Appl Mater Interfaces. 2023; 15: 28922-32.
108. Gong D, Celi N, Zhang D, Cai J. Magnetic Biohybrid Microrobot Multimers Based on Chlorella Cells for Enhanced Targeted Drug Delivery. ACS Appl Mater Interfaces. 2022; 14: 6320-30.
109. Wang X, Cai J, Sun L, Zhang S, Gong D, Li X, et al. Facile Fabrication of Magnetic Microrobots Based on Spirulina Templates for Targeted Delivery and Synergistic Chemo-Photothermal Therapy. ACS Appl Mater Interfaces. 2019; 11: 4745-56.
110. Li Z, Xiao C, Yong T, Li Z, Gan L, Yang X. Influence of nanomedicine mechanical properties on tumor targeting delivery. Chem Soc Rev. 2020; 49: 2273-90.
111. Wilhelm S, Tavares AJ, Dai Q, Ohta S, Audet J, Dvorak HF, et al. Analysis of nanoparticle delivery to tumours. Nat Rev Mater. 2016; 1: 16014.
112. Freeman MW, Arrott A, Watson JHL. Magnetism in Medicine. J Appl Phys. 1960; 31: S404-S5.
113. Zimmermann U, Pilwat G. [Organ specific application of drugs by means of cellular capsule systems (author's transl)]. Z Naturforsch C Biosci. 1976; 31: 732-6.
114. Lubbe AS, Bergemann C, Huhnt W, Fricke T, Riess H, Brock JW, et al. Preclinical experiences with magnetic drug targeting: tolerance and efficacy. Cancer Res. 1996; 56: 4694-701.
115. Lubbe AS, Bergemann C, Riess H, Schriever F, Reichardt P, Possinger K, et al. Clinical experiences with magnetic drug targeting: a phase I study with 4'-epidoxorubicin in 14 patients with advanced solid tumors. Cancer Res. 1996; 56: 4686-93.
116. Alksne JF. Magnetically controlled intravascular catheter. Surgery. 1968; 64: 339-45.
117. Alksne JF. Stereotactic thrombosis of intracranial aneurysms. N Engl J Med. 1971; 284: 171-4.
118. Alksne JF, Fingerhut AG. Magnetically controlled metallic thrombosis of intracranial aneurysms. A preliminary report. Bull Los Angeles Neurol Soc. 1965; 30: 153-5.
119. Yang Z, Zhang L. Magnetic Actuation Systems for Miniature Robots: A Review. Adv Intell Syst. 2020; 2: 2000082.
120. Kong T, Zheng Q, Sun J, Wang C, Liu H, Gao Z, et al. Advances in Magnetically Controlled Medical Robotics: A Review of Actuation Systems, Continuum Designs, and Clinical Prospects for Minimally Invasive Therapies. Micromachines (Basel). 2025; 16: 561.
121. Zughaibi J, Nelson BJ, Muehlebach M. Dynamic Electromagnetic Navigation. IEEE Robot Autom Lett. 2025; 10: 6095-102.
122. Gervasoni S, Pedrini N, Rifai T, Fischer C, Landers FC, Mattmann M, et al. A Human-Scale Clinically Ready Electromagnetic Navigation System for Magnetically Responsive Biomaterials and Medical Devices. Adv Mater. 2024; 36: e2310701.
123. Lubbe AS, Alexiou C, Bergemann C. Clinical applications of magnetic drug targeting. J Surg Res. 2001; 95: 200-6.
124. Alexiou C, Arnold W, Klein RJ, Parak FG, Hulin P, Bergemann C, et al. Locoregional cancer treatment with magnetic drug targeting. Cancer Res. 2000; 60: 6641-8.
125. Tay ZW, Chandrasekharan P, Zhou XY, Yu E, Zheng B, Conolly S. In vivo tracking and quantification of inhaled aerosol using magnetic particle imaging towards inhaled therapeutic monitoring. Theranostics. 2018; 8: 3676-87.
126. Graeser M, Thieben F, Szwargulski P, Werner F, Gdaniec N, Boberg M, et al. Human-sized magnetic particle imaging for brain applications. Nat Commun. 2019; 10: 1936.
127. Liu JF, Lan Z, Ferrari C, Stein JM, Higbee-Dempsey E, Yan L, et al. Use of Oppositely Polarized External Magnets To Improve the Accumulation and Penetration of Magnetic Nanocarriers into Solid Tumors. ACS Nano. 2020; 14: 142-52.
128. Cho MH, Lee EJ, Son M, Lee JH, Yoo D, Kim JW, et al. A magnetic switch for the control of cell death signalling in in vitro and in vivo systems. Nat Mater. 2012; 11: 1038-43.
129. Price PM, Mahmoud WE, Al-Ghamdi AA, Bronstein LM. Magnetic Drug Delivery: Where the Field Is Going. Front Chem. 2018, 6: 619.
130. Kim C, Kim J, Park JO, Choi E, Kim CS. Localization and Actuation for MNPs Based on Magnetic Field-Free Point: Feasibility of Movable Electromagnetic Actuations. Micromachines (Basel). 2020; 11: 1020.
131. Jain RK, Stylianopoulos T. Delivering nanomedicine to solid tumors. Nat Rev Clin Oncol. 2010; 7: 653-64.
132. Ge J, Zhang Y, Dong Z, Jia J, Zhu J, Miao X, et al. Initiation of Targeted Nanodrug Delivery in vivo by a Multifunctional Magnetic Implant. ACS Appl Mater Interfaces. 2017; 9: 20771-8.
133. Vonthron M, Lalande V, Martel S. A MRI-based platform for catheter navigation. Annu Int Conf IEEE Eng Med Biol Soc. 2011; 2011: 5392-5.
134. Pouponneau P, Soulez G, Beaudoin G, Leroux JC, Martel S. MR imaging of therapeutic magnetic microcarriers guided by magnetic resonance navigation for targeted liver chemoembolization. Cardiovasc Interv Radiol. 2014; 37: 784-90.
135. Stauffer PR. Evolving technology for thermal therapy of cancer. Int J Hyperthermia. 2005; 21: 731-44.
136. Xu Y, Wang Y, An J, Sedgwick AC, Li M, Xie J, et al. 2D-ultrathin MXene/DOXjade platform for iron chelation chemo-photothermal therapy. Bioact Mater. 2022; 14: 76-85.
137. Yu L, Xu Y, Pu Z, Kang H, Li M, Sessler JL, et al. Photocatalytic Superoxide Radical Generator that Induces Pyroptosis in Cancer Cells. J Am Chem Soc. 2022; 144: 11326-37.
138. Gu T, Wang Y, Lu Y, Cheng L, Feng L, Zhang H, et al. Platinum Nanoparticles to Enable Electrodynamic Therapy for Effective Cancer Treatment. Adv Mater. 2019; 31: e1806803.
139. Chen L, Zhang J, Xu L, Zhu L, Jing J, Feng Y, et al. Composition tunability of semiconductor radiosensitizers for low-dose X-ray induced photodynamic therapy. J Nanobiotechnology. 2022; 20: 293.
140. Pandey NK, Xiong W, Wang L, Chen W, Bui B, Yang J, et al. Aggregation-induced emission luminogens for highly effective microwave dynamic therapy. Bioact Mater. 2022; 7: 112-25.
141. Gilchrist RK, Medal R, Shorey WD, Hanselman RC, Parrott JC, Taylor CB. Selective inductive heating of lymph nodes. Ann Surg. 1957; 146: 596-606.
142. Li H, Ye Z, Wang X, Yuan J, Guo J, Liu C, et al. Intracellular magnetic hyperthermia reverses sorafenib resistance in hepatocellular carcinoma through its action on signaling pathways. iScience. 2024; 27: 110029.
143. Das P, Colombo M, Prosperi D. Recent advances in magnetic fluid hyperthermia for cancer therapy. Colloids Surf B Biointerfaces. 2019; 174: 42-55.
144. Verde EL, Landi GT, Gomes JA, Sousa MH, Bakuzis AF. Magnetic hyperthermia investigation of cobalt ferrite nanoparticles: Comparison between experiment, linear response theory, and dynamic hysteresis simulations. J Appl Phy. 2012; 111: 123902.
145. Rosensweig RE. Heating magnetic fluid with alternating magnetic field. J Magn Magn Mater. 2002; 252: 370-4.
146. Barick KC, Aslam M, Lin Y-P, Bahadur D, Prasad PV, Dravid VP. Novel and efficient MR active aqueous colloidal Fe3O4 nanoassemblies. J Mater Chem. 2009; 19: 7023-9.
147. Hergt R, Dutz S. Magnetic particle hyperthermia—biophysical limitations of a visionary tumour therapy. J Magn Magn Mater. 2007; 311: 187-92.
148. Lartigue L, Innocenti C, Kalaivani T, Awwad A, Sanchez Duque Mdel M, Guari Y, et al. Water-dispersible sugar-coated iron oxide nanoparticles. An evaluation of their relaxometric and magnetic hyperthermia properties. J Am Chem Soc. 2011; 133: 10459-72.
149. Jeun M, Lee S, Kyeong Kang J, Tomitaka A, Wook Kang K, Il Kim Y, et al. Physical limits of pure superparamagnetic Fe3O4 nanoparticles for a local hyperthermia agent in nanomedicine. Appl Phys Lett. 2012; 100: 092406.
150. Andra W, Bierlich J, Danan H, Bellemann ME. Remote controlled drug release in the alimentary tract by local power deposition in alternating magnetic fields. Biomed Tech (Berl). 2002; 47 736-8.
151. Majeed J, Pradhan L, Ningthoujam RS, Vatsa RK, Bahadur D, Tyagi AK. Enhanced specific absorption rate in silanol functionalized Fe3O4 core-shell nanoparticles: study of Fe leaching in Fe3O4 and hyperthermia in L929 and HeLa cells. Colloids Surf B Biointerfaces. 2014; 122: 396-403.
152. Kafrouni L, Savadogo O. Recent progress on magnetic nanoparticles for magnetic hyperthermia. Prog Biomater. 2016; 5: 147-60.
153. Nandwana V, De M, Chu S, Jaiswal M, Rotz M, Meade TJ, et al. Theranostic Magnetic Nanostructures (MNS) for Cancer. In: Mirkin CA, Meade TJ, Petrosko SH, Stegh AH, editors. Nanotechnology-Based Precision Tools for the Detection and Treatment of Cancer. Berlin, Germany: Springer International Publishing; 2015. p. 51-83.
154. Gupta AK, Naregalkar RR, Vaidya VD, Gupta M. Recent advances on surface engineering of magnetic iron oxide nanoparticles and their biomedical applications. Nanomedicine (Lond). 2007; 2: 23-39.
155. Rao S, Chen R, LaRocca AA, Christiansen MG, Senko AW, Shi CH, et al. Remotely controlled chemomagnetic modulation of targeted neural circuits. Nat Nanotechnol. 2019; 14: 967-73.

156. Huang H, Delikanli S, Zeng H, Ferkey DM, Pralle A. Remote control of ion channels and neurons through magnetic-field heating of nanoparticles. Nat Nanotechnol. 2010; 5: 602-6.
157. Stanley SA, Gagner JE, Damanpour S, Yoshida M, Dordick JS, Friedman JM. Radio-wave heating of iron oxide nanoparticles can regulate plasma glucose in mice. Science. 2012; 336: 604-8.
158. Zhang Y, Zhang Y, Li J, Liang C, Shi K, Wang S, et al. Impact of Nanoheater Subcellular Localization on the Antitumor Immune Efficacy of Magnetic Hyperthermia. Nano Today. 2024; 56: 102226.
159. Clerc P, Jeanjean P, Hallali N, Gougeon M, Pipy B, Carrey J, et al. Targeted Magnetic Intra-Lysosomal Hyperthermia produces lysosomal reactive oxygen species and causes Caspase-1 dependent cell death. J Control Release. 2018; 270: 120-34.
160. Domenech M, Marrero-Berrios I, Torres-Lugo M, Rinaldi C. Lysosomal membrane permeabilization by targeted magnetic nanoparticles in alternating magnetic fields. ACS Nano. 2013; 7: 5091-101.
161. Gordon RT, Hines JR, Gordon D. Intracellular hyperthermia. A biophysical approach to cancer treatment via intracellular temperature and biophysical alterations. Med Hypotheses. 1979; 5: 83-102.
162. Liu X, Zhang Y, Wang Y, Zhu W, Li G, Ma X, et al. Comprehensive understanding of magnetic hyperthermia for improving antitumor therapeutic efficacy. Theranostics. 2020; 10: 3793-815.
163. Sanchez C, El Hajj Diab D, Connord V, Clerc P, Meunier E, Pipy B, et al. Targeting a G-protein-coupled receptor overexpressed in endocrine tumors by magnetic nanoparticles to induce cell death. ACS Nano. 2014; 8: 1350-63.
164. Saeed M, Ren W, Wu A. Therapeutic applications of iron oxide based nanoparticles in cancer: basic concepts and recent advances. Biomater Sci. 2018; 6: 708-25.
165. Ito A, Honda H, Kobayashi T. Cancer immunotherapy based on intracellular hyperthermia using magnetite nanoparticles: a novel concept of "heat-controlled necrosis" with heat shock protein expression. Cancer Immunol Immunother. 2006; 55: 320-8.
166. Lei L, Liu P, Jing W, Wu Z. Advancements in modifying the efficacy of immunotherapies through the thermal effects of nanomaterials. Nano TransMed. 2023; 2: 100022.
167. Yanase M, Shinkai M, Honda H, Wakabayashi T, Yoshida J, Kobayashi T. Antitumor Immunity Induction by Intracellular Hyperthermia Using Magnetite Cationic Liposomes. Japanese J Cancer Res. 1998; 89: 775-82.
168. Srivastava P. Interaction of heat shock proteins with peptides and antigen presenting cells: chaperoning of the innate and adaptive immune responses. Annu Rev Immunol. 2002; 20: 395-425.
169. Suzue K, Zhou X, Eisen HN, Young RA. Heat shock fusion proteins as vehicles for antigen delivery into the major histocompatibility complex class I presentation pathway. Proc Natl Acad Sci U S A. 1997; 94: 13146-51.
170. Meyer RE, Braun RD, Rosner GL, Dewhirst MW. Local 42 degrees C hyperthermia improves vascular conductance of the R3230Ac rat mammary adenocarcinoma during sodium nitroprusside infusion. Radiat Res. 2000; 154: 196-201.
171. Song CW, Shakil A, Griffin RJ, Okajima K. Improvement of tumor oxygenation status by mild temperature hyperthermia alone or in combination with carbogen. Semin Oncol. 1997; 24: 626-32.
172. Kong G, Braun RD, Dewhirst MW. Characterization of the effect of hyperthermia on nanoparticle extravasation from tumor vasculature. Cancer Res. 2001; 61: 3027-32.
173. Toraya-Brown S, Sheen MR, Zhang P, Chen L, Baird JR, Demidenko E, et al. Local hyperthermia treatment of tumors induces CD8+ T cell-mediated resistance against distal and secondary tumors. Nanomedicine. 2014; 10: 1273-85.
174. Sniadecki NJ, Lamb CM, Liu Y, Chen CS, Reich DH. Magnetic microposts for mechanical stimulation of biological cells: fabrication, characterization, and analysis. Rev Sci Instrum. 2008; 79: 044302.
175. Mohammadi H, Sahai E. Mechanisms and impact of altered tumour mechanics. Nat Cell Biol. 2018; 20: 766-74.
176. Jain RK, Martin JD, Stylianopoulos T. The role of mechanical forces in tumor growth and therapy. Annu Rev Biomed Eng. 2014; 16: 321-46.
177. Sengupta S, Balla VK. A review on the use of magnetic fields and ultrasound for non-invasive cancer treatment. J Adv Res. 2018; 14: 97-111.
178. Hubbs AF, Sargent LM, Porter DW, Sager TM, Chen BT, Frazer DG, et al. Nanotechnology: toxicologic pathology. Toxicol Pathol. 2013; 41: 395-409.
179. Chenyang Y, Fang Y, Li S, Yuanyuan M, Stanciu SG, Zihou L, et al. Magnetically switchable mechano-chemotherapy for enhancing the death of tumour cells by overcoming drug-resistance. Nano Today. 2020; 35: 100967.
180. Coste B, Mathur J, Schmidt M, Earley TJ, Ranade S, Petrus MJ, et al. Piezo1 and Piezo2 are essential components of distinct mechanically activated cation channels. Science. 2010; 330: 55-60.
181. Freikamp A, Cost AL, Grashoff C. The Piconewton Force Awakens: Quantifying Mechanics in Cells. Trends Cell Biol. 2016; 26: 838-47.
182. Wu J, Goyal R, Grandl J. Localized force application reveals mechanically sensitive domains of Piezo1. Nat Commun. 2016; 7: 12939.
183. Monticelli M, Conca DV, Albisetti E, Torti A, Sharma PP, Kidiyoor G, et al. Magnetic domain wall tweezers: a new tool for mechanobiology studies on individual target cells. Lab Chip. 2016; 16: 2882-90.
184. Gonzalez-Rodriguez D, Guillou L, Cornat F, Lafaurie-Janvore J, Babataheri A, de Langre E, et al. Mechanical Criterion for the Rupture of a Cell Membrane under Compression. Biophys J. 2016; 111: 2711-21.
185. Cabrera D, Coene A, Leliaert J, Artes-Ibanez EJ, Dupre L, Telling ND, et al. Dynamical Magnetic Response of Iron Oxide Nanoparticles Inside Live Cells. ACS Nano. 2018; 12: 2741-52.
186. Nana ABA, Marimuthu T, Kondiah PPD, Choonara YE, Du Toit LC, Pillay V. Multifunctional Magnetic Nanowires: Design, Fabrication, and Future Prospects as Cancer Therapeutics. Cancers (Basel). 2019; 11: 1956.
187. Yan X, Zhou Q, Vincent M, Deng Y, Yu J, Xu J, et al. Multifunctional biohybrid magnetite microrobots for imaging-guided therapy. Sci Robot. 2017; 2: eaaq1155.
188. Huang HW, Uslu FE, Katsamba P, Lauga E, Sakar MS, Nelson BJ. Adaptive locomotion of artificial microswimmers. Sci Adv. 2019; 5: eaau1532.
189. Lee JU, Shin W, Lim Y, Kim J, Kim WR, Kim H, et al. Non-contact long-range magnetic stimulation of mechanosensitive ion channels in freely moving animals. Nat Mater. 2021; 20: 1029-36.
190. Dupont S, Morsut L, Aragona M, Enzo E, Giulitti S, Cordenonsi M, et al. Role of YAP/TAZ in mechanotransduction. Nature. 2011; 474: 179-83.
191. Cheng Y, Muroski ME, Petit D, Mansell R, Vemulkar T, Morshed RA, et al. Rotating magnetic field induced oscillation of magnetic particles for in vivo mechanical destruction of malignant glioma. J Control Release. 2016; 223: 75-84.
192. Zhao N, Yan L, Xue J, Zhang K, Xu F-J. Degradable one-dimensional dextran-iron oxide nanohybrids for MRI-guided synergistic gene/photothermal/magnetolytic therapy. Nano Today. 2021; 38: 101118.
193. Goiriena-Goikoetxea M, Muñoz D, Orue I, Fernández-Gubieda ML, Bokor J, Muela A, et al. Disk-shaped magnetic particles for cancer therapy. Appl Phys Rev. 2020; 7: 011306.
194. Shen Y, Wu C, Uyeda TQP, Plaza GR, Liu B, Han Y, et al. Elongated Nanoparticle Aggregates in Cancer Cells for Mechanical Destruction with Low Frequency Rotating Magnetic Field. Theranostics. 2017; 7: 1735-48.
195. Park W, Kim SJ, Cheresh P, Yun J, Lee B, Kamp DW, et al. Magneto mitochondrial dysfunction mediated cancer cell death using intracellular magnetic nano-transducers. Biomater Sci. 2021; 9: 5497-507.
196. Wang B, Bienvenu C, Mendez-Garza J, Lançon P, Madeira A, Vierling P, et al. Necrosis of HepG2 cancer cells induced by the vibration of magnetic particles. J Magn Magn Mater. 2013; 344: 193-201.
197. Mirkovic T, Zacharia NS, Scholes GD, Ozin GA. Fuel for thought: chemically powered nanomotors out-swim nature's flagellated bacteria. ACS Nano. 2010; 4: 1782-9.
198. Sanchez S, Soler L, Katuri J. Chemically powered micro- and nanomotors. Angew Chem Int Ed Engl. 2015; 54: 1414-44.
199. Yigit B, Alapan Y, Sitti M. Programmable Collective Behavior in Dynamically Self-Assembled Mobile Microrobotic Swarms. Adv Sci (Weinh). 2019; 6: 1801837.
200. Huang HW, Sakar MS, Petruska AJ, Pane S, Nelson BJ. Soft micromachines with programmable motility and morphology. Nat Commun. 2016; 7: 12263.
201. Kim J, Chung SE, Choi SE, Lee H, Kim J, Kwon S. Programming magnetic anisotropy in polymeric microactuators. Nat Mater. 2011; 10: 747-52.
202. Wang Q, Yang L, Wang B, Yu E, Yu J, Zhang L. Collective Behavior of Reconfigurable Magnetic Droplets via Dynamic Self-Assembly. ACS Appl Mater Interfaces. 2019; 11: 1630-7.
203. Wang H, Pumera M. Coordinated behaviors of artificial micro/nanomachines: from mutual interactions to interactions with the environment. Chem Soc Rev. 2020; 49: 3211-30.
204. Liu JA, Gillen JH, Mishra SR, Evans BA, Tracy JB. Photothermally and magnetically controlled reconfiguration of polymer composites for soft robotics. Sci Adv. 2019; 5: eaaw2897.
205. Huang H-W, Huang T-Y, Charilaou M, Lyttle S, Zhang Q, Pané S, et al. Investigation of Magnetotaxis of Reconfigurable Micro-Origami Swimmers with Competitive and Cooperative Anisotropy. Adv Funct Mater. 2018; 28: 1802110.
206. Ren L, Wang W, Mallouk TE. Two Forces Are Better than One: Combining Chemical and Acoustic Propulsion for Enhanced Micromotor Functionality. Acc Chem Res. 2018; 51: 1948-56.
207. Zrínyi M, Barsi L, Büki A. Deformation of ferrogels induced by nonuniform magnetic fields. J Chem Phys. 1996; 104: 8750-6.

208. Zhao X, Kim J, Cezar CA, Huebsch N, Lee K, Bouhadir K, et al. Active scaffolds for on-demand drug and cell delivery. P Natl Acad Sci U S A. 2011; 108: 67-72.
209. Haider H, Yang CH, Zheng WJ, Yang JH, Wang MX, Yang S, et al. Exceptionally tough and notch-insensitive magnetic hydrogels. Soft Matter. 2015; 11: 8253-61.
210. Schmauch MM, Mishra SR, Evans BA, Velev OD, Tracy JB. Chained Iron Microparticles for Directionally Controlled Actuation of Soft Robots. ACS Appl Mater Interfaces. 2017; 9: 11895-901.
211. Mishra SR, Dickey MD, Velev OD, Tracy JB. Selective and directional actuation of elastomer films using chained magnetic nanoparticles. Nanoscale. 2016; 8: 1309-13.
212. Kim Y, Zhao X. Magnetic Soft Materials and Robots. Chem Rev. 2022; 122: 5317-64.
213. Jeon S, Hoshiar AK, Kim K, Lee S, Kim E, Lee S, et al. A Magnetically Controlled Soft Microrobot Steering a Guidewire in a Three-Dimensional Phantom Vascular Network. Soft Robot. 2019; 6: 54-68.
214. Pancaldi L, Dirix P, Fanelli A, Lima AM, Stergiopulos N, Mosimann PJ, et al. Flow driven robotic navigation of microengineered endovascular probes. Nat Commun. 2020; 11: 6356.
215. Azizi A, Tremblay CC, Gagne K, Martel S. Using the fringe field of a clinical MRI scanner enables robotic navigation of tethered instruments in deeper vascular regions. Sci Robot. 2019; 4: eaax7342.
216. Murasovs N, Lloyd P, Bacchetti A, May YL, Armitage J, Cespedes O, et al. Gradient pulling of a tethered robot via a magnetic resonance imaging system. Device. 2025; 3: 100870.
217. Li J, Esteban-Fernandez de Avila B, Gao W, Zhang L, Wang J. Micro/Nanorobots for Biomedicine: Delivery, Surgery, Sensing, and Detoxification. Sci Robot. 2017; 2: eaam6431.
218. Sun Z, Hou Y. Micro/Nanorobots as Active Delivery Systems for Biomedicine: From Self-Propulsion to Controllable Navigation. Advanced Therapeutics. 2022; 5: 2100228.
219. Huang L, Sun X, Song T, Long J, Chen X, Dong R, et al. The swarmable magnetic-driven nanorobots for facilitating trans-intestinal mucosal delivery of oral vaccines to enhance mucosal and systemic immune responses. Nano Today. 2025; 62: 102721.
220. Srivastava SK, Medina-Sanchez M, Koch B, Schmidt OG. Medibots: Dual-Action Biogenic Microdaggers for Single-Cell Surgery and Drug Release. Adv Mater. 2016; 28: 832-7.
221. Sun Z, Wang T, Wang J, Xu J, Shen T, Zhang T, et al. Self-Propelled Janus Nanocatalytic Robots Guided by Magnetic Resonance Imaging for Enhanced Tumor Penetration and Therapy. J Am Chem Soc. 2023; 145: 11019-32.
222. Yasa IC, Ceylan H, Bozuyuk U, Wild AM, Sitti M. Elucidating the interaction dynamics between microswimmer body and immune system for medical microrobots. Sci Robot. 2020; 5: eaaz3867.
223. Diller E, Sitti M. Three-Dimensional Programmable Assembly by Untethered Magnetic Robotic Micro-Grippers. Adv Funct Mater. 2014; 24: 4397-404.
224. Goudu SR, Yasa IC, Hu X, Ceylan H, Hu W, Sitti M. Biodegradable Untethered Magnetic Hydrogel Milli-Grippers. Adv Funct Mater. 2020; 30: 2004975.
225. Barbot A, Tan H, Power M, Seichepine F, Yang GZ. Floating magnetic microrobots for fiber functionalization. Sci Robot. 2019; 4: eaax8336.
226. Krings T, Finney J, Niggemann P, Reinacher P, Luck N, Drexler A, et al. Magnetic versus manual guidewire manipulation in neuroradiology: in vitro results. Neuroradiology. 2006; 48: 394-401.
227. Ramcharitar S, Patterson MS, van Geuns RJ, van Meighem C, Serruys PW. Technology Insight: magnetic navigation in coronary interventions. Nat Clin Pract Cardiovasc Med. 2008; 5: 148-56.
228. Schiemann M, Killmann R, Kleen M, Abolmaali N, Finney J, Vogl TJ. Vascular guide wire navigation with a magnetic guidance system: experimental results in a phantom. Radiology. 2004; 232: 475-81.
229. Tsuchida K, Garcia-Garcia HM, van der Giessen WJ, McFadden EP, van der Ent M, Sianos G, et al. Guidewire navigation in coronary artery stenoses using a novel magnetic navigation system: first clinical experience. Catheter Cardio Inter. 2006; 67: 356-63.
230. Hong A, Petruska AJ, Zemmar A, Nelson BJ. Magnetic Control of a Flexible Needle in Neurosurgery. IEEE Trans Biomed Eng. 2021; 68: 616-27.
231. Edelmann J, Petruska AJ, Nelson BJ. Estimation-Based Control of a Magnetic Endoscope without Device Localization. J Med Robot Res. 2018; 03: 1850002.
232. Pittiglio G, Barducci L, Martin JW, Norton JC, Avizzano CA, Obstein KL, et al. Magnetic Levitation for Soft-Tethered Capsule Colonoscopy Actuated With a Single Permanent Magnet: A Dynamic Control Approach. IEEE Robot Autom Lett. 2019; 4: 1224-31.
233. Norton JC, Slawinski PR, Lay HS, Martin JW, Cox BF, Cummins G, et al. Intelligent magnetic manipulation for gastrointestinal ultrasound. Sci Robot. 2019; 4: eaav7725.
234. Charreyron SL, Boehler Q, Danun AN, Mesot A, Becker M, Nelson BJ. A Magnetically Navigated Microcannula for Subretinal Injections. IEEE Trans Biomed Eng. 2021; 68: 119-29.
235. Charreyron SL, Gabbi E, Boehler Q, Becker M, Nelson BJ. A Magnetically Steered Endolaser Probe for Automated Panretinal Photocoagulation. IEEE Robot Autom Lett. 2019; 4: 284-90.
236. Ullrich F, Lussi J, Chatzopoulos V, Michels S, Petruska AJ, Nelson BJ. A Robotic Diathermy System for Automated Capsulotomy. J Med Robot Res. 2017; 03: 1850001.
237. Leon L, Warren FM, Abbott JJ. Optimizing the Magnetic Dipole-Field Source for Magnetically Guided Cochlear-Implant Electrode-Array Insertions. J Med Robot Res. 2018; 3: 1850004.
238. Bruns TL, Riojas KE, Ropella DS, Cavilla MS, Petruska AJ, Freeman MH, et al. Magnetically Steered Robotic Insertion of Cochlear-Implant Electrode Arrays: System Integration and First-In-Cadaver Results. IEEE Robot Autom Lett. 2020; 5: 2240-7.
239. Lloyd P, Hoshiar AK, Veiga Td, Attanasio A, Marahrens N, Chandler JH, et al. A Learnt Approach for the Design of Magnetically Actuated Shape Forming Soft Tentacle Robots. IEEE Robot Autom Lett. 2020; 5: 3937-44.
240. Kim Y, Parada GA, Liu S, Zhao X. Ferromagnetic soft continuum robots. Sci Robot. 2019; 4: eaax7329.
241. Wang B, Hu S, Teng Y, Chen J, Wang H, Xu Y, et al. Current advance of nanotechnology in diagnosis and treatment for malignant tumors. Signal Transduct Target Ther. 2024; 9: 200.
242. Bhattacharya S, M KR, Priyadarshani J, Ganguly R, Chakraborty S. Targeting Magnetic Nanoparticles in Physiologically Mimicking Tissue Microenvironment. ACS Appl Mater Interfaces. 2022; 14: 31689-701.
243. Gwisai T, Mirkhani N, Christiansen MG, Nguyen TT, Ling V, Schuerle S. Magnetic torque-driven living microrobots for increased tumor infiltration. Sci Robot. 2022; 7: eabo0665.
244. Yang N, Sun X, Zhou Y, Yang X, You J, Yu Z, et al. Liquid metal microspheres with an eddy-thermal effect for magnetic hyperthermia-enhanced cancer embolization-immunotherapy. Sci Bull (Beijing). 2023; 68: 1772-83.
245. Price DN, Stromberg LR, Kunda NK, Muttil P. In Vivo Pulmonary Delivery and Magnetic-Targeting of Dry Powder Nano-in-Microparticles. Mol Pharm. 2017; 14: 4741-50.
246. Manshadi MKD, Saadat M, Mohammadi M, Kamali R, Shamsi M, Naseh M, et al. Magnetic aerosol drug targeting in lung cancer therapy using permanent magnet. Drug Deliv. 2019; 26: 120-8.
247. Zhou Z, Shen Z, Chen X. Tale of Two Magnets: An Advanced Magnetic Targeting System. ACS Nano. 2020; 14: 7-11.
248. Belyanina I, Kolovskaya O, Zamay S, Gargaun A, Zamay T, Kichkailo A. Targeted Magnetic Nanotheranostics of Cancer. Molecules. 2017; 22: 975.
249. Cho MH, Kim S, Lee JH, Shin TH, Yoo D, Cheon J. Magnetic Tandem Apoptosis for Overcoming Multidrug-Resistant Cancer. Nano Lett. 2016; 16: 7455-60.
250. Heunis C, Sikorski J, Misra S. Flexible Instruments for Endovascular Interventions: Improved Magnetic Steering, Actuation, and Image-Guided Surgical Instruments. IEEE Robot Autom Mag. 2018; 25: 71-82.
251. Kafash Hoshiar A, Jeon S, Kim K, Lee S, Kim JY, Choi H. Steering Algorithm for a Flexible Microrobot to Enhance Guidewire Control in a Coronary Angioplasty Application. Micromachines (Basel). 2018; 9: 617.
252. Martin JW, Scaglioni B, Norton JC, Subramanian V, Arezzo A, Obstein KL, et al. Enabling the future of colonoscopy with intelligent and autonomous magnetic manipulation. Nat Mach Intell. 2020; 2: 595-606.

Author Biographies

Shuang Bai is currently an associate professor in the First Affiliated Hospital of Xi'an Jiaotong University. She received her Ph.D.

degree from Xiamen University in 2023. Her research interests focus on the functional micro/nanomaterials for biomedical application. She has published more than 40 papers and been awarded the Sanqin Talent Introduction Plan-Youth Project of Shaanxi Province and Xi'an Jiaotong University Young Top-Talent Support Program.

Kai Ma received his M.S. degree from the School of Bioengineering and Food Science at the Hubei University of Technology in 2023. He is currently pursuing his PhD degree at Xi'an Jiaotong University. His research interests focus on anti-tumor drug delivery systems.

Yi Lv is currently a professor at the Xi'an Jiaotong University. He is an academician of the Academia Europaea, a specialist in hepatobiliary surgery, the Vice President of Xi'an Jiaotong University, and serves as the President of the First Affiliated Hospital of Xi'an Jiaotong University. He has long been engaged in hepatobiliary surgery and liver transplantation, and is also a pioneer in the magnetic surgery in China, having proposed the concept and system of magnetic surgery. He has published more than 300 papers in SCI-indexed journals, and won the second prize of National Award for Science and Technology Progress as the first principal investigator. He has held nine consecutive International Conferences of Magnetic Surgery.